IN SILICO ANALYSIS OF NEUTRAL SPHINGOMYELINASE 2

by

Zarife Begüm Yağcı

B.S., Chemical Engineering, Boğaziçi University, 2016

Submitted to the Institute for Graduate Studies in
Science and Engineering in partial fulfillment of
the requirements for the degree of
Master of Science

Graduate Program in Chemical Engineering

Boğaziçi University

2018

ACKNOWLEDGEMENTS

I would like to express my sincere gratitude and appreciation to my thesis supervisor Prof. Kutlu Ülgen and thesis co-supervisor Assoc. Prof. Elif Özkırımlı Ölmez for providing patient guidance and valuable support during this research work.

I would like to thank my committee members; Prof. Berna Sarıyar Akbulut, Prof. Türkan Haliloğlu, and Assoc. Prof. Burak Alakent. Their willingness to spend time on my thesis and provide guidance and recommendations has been greatly appreciated.

I wish to acknowledge the help provided by Prof. Yusuf Hannun. His valuable and constructive recommendations have been a great help throughout my research.

I am forever thankful to my fellow friends; Elif Esvap, Merve Yüce and Özlem Özbek for being by my side through thick and thin, and the wonderful times we have shared together. Our 'coffee sessions' will always be among my fondest memories. I would like to thank my dear friends; Selin Baç, Dilara Göreke, Ayşegül Karakuş, İlke Kaykanat, Müge Kasım, Feyza Öner, Ezgi Öztürk, Özge Selçuk and Aysun Urhan for their encouragement and continuous optimism. I cannot thank enough to my best friends; Sinem, Ecem, Esra and Yeşim for their endless support and unparalleled love. I am grateful for the assistance provided by my mentor and dear friend Ayşe Eren.

Finally, my grateful thanks are extended to my family for their invaluable support, continued patience and encouragement throughout my entire life. This journey would not have been possible without them. They will always be my inspiration. Thank you for believing in me. I dedicate this thesis to them.

The support provided by the Scientific and Technological Research Council of Turkey (TÜBİTAK) under the grant number of 115S208 is gratefully acknowledged.

ABSTRACT

IN SILICO ANALYSIS OF NEUTRAL SPHINGOMYELINASE 2

Neutral sphingomyelinase 2 (nSMase2) is an important sphingolipid metabolism enzyme that generates ceramide through the hydrolysis of sphingomyelin (SM) present in the plasma membrane. It has been suggested as a therapeutic target for many diseases from Alzheimer's disease to cancer because of its possible role in several cellular processes including exosome secretion and inflammation. Mammalian nSMases comprise catalytic and membrane domains, and the crystal structure of the catalytic domain of human nSMase2 was recently resolved facilitating detailed structural analysis of this enzyme. The aim of this current study was to investigate the structure and dynamics of human nSMase2 by comparison with bacterial sphingomyelinase (*Bc*-SMase) structures to unveil its catalytic mechanism. Docking and MD simulations were performed on apo and SM-bound bacterial and human nSMase catalytic domains. The simulations suggested that the membrane-associated N-terminal domain of human nSMase2 may be important for the stability of this enzyme. SM interacted with Glu53 and Mg^{2+} in *Bc*-SMases and with the corresponding Glu364 and Ca^{2+} in human nSMase2 highlighting the importance of these residues and ions in SM binding. The possible binding site and binding mode of the experimentally determined nSMase2 inhibitor GW4869 were identified through SiteMap and molecular docking analysis, and MD simulations were carried out on GW4869-bound structures to further investigate the catalytic mechanism of human nSMase2.

ÖZET

NÖTRAL SFİNGOMYELİNAZ 2'NİN *İN SİLİKO* ANALİZİ

Nötral sfingomiyelinaz 2 (nSMaz2), plazma membranında bulunan sfingomiyelinin (SM) hidrolizi yoluyla seramidi oluşturan, önemli bir sfingolipid metabolizma enzimidir. Alzheimer hastalığından kansere kadar birçok hastalık için, ekzozom sekresyonu ve iltihaplanma dahil olmak üzere çeşitli hücresel süreçlerdeki muhtemel rolü nedeniyle terapötik bir hedef olarak önerilmiştir. Memeli nSMazları, katalitik ve membran domainlerini içerir ve yakın zamanda bulunun insan enziminin katalitik domaininin kristal yapısı, bu enzimin ayrıntılı yapısal analizini kolaylaştırdı. Bu çalışmanın amacı, insan nSMaz2'nin katalitik mekanizmasını ortaya çıkarmak için insan nSMaz2'nin yapısını ve dinamiklerini bakteri sfingomiyelinaz (*Bc*-SMaz) yapıları ile karşılaştırmaktır. Doklama ve MD simülasyonları, apo ve SM-bağlı bakteri ve insan nSMaz katalitik domainleri üzerinde gerçekleştirilmiştir. Simülasyonlar, insan nSMaz2'nin membrana bağlı N-terminal domaininin bu enzimin stabilitesi için önemli olabileceğini göstermiştir. SM'nin *Bc*-SMazları içinde Glu53 ve Mg^{2+} ile ve insan nSMaz2'de karşılık gelen Glu364 ve Ca^{2+} ile etkileşime girmesi bu aminoasitlerin ve iyonların SM bağlanmasındaki önemini vurgulamıştır. Deneysel olarak belirlenen nSMaz2 inhibitörü GW4869'un olası bağlanma yeri ve bağlanma modu, SiteMap ve moleküler doklama analizi yoluyla tanımlanmış olup, insan nSMaz2'nin katalitik mekanizmasını daha fazla araştırmak amacıyla GW4869-bağlı yapılar üzerinde MD simülasyonları gerçekleştirilmiştir.

TABLE OF CONTENTS

LIST OF FIGURES

LIST OF TABLES

LIST OF SYMBOLS

E	Energy
e	Enclosure Score
G	Gibbs Free Energy (kcal/mol)
H	Enthalpy (kcal/mol)
N	Number of Atoms
n	Number of Site Points
p	Hydrophilic Score
r	Position
S	Entropy
T	Temperature (K)
t	Time (ns)
T	Trajectory Time (ns)

LIST OF ACRONYMS/ABBREVIATIONS

2D	Two Dimensional
3D	Three Dimensional
A	Alanine
AD	Alzheimer's Disease
Ala	Alanine
APL	Anionic Phospholipid
Arg	Arginine
aSMase	Acid Sphingomyelinase
Asp	Aspartic Acid
Avg	Average
AWD	All Water Deleted Structure
Bc-SMase	*Bacillus cereus* Sphingomyelinase
C	Cysteine
C16-SM	d18:1C16-Sphingomyelin
C1P	Ceramide-1-Phosphate
CTD	C-terminal Domain
Cys	Cysteine
DK	Asp126-Lys131 in *Bc*-SMase, Asp430-Lys435 in Human nSMase2
E	Glutamic Acid
eq	Equilibrium
F	Phenylalanine
G	Glycine
GB	Generalized Born
Gln	Glutamine
Glu	Glutamic Acid
Gly	Glycine
GPU	Graphics Processor Unit

GScore	Glide Score
GSH	Glutathione
GW	GW4869
H	Histidine
H(b)	Hydrogen Bonding (Backbone)
H(s)	Hydrogen Bonding (Side Chain)
His	Histidine
Hyd	Hydrophobic Interactions
I	Isoleucine
ICAM	Intracellular Adhesion Molecule
IFD	Induced Fit Docking
IFN	Interferon
IL	Interleukin
IL-1β	Interleukin 1-Beta
IL-1R	Interleukin-1 Receptor
Ile	Isoleucine
Ins	Insertion
IRAK-1	Interleukin-1 Receptor Activated Kinases
K	Lysine
L	Leucine
Leu	Leucine
Lys	Lysine
M	Methionine
Met	Methionine
MA-nSMase	Mitochondrial-Associated nSMase
MBW	Metal Bound Water Kept Structure
MD	Molecular Dynamics
Metal Coor	Metal Coordination
MM	Molecular Mechanics
N	Asparagine
NPT	Isothermal-Isobaric Ensemble

nSMase	Neutral Sphingomyelinase
NTD	N-terminal Domain
P	Proline
PB	Poisson-Boltzmann
PDB	Protein Data Bank
PM	Plasma Membrane
PMA	Phorbyl 12-Myristate 13-Acetate
PPW	Protein Preparation Wizard
Pro	Proline
PS	Phosphatidylserine
Q	Glutamine
R	Arginine
RMSD	Root Mean Square Deviation
RMSF	Root Mean Square Fluctuations
S	Serine
S1P	Sphingosine-1-Phosphate
SA	Surface Area
Salt b	Salt Bridge
SASA	Solvent Accessible Surface Area
SEA	Simulation Event Analysis
Ser	Serine
SID	Simulation Interactions Diagram
SM	Sphingomyelinase
SMS	SM Synthases
SPC	Simple Point Charge Model
SSE	Secondary Structure Elements
sSMase	Secretory Sphingomyelinase
StDev	Standard Deviation
Struct	Structure
T	Temperature
T	Threonine

t	Time
Thr	Threonine
TLR	Toll-like Receptor
TNF	Tumor Necrosis Factor
Trp	Tryptophan
Tyr	Tyrosine
V	Valine
Val	Valine
VCAM	Vascular Cell Adhesion Molecule
vdW	van der Waals
VMD	Visual Molecular Dynamics
VSGB	Variable-Dielectric Generalized Born Model
W	Tryptophan
Wb	Water Bridge
WW5M	Water within 5 Å of Metal Ion Kept Structure
XP	Extra Precision
Y	Tyrosine

1. INTRODUCTION

Neutral sphingomyelinase 2 (nSMase2), a key enzyme in sphingolipid metabolism, hydrolyzes sphingomyelin to generate phosphocholine and ceramide at neutral pH in a divalent metal ion-dependent manner [1, 2]. It was reported to play a major role in stress-induced ceramide generation [3], and its product ceramide is a crucial sphingolipid metabolite involved in regulating many cellular signaling pathways that are related with cell proliferation, differentiation and apoptosis [4–6]. Due to its role in various cellular processes including bone mineralization, exosome formation, inflammatory response, cell growth arrest, and cellular stress responses, nSMase2 has been implicated in the pathogenesis of many diseases such as Alzheimer's disease (AD) and cancer [1, 4, 7]. Hence understanding its catalytic mechanism will enable developing new therapeutic agents that target nSMase2 [1].

Bacterial and mammalian nSMases share a similar catalytic mechanism and protein fold even though their sequence identity is low. Mammalian nSMases are integral membrane proteins while bacterial ones are soluble [2, 7, 8]. In addition to the highly conserved residues at the active site, Airola *et al.* suggested another conserved region, the so-called DK Switch, which was proposed to regulate the interaction between N-terminal domain and the catalytic domain of nSMase2, and have different conformations depending on whether the nSMase2 has an active state or not [1].

Several studies have being carried out to unveil the structural and dynamical details about human nSMase2. The newly discovered crystal structure of catalytic domain of human nSMase2 (PDB ID: 5UVG) [1] has contributed to elucidating the catalytic mechanism of nSMase2. Yet, the conformational activation mechanism of nSMase2 is still not clear.

The aim of this work is to comparatively analyze the structures and dynamics of bacterial and human nSMases by making use of their shared catalytic mechanism and

protein fold [1], and to shed light on the catalytic mechanism of nSMase2. For this purpose, molecular dynamics simulations were performed on the apo and ligand-bound forms of *Bacillus cereus* SMases (PDB IDs: 2DDS and 2UYR [2]) and human nSMase2 (PDB ID: 5UVG). The results were comparatively analyzed with a special focus on the DK switch and active site regions.

This thesis is organized as follows: Background information on sphingolipids with a special focus on the function and structure of nSMase2 and bacterial sphingomyelinases is given in the Theoretical Background section. The computational tools utilized and the parameters used for docking and molecular dynamics simulations are described in the Methods section. Results and Discussion section includes the comparative analysis and interpretation of the docking and MD simulations results on apo, SM-bound and GW4869-bound SMases. Conclusion and Recommendation section contains the summary of the main findings of this study and the recommendations on how to improve this research for future work. Supplementary data for the results of the MD simulations are provided in the Appendix section.

2. THEORETICAL BACKGROUND

2.1. Sphingolipids and Sphingomyelinases

Sphingolipids are an important family of membrane lipid molecules that have a structural role in the cellular membrane and take part in several cellular processes including inflammatory signaling, apoptosis, proliferation, and pain sensing [4, 9, 10]. They have been implicated in the pathogenesis of many diseases such as cancer, lysosomal storage disorders, inflammatory bowel disease, lung disease, diabetes, and Alzheimer's disease [4, 9].

Sphingolipids have a long-chain sphingoid backbone known as sphingosine which is derived from the condensation of an amino acid (mainly serine) and a fatty acid (mainly palmitate) [4, 9, 11]. Ceramide has a structure of sphingosine attached to a fatty acid moiety, and it is a bioactive lipid involved in several cellular functions including inflammation and apoptosis [1, 2, 4, 9, 12]. The phosphorylation of the 1-hydroxyl groups of ceramide and sphingosine generates ceramide-1-phosphate (C1P) and sphingosine-1-phosphate (S1P), respectively (see Figure 2.1). Complex sphingolipids have different headgroups attached to ceramide. For example, sphingomyelin (SM) contains a phosphorylcholine headgroup, whereas the basic glycosphingolipids have a single sugar molecule headgroup [4, 9]. These various moieties, i.e. differences in the structures of sphingolipid types, enable these metabolites to have different roles in cellular metabolism including the regulation of signaling pathways [9, 13].

Sphingomyelinases (SMases) are enzymes which hydrolyze sphingomyelin to produce ceramide and phosphocholine [4]. They are classified into five categories according to their optimal pH, metal ion requirement and localization. These SMase types are acid sphingomyelinase (aSMase), secretory sphingomyelinase (sSMase), neutral Mg^{2+}-dependent sphingomyelinase (nSMase), Mg^{2+}-independent neutral sphingomyelinase,

and alkaline sphingomyelinase. Bacterial sphingomyelinase-phospholipase C was also reported to be under the classification of sphingomyelinases [6, 8].

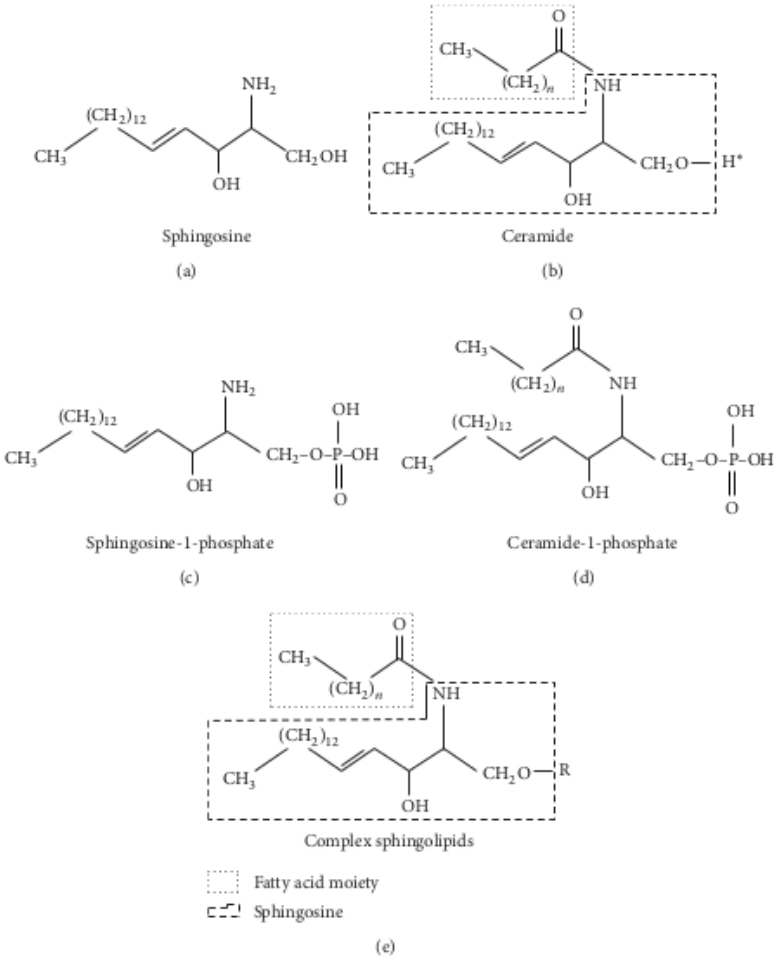

Figure 2.1. Structures of bioactive sphingolipids [9].

The first identified sphingomyelinase, aSMase (*SMPD1*) has an optimum activity at around pH 5 and is localized in lysosomes. The deficiency of this enzyme leads to a neurodegenerative disorder known as Niemann-Pick syndrome. sSMase is a secretory enzyme activated by Zn^{2+}, however it has been suggested that zinc-independent forms of this enzyme may exist. Alkaline sphingomyelinase has been suggested to be expressed in intestine and not in other organs. Bile salts are needed for its activity and it is Mg^{2+}-independent. Deficiency in this enzyme may contribute to colon carcinogenesis [8]. Neutral sphingomyelinases with a special focus on nSMase2 are explained in detail in the next sections.

2.2. Neutral Sphingomyelinase (nSMase)

Neutral sphingomyelinases (nSMases) are among the key enzymes in sphingolipid metabolism. They hydrolyze sphingomyelin to produce ceramide and phosphocholine at around pH 7.4. Ceramide and other sphingolipid metabolites are essential for regulating several cellular signaling pathways, involved in cell proliferation, differentiation and apoptosis, and implicated in the pathogenesis of many diseases [4–6].

Among the four mammalian nSMase enzymes that have been identified (nSMase1 (*SMPD2*), nSMase2 (*SMPD3*), nSMase3 (*SMPD4*), and MA-nSMase (mitochondrial-associated nSMase; *SMPD5*)), nSMase2 is the most widely investigated one. Neutral SMase2 has a role in bone mineralization, exosome formation, inflammatory response, cell growth arrest, and cellular stress responses [4]. nSMase2 has been suggested as a therapeutic target for cancer and Alzheimer's disease [1].

SMPD3 gene encodes nSMase2 enzyme that consists of 655 amino acids [7]. The deletion mutant of *SMPD3* demonstrated that in the absence of this gene, nSMase2 activity in liver and brain was decreased. In the absence of both *SMPD3* and *SMPD2* genes, i.e. in the absence of nSMase2 and nSMase1, all neutral SMase activity was disrupted [7].

Human nSmase2 shares sequence identity about 90% with mouse nSMase2 [7]. Even though there are multiple nSMase types, the studies conducted on nSMase2-deficient mice demonstrated that majority of the nSMase activity is abolished in many organs due to the disruption of nSMase2. Hence, nSMase2 is a crucial nSMase. In addition to decreasing nSMase activity, nSMase2 knockout animals were reported to have lower levels of growth hormone [13]. Being the most prominent mammalian nSMase, nSMase2 is a key mediator of cellular stress-induced ceramide production [4]. Hence it is involved in the ceramide-mediated cell regulation such as the regulation processes of cytokine signaling, toxic agents and stress. Ceramide is crucial for cell regulatory pathways including cell growth, differentiation and apoptosis [14].

In the mouse model of osteogenesis and dentinogensis imperfecta (the *fro/fro* mouse), a partial deletion of intron 8 and exon 9 in *SMPD3* gene was observed. This mutation was found to be corresponding to the deletion of 33 amino acids from C-terminal of nSMase2. This region includes the critical catalytic residues Asp638 and His639. This indicates that nSMase2 inactivity might be one of the reasons for the phenotype of *fro/fro* mouse [13]. The mouse model studies showed that nSMase2 has a role in bone maturation during development [15].

nSMase2 is abundantly found in the plasma membrane, particularly in the inner leaflet of the plasma membrane (PM). nSMase2's natural substrate, sphingomyelin is initially generated in the Golgi compartment by SM synthases (SMSs); SMS1 and SMS2 from ceramide and phosphocholine, and then through vesicular transport, it is delivered to the PM. The cellular level of SM is regulated by many enzymes including sSMase, SMS2 and nSMase2. In addition to the regulation of SM and ceramide levels at the PM, SM and ceramide can also be converted into other bioactive sphingolipids including sphingosine and S1P by these enzymes, if necessary. It is known that ceramide is a precursor molecule to other signaling lipids. Hence at the PM, SMS and SMase activities regulate signal transduction by modulating ceramide levels [5].

2.3. nSMase2 in the Inflammatory Pathway

Inflammation is a critical immune response against harmful stimuli such as infection or injury, and it enables survival and maintains tissue homeostasis. Inflammatory response has been divided into four groups by Medzhitov: inducers, sensors, mediators and target tissues. Inducers such as infection or tissue damage initiate the inflammatory pathway, and they are sensed by sensors including Toll-like receptors (TLRs) expressed on mast cells, dendritic cells and macrophages. These TLRs trigger mediators such as cytokines (e.g. tumor necrosis factor (TNF), interleukin (IL), interferon (IFN)). Consecutively, these mediators act on the target tissues to change their functional states to enable survival [16].

Both SMS2 and nSMase2 are involved in development, cell death and inflammatory signaling pathways, and SM and ceramide concentrations at the PM are critical for cellular signaling [5, 13]. nSMase2 was reported to be involved in inflammation in response to pro-inflammatory cytokine; interleukin 1-beta (IL-1β). When nSMase2 is induced by IL-1β, nSMase2 amplifies the IL-1β signaling pathway by inducing ceramide-activated protein phosphatase 2 (PP2A) which hinders the phosphorylation and ubiquitination of interleukin-1 receptor activated kinases (IRAK-1) that are the key mediators in the signaling pathways of TLRs/IL-1Rs (Toll-like receptors/IL-1 receptors) [5, 17, 18].

Increased sensitivity to IL-1β in aging rats suggested that nSMase2 activity is a key contributor to IL-1β hypersensitivity. In this study which was conducted on the aging rats, it was observed that the activity of nSMase2 increased even though the expression levels of IL-1β receptor and IRAK-1 were not significantly different from that of the young rats [13,19]. Oxidative stress was noted to increase nSMase2 activity due to a decrease in hepatic glutathione (GSH) content during aging to regulate the hepatic response to IL-1β [5, 20].

nSMase2 was reported to be a TNF-α-responsive enzyme. The stimulation of nSMase2 with TNF-α was found to enhance PM localization and increase the activity of nSMase2 [13]. nSMase2 induced by TNF-α was reported to play a role in vascular inflammatory responses including the expression of vascular cell adhesion molecule (VCAM) and intracellular adhesion molecule (ICAM) in lung epithelial cells [5, 21]. In addition to TNF-α, PMA (phorbyl 12-myristate 13-acetate), H2O2 and cell confluence were noted to stimulate the translocation of nSMase2 from Golgi to PM, and increase the activity of nSMase2. This translocation is important for the activity of nSMase2 since it may control access to SM, activate anionic phospholipids (APLs), and regulate other mechanisms related to nSMase2 activity [4].

nSMase2 has been suggested to have a role in lung injury mediated by ceramides. An increase in nSMase2 activity was seen due to the oxidants present in cigarette

smoke and hydrogen peroxide. Increased ceramide levels due to nSMase2 activity caused increased apoptosis in rodent's bronchial epithelial cells and lung tissues [4].

nSMase/ceramide pathway has also been associated with some neurodegenerative diseases, especially with Alzheimer's disease (AD). Amyloid-β peptide, which is toxic to neurons and oligodendrocytes, was reported to contribute to the pathogenesis of AD. It has been suggested that the increased activity of nSMases was associated with the amyloid-β peptide cytotoxicity since several studies showed that the cultured neuronal cells treated with amyloid-β peptide increased nSMase activity, and the various inhibitors of nSMases including GW4869 abated the cytotoxic effects of amyloid-β peptide [13]. Decrease in exosome-mediated amyloid plaque formation by GW4869 suggests that nSMase2 may be a potential therapeutic target for AD [1, 13, 22]. With the induction of pro-inflammatory cytokines including IL-1β and TNF-α by amyloid-β peptide-activated astrocytes and microglia, nSMase2 was induced to generate ceramide which can result in apoptosis. Hence chronic neuroinflammation seen with AD progression may also be reduced by inhibiting nSMase2 [22].

2.4. *Bacillus cereus* Sphingomyelinase

Bacillus cereus sphingomyelinases (*Bc*-SMases) are Mg^{2+}-dependent neutral SMases; hence SM hydrolysis is conducted in a water-bridged divalent metal ion-dependent manner in *Bc*-SMase [2,6]. *Bc*-SMase is a homologue of mammalian nSMase, suggesting that it can be a good model for mammalian nSMase [2]. As an extracellular soluble toxin, this enzyme shows hemolytic activity against SM-rich erythrocytes in mammals [6]. Apart from its hemolytic activity, it also exhibits hydrolytic and phospholipase C activities [2].

Bc-SMase was suggested to be activated by Mg^{2+}, Mn^{2+} and Co^{2+} cations, but inhibited by Ca^{2+}, Cu^{2+} and Zn^{2+} [6]. In another study, it was stated that Mg^{2+}, Mn^{2+} or Co^{2+} bound *Bc*-SMase showed high catalytic activity, whereas Ca^{2+} or Sr^{2+} bound *Bc*-SMase showed lower catalytic activity. Mg^{2+} and additional Ca^{2+} ions are required

for the hydrolytic and hemolytic activities, respectively [2,6,23]. Asn16, Glu53, His151, Asp195, Asn197, Asp253, Asp295 and His296 are important residues involved in divalent metal ion binding at the active site of *Bc*-SMase [1, 2, 6, 23], and except for Asn16 which was Val in mammalian nSMases, all of these residues were stated as the conserved residues in both bacterial and mammalian nSMases [2]. However, Airola *et al.* has recently noted that Asn16 in *Bc*-SMase was also conserved in mammalian nSMases and it corresponded to Asn130 in human nSMase2 [1]. Taken together, a common catalytic mechanism exists for these organisms [2, 6, 23].

Ago *et al.* and Obama *et al.* carried out several studies on mutant *Bc*-SMases. E53A and E53Q mutations interrupted the hemolytic and SM-hydrolyzing activities. E53D mutation partially decreased the activity of the enzyme. Hemolytic activity of this latter mutant was decreased to less than 40% in comparison with the wild type enzyme. E53D mutation led to a decrease in the binding affinity of Mg^{2+} suggesting that Glu53 was an essential amino acid for Mg^{2+} binding [2, 6]. E53D did not affect the binding of Ca^{2+}, Cu^{2+} and Zn^{2+} [6].

H296F, H296Y and H296A mutations listed for His296, as well as all of the mutations listed for His151 (H151A, H151F, H151R, H151K, H151Y, H151D, H151E, H151N) interrupted both hemolytic activity and hydrolytic activity suggesting that His296 acted as a general base in catalysis. Asp195 mutations (D195E, D195N and D195A) showed that Asp195 was important for hemolytic activity [23].

Bc-SMase, like nSMase2, has a similar fold to bovine pancreatic DNase I. Even though their substrates are different, SM for SMase and DNA for DNase I, their catalytic mechanism is similar; i.e. they both catalyze the hydrolysis of phosphodiester bonds of their substrates in a Mg^{2+}-dependent manner. Hence they share structural and catalytic similarity with each other [23]. However, SMase has a hydrophobic β-hairpin structure unlike DNase I. This β-hairpin structure, which is between Trp279 and Tyr290, was suggested to be critical for the attachment of *Bc*-SMase to the cell surface during hemolytic activity by Ago *et al.* (see Figure 2.2). Trp284 and Phe285

are at the apex of this structure. W284A and F285A mutants exhibited lower liposome disruption activity, lower catalytic activity and lower hemolytic activity compared to the wild-type *Bc*-SMase [2]. This β-hairpin structure is absent in human nSMase2, but was suggested to be replaced by N-terminal domain (NTD) and palmitoylation sites present in the catalytic domain of nSMase2 [1].

There are four *Bc*-SMase crystal structures available in Protein Data Bank [24]; 2DDS, 2UYR, 2DDR and 2DDT. 2DDS is the sphingomyelinase structure with cobalt ion. 2UYR is the mutant sphingomyelinase structure (N57A). 2DDR is the sphingomyelinase structure with calcium ion. 2DDT is the sphingomyelinase structure with magnesium ion. The calcium-bound *Bc*-SMase was stated as the inhibited one, whereas the cobalt-bound and magnesium-bound ones were reported as active [3]. The missing residues on these crystal structures are tabulated in Table 2.1. The crystal structure 2DDT is missing the DK Switch loop residues; Gly124-Asp126. These *Bc*-SMase structures all have a β-sandwich topology and are composed of α/β elements [2] (see Figure 2.2).

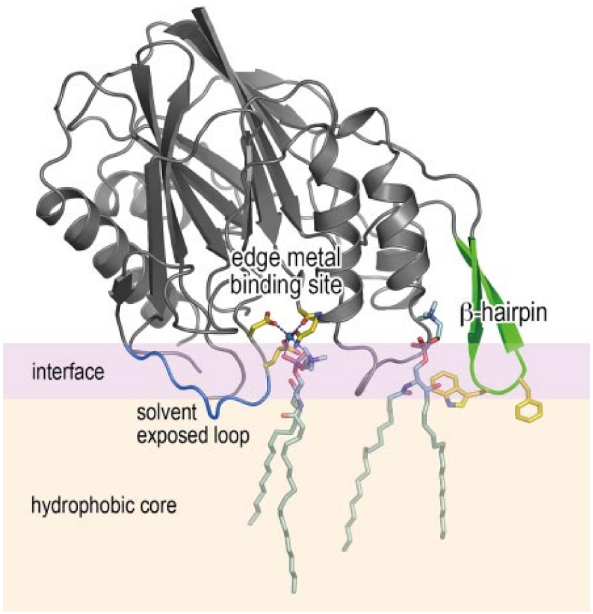

Figure 2.2. Model of *Bc*-SMase with β-hairpin structure attached to the PM [2]. SM (with its long acyl chains embedded in the PM) binding of *Bc*-SMase is also shown.

Missing residues on the crystal structures of *Bc*-SMases and human nSMase2 along with the residues interacting with the metals bound these crystal structures are tabulated in Table 2.1. Metals bound to Chain As of 2DDS and 2DDT and to Chain C of 2DDR along with the residues interacting with these metal ions are tabulated in Table 2.1. 5UVG is the crystal structure of the catalytic domain of human nSMase2 and the NTD residues; 1-115 and 175-335 are also missing.

The conserved residues between *Bc*-SMases and human nSMase2 are listed in Table 2.2. The active site residues are indicated by asterisks.

2.5. Primary Structure of Human nSMase2

nSMases are integral membrane proteins in mammals, whereas they are soluble proteins in bacteria. nSMase2 in mammals requires Mg^{2+} or Mn^{2+} for its activity. This enzyme is present in mammalian tissues, but shows the highest activity in brain [8]. Most nSMases, from bacteria to mammals, have a DNase I-type catalytic core [1, 4]. This suggests that most nSMases (excluding nSMase3) hydrolyze sphingomyelin through a common catalytic mechanism [4]. Eight metal-binding residues define the active site of nSMases, which are Asn130, Glu364, His461, Asp510, Asn512, Asp607, Asp638 and His639 for nSMase2 [1]. There are also highly conserved residues near the active site that are suggested to be important for the catalytic activity [4].

Human nSMase2 consists of two domains; a two-segment hydrophobic NTD which binds nSMase2 to the membrane and a C-terminal domain (CTD) which contains the catalytic domain as seen in Figure 2.3. The hydrophobic domain that consists of two putative helical segments (HS1 and HS2) helps bind the catalytic domain of nSMase2 to the membrane [4]. Catalytic region on nSMase2 faces the inner leaflet of the PM where sphingomyelin is hydrolyzed [14]. This domain was suggested to share a similar fold with DNase I superfamily of enzymes [1].

Table 2.1. Missing residues and metal binding residues in the *Bc*-SMase and human nSMase2 crystal structures.

PDB ID	**Missing Residues**	**Metal**	**Interacting Residues and Water Molecules**
2UYR	**Chain X:** Glu1-Gln6, Lys306	Mg(1306)	Glu53, HOH2083, HOH2009, HOH2010, HOH2084, HOH2086
2DDS	**Chain A:** Glu1-Gln6, Lys306 **Chain B:** Glu1-Gln6, Gly124-Asn127, Asp156-Thr162, Lys306 **Chain C:** Glu1-Asn7, Lys306 **Chain D:** Glu1-Gln6, Gly124-Asp126, Met158-Thr162, Lys306	Co(1117)	Glu53, HOH1141, HOH1138, HOH1144, HOH1130
		Co(1121)	Phe55, Asn57, Glu99, Asp100, HOH1168, HOH1159
		Co(1127)	His296, HOH1164, HOH1130
2DDT	**Chain A:** Glu1-Asn7, Gly124-Asp126, Asp156-Thr162, Lys306 **Chain B:** Glu1-Asn7, Gly124-Asn127, Asp156-Thr162, Lys306	Mg(310)	Glu53, HOH322, HOH352, HOH367, HOH326, HOH384
		Mg(311)	Phe55, Asn57, Glu99, Asp100, HOH330, HOH372
2DDR	**Chain A:** Glu1-Gln6, Gly124-Asn127, Asp156-Thr162, Lys306 **Chain B:** Glu1-Gln6, Gly124-Asp126, Asp156-Thr162, Lys306 **Chain C:** Glu1-Asn7, Lys306 **Chain D:** Glu1-Asn7, Lys306	Ca(1328)	Phe55, Asn57, Glu99, Asp100, HOH1337, HOH1332
		Ca(1329)	Glu53, HOH1390, HOH1341, HOH1397, HOH1464
5UVG	**Chain A:** Ser116-Pro120, Cys394-Lys401, Ser493-Asn497, Gly556-Glu560, Asp561	Ca(701)	Glu364, HOH873, HOH869, HOH906

Table 2.2. Conserved residues between *Bc*-SMase and human nSMase2 [1].

nSMase2	**Residue**	***Bc*-SMase**		**nSMase2**	**Residue**	***Bc*-SMase**
130	N*	16		461	H*	151
150	R	33		472	R	168
358	D	47		475	Q	171
364	E*	53		509	G	194
374	L	63		510	D*	195
406	G	102		512	N*	197
411	S	107		607	D*	253
414	P	110		608	Y	254
430	D*	126		638	D*	295
435	K*	131		639	H*	296

Between the two domains, serine phosphorylation sites (Pi) and a calcineurin-binding site have been identified [4]. The binding site for serine/threonine phosphatase Calcineurin (protein phosphatase 2B) was found to be a motif, PQIKIY (residues 165-170), located between NTD and CTD. Calcineurin was suggested to regulate nSMase2 activity by dephosphorylating nSMase2 [7, 25]. A mutant nSMase2 lacking the calcineurin binding site was observed to have an elevated level of phosphorylation and an increased activity compared to the wild type nSMase2. During oxidative stress, both the phosphorylation and activity of nSMase2 were increased, whereas the calcineurin activity was hindered [25]. The phosphoserine site of nSMase2 (Ser173, Ser209, Ser291, Ser294 and Ser301) is near this calcineurin binding site and needed for full nSMase2 activity [1, 7].

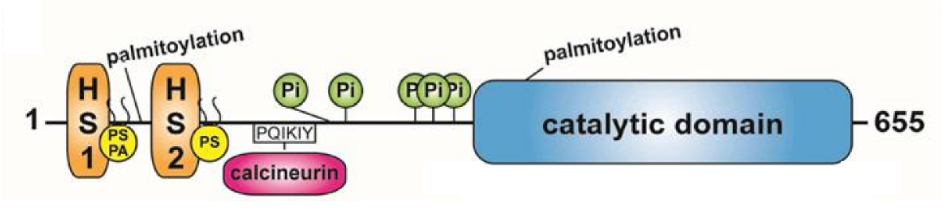

Figure 2.3. Predicted topology of human nSMase2 [7].

nSMase2 has two palmitoylation sites; one is at the beginning of the catalytic site (Cys397 and Cys398 [26, 27], the other one is between the putative two-segment hydrophobic NTD (Cys53, Cys54, Cys59) [5, 7]. The covalent lipid modification of the side chain of cysteine residue with palmitate is known as S-palmitoylation, and it is important for regulation of protein subcellular localization, trafficking, stability and translocation to lipid rafts [28]. These palmitoylation sites within nSMase2 were suggested to be crucial for membrane association, PM localization and protein stability [4, 5, 13].

nSMase2 is activated by anionic phospholipid (APL) phosphatidylserine (PS), which is located abundantly in the inner leaflet of the PM, and unsaturated fatty acids in vitro [1, 5, 7]. nSMase2 has low basal SMase activity in vitro and needs APLs for activation [4]. APL-binding domain was found to be localized in the NTD at two different positively charged regions; at the first site, both PS and phosphatidic acid (PA) bind Arg33 and the amino acids located between 45 and 48, whereas at the second site, PS and Arg92-Arg93 are selectively bound [7]. These three conserved Arg residues are required for APL binding, APL-mediated activation, and correct nSMase2 trafficking [4].

2.6. Crystal Structure of Human nSMase2

Understanding the structure and mechanism that regulates the activity of nSMase2 is very important for deciphering the underlying mechanisms of various diseases including Alzheimer's disease and cancer, and the development of new therapeutic options [1, 7]. Until recently, the structure and catalytic mechanism for nSMase2 were analyzed by examining related bacterial SMases [7]. However, the discovery of the crystal structure of the human nSMase2 catalytic domain (PDB ID: 5UVG, see Figure 2.4) by Hannun's group has provided valuable information on the shared and different characteristics of nSMases [1].

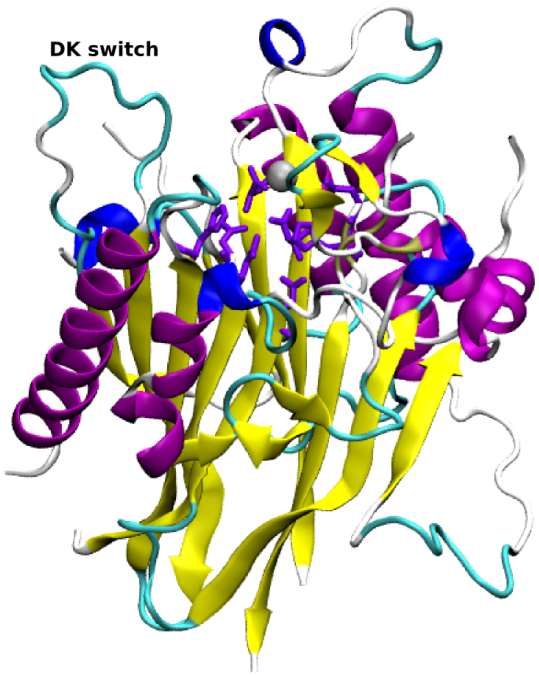

Figure 2.4. Crystal structure of human nSMase2 (PDB ID: 5UVG). Active site residues and calcium ion are shown in violet licorice and gray vdW forms, respectively.

SMases of several pathogenic bacteria, including that of *Bacillus cereus* and *Staphylococcus aureus*, are homologous to mammalian nSMases [2, 12]. Similar metal ion dependence-manner and considerable sequence identity between *Bc*-SMase and human nSMase2, which is 24% according to BLAST analysis [29], suggest that a similar hydrolytic mechanism may exist between these enzymes [2]. Even though the sequence identity is low and the structure of their active site pockets are different (bowl-like cavity in human nSMase2, whereas lipid-like contoured active site in bacterial SMase) [1], they share a similar protein fold and catalytic mechanism due to their similar metal ion dependence and common conserved active site residues [1, 2, 7, 12].

The construct used for determining the crystal structure of the human nSMase2 catalytic domain (PDB ID: 5UVG) contains the residues between 119 and 174 and between 340 and 651; i.e. the residues between 175 and 339, or namely the insertion (*Ins*) region, are missing (*Δ175-339* or *ΔIns*). *ΔIns* region contains regulatory elements including serine/threonine phosphatase Calcineurin binding and phosphoserine

sites. Airola *et al.* noted that while *ΔIns* region regulated the function of nSMase2, it was not crucial for its activity [1]. In addition to *ΔIns* region, the crystal structure of human nSMase2 (5UVG) is missing NTD and the following residues; Ser116-Pro120, Cys394-Lys401, Ser493-Asn497 and Gly556-Glu560. Among these missing residues is the palmitoylation site containing Cys397 and Cys398.

In 5UVG, the active site pocket contains Ca^{2+} ion instead of a Mg^{2+} ion possibly due to the exogenous calcium ions present in the crystallization conditions [1]. The β-sandwich core of the active site contains the highly conserved residues; Asn130, Glu364, His461, Asp510, Asn512, Asp607, Asp638 and His639. These highly conserved residues and the metal ion presence at the active site indicate that mammalian and bacterial nSMases share similar catalytic mechanisms [1].

Airola *et al.* suggested that the catalytic domain of nSMase2 is activated by the membrane-associated NTD, and this interaction and activation is regulated by a conserved flexible catalytic motif which they named as DK switch (Asp430-Lys435). This highly conserved region was reported to have different conformations; loop or helical conformations, in *Bc*-SMase (Asp126-Lys131) and human nSMase2 structures [1]. These conformational differences of the DK Switch loop regions are shown in Figure 2.5. In the crystal structure of human nSMase2, DK switch is an extended loop, the residue Asp430 faces away from the active site, and the entrance of the hydrophobic groove is blocked. In the crystal structure of *Bc*-SMase, the DK switch is a loop with the residue Asp126 being directed away from the active site (PDB ID: 2DDS), or it is a short α-helix with Asp126 facing the active site and forming a salt bridge with Lys131 (PDB ID: 2UYR). The reason for these conformational differences in the DK switch regions of *Bc*-SMase is unclear [1].

The helical conformation of DK switch where the residue Asp could participate in catalysis was proposed to be the active state of neutral sphingomyelinases. This helical conformation is seen in one of the *Bc*-SMase structures; 2UYR (see Figure 2.5). The active state of nSMase2 was suggested to have a helical DK switch conformation [1]

as seen in one of the *Bc*-SMase structures; 2UYR. The other crystal structures do not have a helical DK switch conformation hence they might be in 'inactive' state. Airola *et al.* also mentioned that the DK Switch regions might be affected by the crystal contacts [1]. The non-competitive inhibitor, GW4869 was also suggested to inhibit nSMase2 activity by targeting DK switch [1].

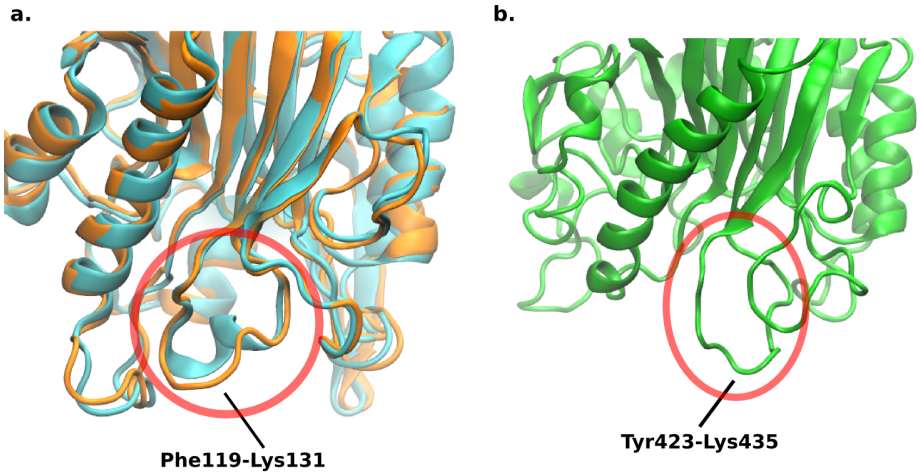

Figure 2.5. DK switch loops of the crystal structures of inactive (PDB ID: 2DDS, orange) and active (PDB ID : 2UYR, cyan) *Bc*-SMases (a) and inactive human nSMase2 (PDB ID: 5UVG, green) (b). DK Switch regions are indicated by red circles.

Juxtamembrane (JX) region of NTD was suggested to be required for inter-domain interactions and enhancing nSMase2 activity by affecting DK Switch to attain an active conformation [1]. However, this region is absent in the crystal structure.

The aforementioned important residues for stability and activation of nSMase2 and their presence in the crystal structure of human nSMase2, 5UVG are tabulated in Table 2.3.

The number and type of the metal ions in the active site of the crystal structures of *Bc*-SMases and human nSMase can vary. The inactive form of *Bc*-SMase has two cobalt ions in the active site (bound to Glu53 and His296) while the active form of *Bc*-SMase and the human nSMase2 each have a single magnesium ion (bound to Glu53)

Table 2.3. Important residues for nSMase2 stability and activity.

Site	Residues	Presence in Crystal Structure
Active Site [1]	N130, E364, H461, D510, N512, D607, D638, D639	Present
Phosphoserine Site [7]	S173, S209, S291, S294, S301	Absent
Calcineurine Site [7]	P165-K170 (PQIKIY motif)	Absent
Palmitoylation Site 1 [7]	C53, C54, C59	Absent
Palmitoylation Site 2 [26,27]	C397, C398	Absent
APL Binding Site [7]	R33, R92, R93	Absent
DK Switch [1]	D430, K435	Present

and calcium ion (bound to Glu364), respectively. Ago *et al.* proposed that the water molecule activated by the metal ion bound to His296 and the side chains of Asp195 and Asn197 in *Bc*-SMase acts as a nucleophile and attacks the phosphate moiety of SM to form a pentavalent phosphorus. This, in turn, facilitates the hydrolysis of SM due to increasing negative charge on the oxygens of this pentavalent phosphorus (see Figure 2.6) [2]. Mg^{2+} ion at the active site was suggested to bind and stabilize the phosphodiester bond of SM [1].

Airola *et al.* suggested that nSMases extract SM partially from the PM to hydrolyze it since they observed that the aliphatic chains of SM were not fully enclosed by bacterial SMases when SM was placed at the active site. The same group also suggested that human nSMase2 needed to undergo some conformational changes to accommodate SM [1].

Table 2.4 shows the residues on *Bc*-SMase that might interact with SM. The interacting residues for 2DDS were proposed by Ago *et al.* [2], and the interacting residues tabulated for 2DDR were the docking results of Sergelius *et al.* [30].

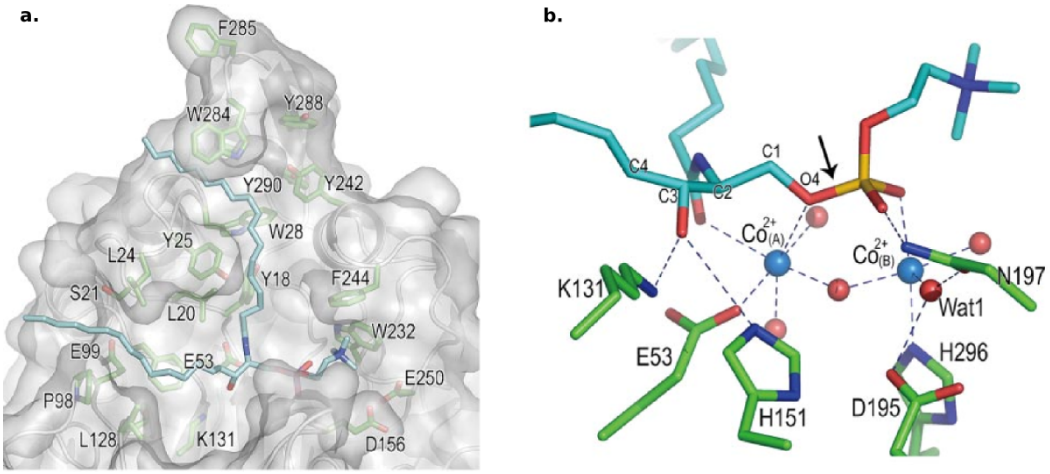

Figure 2.6. Proposed SM binding mode to *Bc*-SMase (2DDS) [2]. (a) Binding pocket of SM. (b) Residues interacting with SM. The activated water is named as Wat1.

A similar catalytic mechanism has been suggested for aSMases by Gorelik *et al.* [31]; the hydrolysis of SM is facilitated by a nucleophilic attack on the phosphate group of SM by a water molecule activated by a zinc ion and protonation of the ceramide by a histidine residue present at the active site with the help of an aspartic acid residue [31].

Table 2.4. *Bc*-SMase residues interacting with SM.

Structure	**Interacting Residues**
***Bc*-SMase (2DDS) [2]**	K131, H151, N197, Co1127, Co1117
***Bc*-SMase (2DDR) [30]**	E53, K131, N156, Mg^{2+}

2.7. Natural Substrate of Bacterial and Human Neutral Sphingomyelinases: Sphingomyelin

SM consists of a phosphocholine-head group and a ceramide, a central hub in the sphingolipid network [5, 30]. The acyl chain length of sphingolipids is believed to be tissue- and cell-specific [32]. Sphingomyelin species in cell membranes can have different length of acyl chains with C16 (see Figure 2.7), C18 and C24 being the dominant ones [33, 34]. The role of SM in cell apoptosis, migration and proliferation

and its involvement in various disorders including cancer suggests that the enzymes that regulate SM levels can be potential therapeutic targets [35]. The formation of SM is catalyzed by SMS1 and SMS2 in the Golgi compartment, and by SMS2 in the plasma membrane [30]. SM can be hydrolyzed to generate ceramide by acid, neutral and alkaline SMases. SM levels can be regulated in lysosomes, cell membranes and intestinal cells by aSMase, nSMase2 and alkaline SMase, respectively [30].

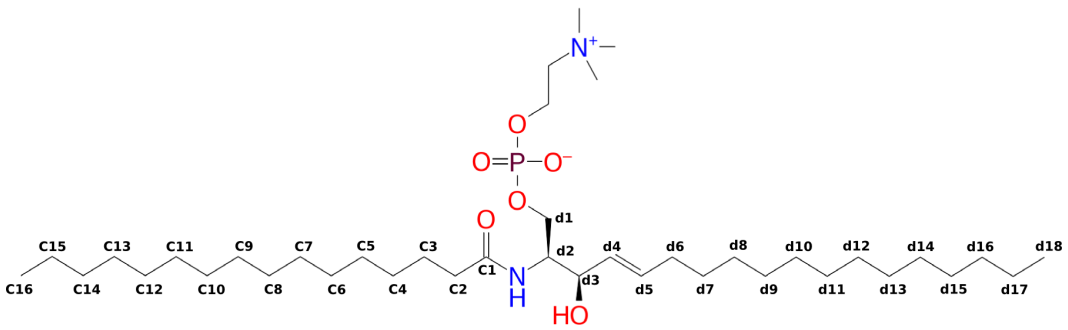

Figure 2.7. d18:1C16-SM (C16-SM) structure with its carbons cropped labeled.

SM is the natural substrate of SMases which hydrolyze this substrate to produce ceramide and phosphocholine. Many cell membranes contain SM predominantly in their outer leaflet. The SM content in mammalian tissues is about 2-15% of the total organ phospholipid, however, depending on the localization of the tissue such as in the case of brain tissues, this content can be even higher [32]. SMs, along with other sphingolipids and sterols including cholesterol, have been suggested to constitute the dynamic lateral membrane rafts, also called lipid rafts, in membranes [30, 36]. The asymmetric structure of SM with long acyl chains as well as its highly saturated structure are thought to be essential for its role in the formation of lipid rafts. SM has potential to form several hydrogen bonds with a receptor [32]. Hence the morphology of SM is highly important when forming interactions with other lipids and membrane proteins, and also in lipid raft formation [30]. Lipid rafts play important roles in signal transduction and other cellular processes [5]. The lipid phase order and the fluidity of membrane can be highly affected by the molecular structures of sphingolipids [36].

The role of lipid rafts in signal transduction at the PM and the sphingomyelin content in these rafts indicate that both SMS and SMases seem to be involved in the regulation of receptor-induced cell apoptosis and inflammatory signaling pathways [5].

A docking simulation conducted on SM binding to *Bc*-SMase (2DDR [2] with calcium ion replaced by magnesium) by Sergelius *et al.* showed that SM formed hydrogen bonds with Glu53 (with 3OH group of SM), Lys131 (with carbonyl oxygen of SM) and Asp156 (with 2NH group of SM) and its 3OH group was coordinated by Mg^{2+} ion (see Figure 2.8) [30]. The hydrogen bonds between Lys131 and carbonyl oxygen of SM and between Asp156 and 2NH group of SM have been suggested to be important for keeping SM in a proper location at the active site during catalysis so that catalysis can occur efficiently. Their MD simulation results also showed that the loops; Val118-Gly132 and Thr150-Pro164 adjusted their conformations to facilitate the interaction between Asp156 and 2NH group of SM which was believed to be important for efficient catalysis [30].

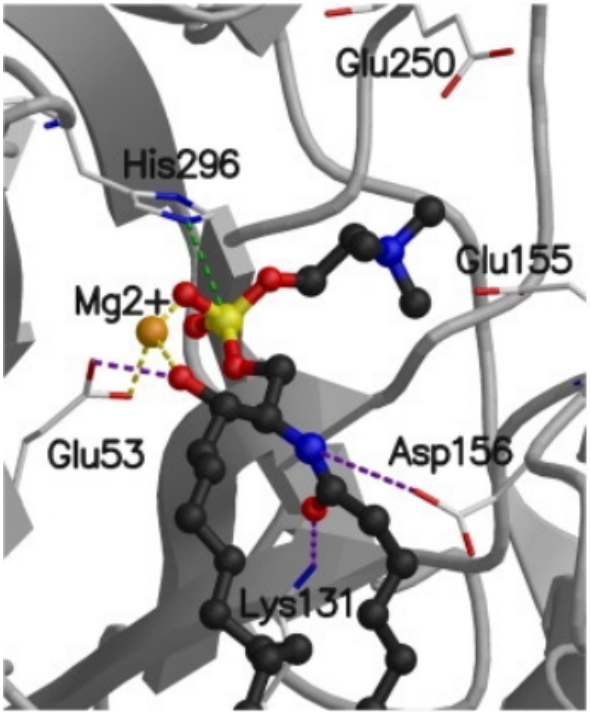

Figure 2.8. *Bc*-SMase-SM complex structure proposed by Sergelius *et al.* [31]. The hydrogen bonds and metal coordination are shown with purple and yellow lines [31].

As stated before, *Bc*-SMase has been suggested as a homologue of mammalian nSMase due to their similar catalytic mechanisms. They both hydrolyze sphingomyelin in a divalent metal ion-dependent manner [2]. Although bacteria cannot generate sphingolipids by themselves, some of them are able to produce proteins with activities that are similar to that of nSMases. These proteins are secretory proteins which exploit host cell lipids [5].

2.8. nSMase2 Inhibitors

The non-competitive nSMase2 inhibitor, GW4869, has been suggested to inhibit nSMase2 by hindering APL activation [4, 7]. GW4869 is a specific inhibitor for nSMase2 with an IC50 of 1 μM. Scyphostatin and Manumycin A were also reported as inhibitors for nSMase2 [15]. Scyphostatin was also reported to inhibit aSMase at higher IC50 values [7]. Among these inhibitors, GW4869 is the most widely studied one for investigating the nSMase2 specific functions and the role of nSMase2 in cellular response and physiological function [7, 13].

3. METHODS

The crystal structures for *Bc*-SMases (PDB IDs: 2UYR and 2DDS [2]) and human nSMase2 (PDB ID: 5UVG [1]) were retrieved from Protein Data Bank (PDB) [24]. Prior to docking and molecular dynamics (MD) simulations, the protein structures and ligands were prepared, and then, these ligands were docked to the possible binding sites on the prepared target proteins. The programs that were integrated within the software Schrödinger Suite's interface, Maestro [37] including Protein Preparation Wizard [38–40], LigPrep [41], SiteMap [42–44], Induced Fit Docking [45–48] and Desmond [49, 50] were utilized for protein preparation, ligand preparation, binding site determination, docking and MD simulations, respectively. These steps were crucial for the analysis of the protein and protein-ligand interactions from a structural and dynamical point of view.

3.1. Protein Preparation

A complete starting structure is crucial when performing simulations. However, the X-ray crystal structures of the proteins may have missing residues, missing hydrogen atoms, steric clashes, incorrect charge states or orientations, and so on, even when their resolution is high. These problems can lead to incorrect or incomplete simulation outputs. To obtain more reliable results from the simulations, the protein structures are required to be prepared and corrected from their structural defects [38,39]. For this purpose, Protein Preparation Wizard (PPW) [38–40] in Schrödinger's Suite was utilized to prepare the protein structures; 2DDS, 2UYR and 5UVG which were retrieved from the RCSB PDB [24].

5UVG and 2UYR are monomers while 2DDS is a quadromer that consists of four identical chains. For computational efficiency, all chains except for Chain A were deleted from 2DDS structure. When selecting the chain, the missing residues presented

in Table 2.1 were taken into account since Chain B and Chain D had more missing residues than Chain A and Chain C, they were automatically eliminated.

The crystal structures were prepared according to the three main steps determined by PPW. In the first step, hydrogens were added, disulfide bonds were created and the missing side chains and loops were filled in by using Prime [51]. The missing residues that were filled by PPW are tabulated in Table 3.1. When Table 2.1 and Table 3.1 are compared, it can be seen that not all the missing residues were filled. Generally, the software cannot fill in the missing residues at the beginning and end of the chain. However, since the start and end of the chains of the nSMase structures are not relevant to the catalytic activity, these missing residues part can be disregarded.

Table 3.1. Missing residues filled in by PPW.

PDB ID	**Missing Residues Filled**
2DDS (Chain A)	-
2UYR	-
5UVG	Cys394-Lys401, Ser493-Asn497, Gly556-Glu560, Asp561

Two sets of protein were prepared. In the first set, the waters beyond 5 Å from the het groups (metal ions) were deleted. Since the water molecules around the metal ions are important for the catalytic activity of nSMases, water molecules within 5 Å of the metal ions were not deleted for all three structures. In the second set, only the water molecules bound to metal ion were kept; i.e. the other water molecules were all deleted. The water molecules not deleted in these two protein sets are tabulated in Table 3.2.

In the second step of PPW, the possible states of the metal ions present in the crystal structures were generated within a pH range of 7.2±0.5. The original states were selected for all the metal ions.

In the final step, the protein structures were optimized and minimized. The optimization of the hydrogen-bonding network was performed by reorienting hydroxyl and thiol groups and water molecules, and determining the protonation states of the residues; histidine, aspartic acid and glutamic acid according to the optimum pH value which was 7.5 for nSMases [1]. After optimization, a minimization step was run to relieve the strain on the processed protein structures by allowing hydrogen atoms to be refined and converging heavy atoms to an RMSD about 0.30 Å. OPLS2005 was utilized during minimization process.

Table 3.2. Water molecules around the metal ion.

PDB ID	**Metals**	**Only Metal Bound Water Kept**	**Only Water within 5 Å of Metal Ion Kept**
2UYR	Mg1306	HOH2009, HOH2010, HOH2083, HOH2084, HOH2086	HOH2002, HOH2009, HOH2010, HOH2017, HOH2026, HOH2032, HOH2035, HOH2048, HOH2083, HOH2084, HOH2086
2DDS	Co(1117)	HOH1141, HOH1138, HOH1144, HOH1130	HOH1130, HOH1135, HOH1138, HOH1141, HOH1144, HOH1164, HOH1183, HOH1209, HOH1229, HOH1392, HOH1400, HOH1406, HOH1407
	Co(1121)	HOH1168, HOH1159	
	Co(1127)	HOH1164, HOH1130	
5UVG	Ca701	HOH869, HOH873, HOH906	HOH807, HOH869, HOH873, HOH906

3.2. Ligand Preparation

Many databases generally contain 2D structures of the ligands that should be converted into their 3D conformations prior to any computational simulations including molecular docking. Hence accurate 3D models of the ligands should be generated to obtain reliable results from the simulations [41].

The 2D structures of the ligands; d18:1C16-SM (C16-SM) and GW4869 were retrieved from PubChem under the PubChem CIDs of 9939941 [52] and 16078967 [53], respectively. These structures were converted to their 3D conformations by using Lig-

Prep [41] in Schrödinger Suite. Prior to the ligand preparation, C16-SM was cropped and several cropped SM structures (from C3 to C16 in fatty acid tail and d5 to d18 in sphingosine backbone) were prepared. As stated before, C16-SM has a long hydrophobic tail which was embedded in PM, and C16-SM was possibly partially extracted from PM by nSMases [1]. Hence C16-SM was cropped from both of its tails and several cropped SM structures (lengths of both tail ends varied between C3 and C16, and d5 and d18) were prepared (see Figure 2.7) to test to what extent C16-SM was extracted from PM by nSMase2. The cropping was stopped at C3 and d5 from the tails to preserve the head group of SM. This cropping procedure was not performed on GW4869.

After retrieving the 2D structures from PubChem and cropping C16-SM, LigPrep was utilized to prepare the structures for molecular docking simulations. Hydrogen atoms were added. 'Desalt' option was chosen to remove the two hydrogen chloride molecules from the GW4869 inhibitor structure. No possible tautomer structure was available for SM and GW4869. Only one low energy ring conformation generation per ligand was selected.

The possible ionization states at a target pH range of 7.0±2.0 were generated by using Epik [54–56] in LigPrep [41]. 'Add metal binding states' option was also taken into account when generating the possible states because *Bc*-SMases and nSMase2 are metalloproteins with Co^{2+}, Mg^{2+} and Ca^{2+} in their active sites. These metal ions occupied a space in the active site, hence generating the metal binding sites could be important for the ligand to fit into the active site [41]. Only one state was generated for each cropped SM ligand while three states were generated for GW4869 with two of them being the metal binding states (see Figure 3.1). The metal binding states of TC, CT and CC isomers of GW4869 are not shown in Figure 3.1. Finally, the geometries of the generated ligand structures were optimized with a force field of OPLS2005 [41].

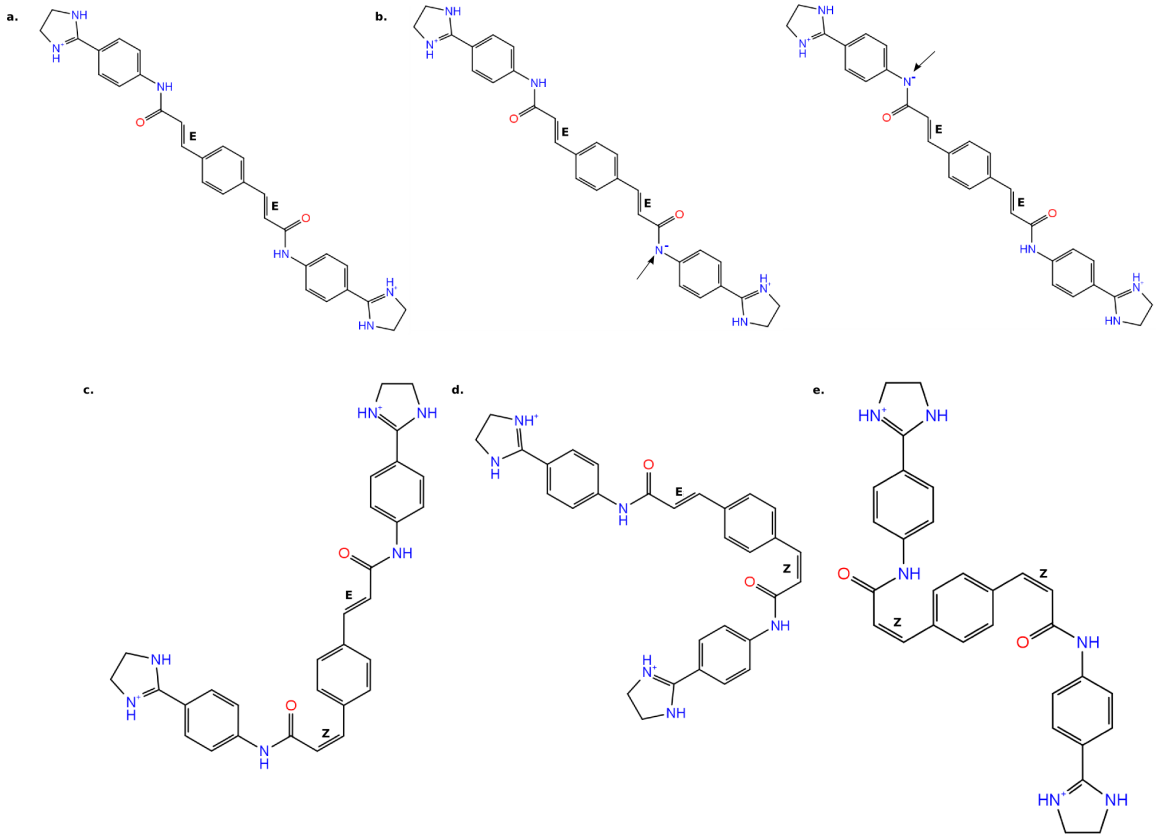

Figure 3.1. 2D structure of trans-trans (TT) GW4869 (a) along with its metal binding states (b) and GW4869 isomers; (c) trans-cis (TC), (d) cis-trans (CT) and (e) cis-cis (CC). The deprotonated regions of the metal binding states are shown with an arrow.

3.3. Induced Fit Docking

Molecular docking simulations are widely used to identify new possible ligands for a target protein and determine the binding modes and binding affinities between these ligands and the target protein [57]. The ligand bound to the protein can induce conformational changes in the active site of the protein so that the ligand can fit into the protein. This is also known as induced fit model. Hence to take the conformational changes in both the ligand and the protein into account, Induced Fit Docking (IFD) protocol of Schrödinger Suite [45–48] was utilized when docking SM and GW4869 into *Bc*-SMases and nSMase2. The protein structures used during docking were the crystal structures which were prepared with PPW prior to docking.

IFD protocol utilizes Glide [58–61] and Prime [51, 62, 63] tools in Schrödinger Suite to dock the ligands into the protein and induce conformational changes in the binding site of the protein. IFD standard protocol consists of three main steps; Glide docking, Prime refinement and Glide redocking.

Prior to Glide docking, a receptor grid box was generated on each protein structure. Box center of the receptor grid was taken as the centroid of the specified residues that defined the binding site of the protein. The box size was set to 26 Å on a side by selecting the 'Auto' option [45]. Ligands were allowed to sample ring conformations with an energy window of 2.5 kcal/mol. Nonplanar conformations of amide bonds were penalized. OPLS3 was selected as the force field for IFD. Number of Glide and Prime CPUs were both set to 1.

After setting the receptor and ligand parameters, the ligands were initially docked into the specified binding site with receptor and ligand van der Waals scalings of 0.50 by utilizing Glide. A maximum number of 20 poses were generated in this step. In the second step, the side chains of the residues within 5 Å of each ligand were refined by using Prime. The residues that are interacting with the metal ion were excluded from refinement (see Table 3.3) as suggested by the IFD protocol [45]. The side chains

of the refined residues were optimized. A Prime minimization was performed on these protein/ligand complexes. Finally, the ligands were redocked into the protein with extra precision (XP). Redocking was performed on the structures within 30 kcal/mol of the best structure which was the lowest-energy structure [45].

Table 3.3. Specified residues for receptor grid generation and metal-bound residues that were excluded from Prime refinement.

Ligand	**PDB ID**	**Site (Specified residues for receptor grid generation**	**Metal-bound residues that were not refined**
SM	2UYR	16,53,151,195,197,253,295,296	53
	2DDS	16,53,151,195,197,253,295,296	53, 296
	5UVG	130,364,461,510,512,607,638,639	364
GW4869	2UYR	Possible Binding Sites Suggested by SiteMap	53
	2DDS	Possible Binding Sites Suggested by SiteMap	53, 296
	5UVG	Possible Binding Sites Suggested by SiteMap	364

IFD protocol also estimated the binding affinity for the generated protein-ligand complexes in terms of XP GScores (kcal/mol). XP GScore takes many aspects into account including lipophilicity, hydrophobicity, electrostatic interactions, pi-pi stacking and pi-cation interactions, hydrogen bonding, polar atom burial [45].

3.4. Determination of Possible Binding Sites on *Bc*-SMases and Human nSMase2

The possible binding sites on *Bc*-SMases and nSMase2 were found by utilizing SiteMap module of Schrödinger [42–44]. SiteMap initially finds the sites that can be suitable for ligand-protein binding. To locate the possible binding sites, SiteMap

utilizes a grid of points, namely 'site points'. A 1 Å grid of possible site points is placed over the whole protein at the beginning of the SiteMap algorithm. The points that are in good van der Waals contact with the protein are selected as candidates for binding site points. These site points are then merged, if the gap between them is small, to generate the possible binding sites. These sites are then further analyzed by assessing their various properties including their hydrophobicity and hydrophilicity [42–44]. Finally, SiteMap tabulates the possible binding sites with their properties including SiteScores, size of the site, hydrophilic and hydrophobic character.

The scores provided by SiteMap have average or threshold values computed by taking tight-binding (binding affinity $\leq$ 1 μM) sites of an extensive set of proteins available in literature into account [42–44].

For a SiteScore, a value of 0.80 is defined as the threshold level for distinguishing between drug-binding and non-drugbinding sites. The calibration value for SiteScore is 1.0, hence if the SiteScore of a binding site is greater than 1, it indicates that it is a very promising site [42–44].

In Dscore, hydrophilicity plays a special role when calculating this score. Hydrophilicity is capped at 1 when calculating SiteScore, however in Dscore, it is not capped. This is done to distinguish between drug-binding and non-drug-binding sites. For example, some of the ligands can be highly active (they have charged structures) and not drug-like, hence SiteMap aims to recognize the non-drug-binding sites that can bind these active, charged and not drug-like ligands. The higher this score, the more "druggable" the site is. The calibration value for Dscore is also 1 [42–44].

SiteScore and Druggability Score (Dscore) are calculated by using the following equations:

$$SiteScore = 0.0733\sqrt{n} + 0.6688e - 0.20p \tag{3.1}$$

$$Dscore = 0.094\sqrt{n} + 0.60e - 0.324p \tag{3.2}$$

where n is the number of site points which defines the size of the site, and e and p are the enclosure and hydrophilic scores, respectively. The hydrophilic score is capped at 1 if it is higher than 1 when calculating SiteScore [42–44].

Enclosure is a measure of how open the site is to solvent. It evaluates whether the ligand can be enclosed by the protein or not. It is calculated by drawing radial rays from the site points. The fraction of radial rays that hit the protein surface within a specified distance gives the enclosure. The higher this score, the better it is. An average value of 0.78 is determined for a tight-binding (binding affinity ≤ 1 μM) site [42–44].

SiteMap analysis on *Bc*-SMases and human nSMase2 was performed to find the possible binding site of nSMase2 inhibitor, GW4869. This inhibitor was proposed to bind to the DK Switch site [1]. The possible binding site that contained DK Switch residues was sought to identify the possible binding site of GW4869. The receptor grid for IFD simulations of GW4869 was defined based on these SiteMap results.

The top-ranked potential receptor binding sites on *Bc*-SMases and human nSMase2 were identified with SiteMap. All the water molecules and metal ions present in the prepared crystal structures of the *Bc*-SMases and human nSMase2 were deleted prior to SiteMap analysis as suggested by the SiteMap instructions [42–44]. The default options were used when running SiteMap. 15 site points per reported site was set as the lower limit for defining a site so that even relatively small binding sites could be identified. At most 5 sites were reported per receptor. More restrictive definition of hydrophobicity was selected since it took the hydrophilic regions into account and reduced their hydrophobic scores [42–44].

3.5. Molecular Dynamics Simulations

Proteins are dynamic in nature, not static, hence the conformational changes that they undergo are crucial for their function, and to understand the role of their structures in their action mechanisms, their dynamic nature should be analyzed [64]. Molecular dynamics simulations are widely used computational method to analyze the protein folding, the conformational changes that a protein undergoes and the effect of these changes on catalytic mechanism and ligand binding [65].

Time-based behavior of a protein can be computed by changing the conformation of a protein according to the Newton's equation of motion [66]. Initial coordinates of the atoms in a protein which can be retrieved from the crystal structure information and the potential which can be derived from a force field and the coordinates are required for the calculation of the time-based behavior of a biological macromolecular system [65]. Force field consists of various atomic forces which are defined by the potential energy parameters including bond lengths, vibrational energies, van der Waals atomic radii and atomic charges [67].

MD simulations were performed on the apo and ligand-bound forms of *Bc*-SMases and human nSMase2 to analyze the conformational changes that might be important for their catalytic mechanism. For this purpose, Desmond tool in Schrödinger's Suite [49, 50] was utilized. Desmond is an explicit-solvent molecular dynamics tool [49, 50], hence the interactions between all pairs of solute and solvent are explicitly calculated in contrast to implicit-solvent methods which treat the discrete solvent as a continuum. Hence the explicit-solvent methods are much more accurate, and as a result longer in time, than the implicit-solvent methods [68].

Prior to MD simulations, the protein structures and ligands were prepared by using PPW and LigPrep. The ligand-bound forms of the proteins were generated by using IFD. After preparing the structures, an aqueous system was built for each protein structure. The solvent/water model was chosen as SPC. SPC water model is among the

widely used solvent models [69]. Boundary conditions were defined with a simulation box shape of orthorhombic and a buffer distance of 10 Å on each side of the box. No membrane was set up. The default force field OPLS2005 was utilized. The system was neutralized by adding sodium or chloride ions. The minimum number of the ions required to neutralize the systems was calculated by Desmond. An amount of 0.15 M of salt (NaCl) was added to the system to simulate the physiological conditions [49,50].

After building the system for each protein, molecular dynamics simulation was performed. MD simulations with a simulation time range of 100 ns to 500 ns were carried out with recording intervals of 4.8 ps for trajectory and 1.2 ps for energy. An approximate number of 104167 frames were calculated for each 500 ns MD simulation. The ensemble class was chosen as NPT (isothermal-isobaric ensemble) with a temperature of 310 K and a pressure of 1.01325 bar. The model system was relaxed before simulation. The thermostat and barostat methods were chosen as Langevin. The short range method of coulombic interactions was defined with a cutoff radius of 9.0 Å. The seed number was set to the default value 2007 [49,50]. All the MD simulations parameters were actually at their default values except for the simulation time [49, 50], the temperature and the thermostat-barostat methods. 310 K was opted to simulate the physiological temperature at the proteins function. Finally, the MD simulation was run on a single graphics processor (GPU).

3.6. Analysis of the Simulation Results

MD trajectories were analyzed by using Simulation Interactions Diagram (SID) and Simulation Event Analysis (SEA) in Desmond Maestro [37, 49, 50]. The protein-ligand interactions over the trajectory, e.g. the stability of the protein-ligand interactions and the flexibility of the ligand in the binding site, were investigated by using SID. SID analysis encompasses RMSD and RMSF profiles of the proteins and ligands, the content of the secondary structure elements and the protein-ligand contacts over simulation trajectory [49, 50].

Root-mean-square deviation (RMSD) backbone profiles of the proteins and their ligands relative to the first frame of the MD simulation (0 ns) were plotted to see whether the simulation equilibrated, i.e. RMSD reached a plateau, or not. The simulations were extended if they did not reach equilibrium.

RMSD provides information on how much the conformation of a protein or a ligand deviates from its reference structure (usually the first frame). The changes over 3 Å may indicate that protein goes through large conformational changes. If RMSD reaches a plateau over time, it indicates that the system has equilibrated. If not, the simulation time should be extended [49].

RMSD for frame x of a protein or a ligand was calculated by Schrödinger with the following equation [37, 49, 50]:

$$RMSD_x = \sqrt{\frac{1}{N}\sum_{i=1}^{N}(\mathbf{r_i}'(t_x) - \mathbf{r_i}(t_{ref}))^2} \tag{3.3}$$

where N is the number of atoms, t_{ref} is the reference time, t_x is the time at which frame x occurs, r_i' is the position of atom i at frame x. RMSD values was calculated for each frame in the simulation [49, 50].

Secondary structure elements (SSE); strand, helix and loop, were also investigated to see the change in the secondary structure content over time for each protein structure, i.e. whether the structure of a helix or a strand was maintained or not, or whether an SSE was formed over time [49, 50].

Root-mean-square fluctuations (RMSF) were calculated for the backbone atoms of each residue in a protein over the entire simulation time based on a reference frame of 0 ns. RMSF profiles showed the regions that were highly mobile on the protein. RMSF profiles were also computed for the ligand by superposing the ligand on a reference frame of 0 ns to see the internal fluctuations, or by superposing the protein-ligand

complex on the protein backbone to see its fluctuations based on the binding site. The RMSF for residue i was calculated by Schrödinger with the following equation [49, 50]:

$$RMSF_i = \sqrt{\frac{1}{T}\sum_{i=1}^{T} < (\mathbf{r_i}'(t) - \mathbf{r_i}(t_{ref}))^2 >} \tag{3.4}$$

where T is the trajectory time, t_{ref} is the reference time, r is the position of the atoms on residue i at time t_{ref}, r' is the position of atoms on a residue after aligned on the reference structure [49, 50].

Protein-ligand contacts from the MD simulations were examined to see which residues interacted with the ligand as a function of time. Hydrogen bonding, hydrophobic, ionic and water bridge interactions were analyzed. The Maestro default values were utilized for the maximum distances that defined these interactions; 2.5 Å (between donor and acceptor) for hydrogen bonding, 4.5 Å for pi-cation interactions (between aromatic and charged groups), 3.7 Å for ionic interactions (between oppositely charged atoms), and 2.7 Å (between donor and acceptor) for water bridge [49, 50].

SEA was utilized to calculate the RMSD profiles of the backbone atoms of the regions of interest, especially the active site and the DK switch loop. These profiles were analyzed to see whether the region of interest underwent some major conformational changes over time [49, 50].

The visual inspection of the protein structures, docking simulations and MD simulations were carried out with Stride and Visual Molecular Dynamics (VMD) tools [70, 71], in addition to Maestro in Schrödinger's Suite [37].

3.7. Calculation of the Binding Free Energies of the Protein-Ligand Complexes and the Ligand Strain Energies

The Molecular Mechanics/Generalized Born Surface Area (MM/GBSA) is a computational method to compute the binding free energy of a protein-ligand complex. It utilizes continuum solvation models. Compared to the Molecular Mechanics/Poisson-Boltzmann Surface Area (MM/PBSA), it is computational efficient hence, much faster [72].

The binding free energies of protein-ligand complexes and the ligand strain energies were computed by using Prime MM/GBSA tool in Schrödinger's Suite [51,62,63]. Since an implicit solvent model was utilized in MM/GBSA, all the waters and ions were suggested to be removed from the protein. The solvation model was selected as VSGB (variable-dielectric generalized Born model) 2.0 [73]. Default parameters were used in Prime MM/GBSA.

The binding energies were calculated for the frames selected from the MD simulations. The binding energy was calculated based on the following equation [51]:

$$\Delta G_{bind} = E_{complex} - (E_{ligand} + E_{receptor}) \tag{3.5}$$

where $\Delta\ G_{bind}$ and E were used to denote the binding free energy and the minimized energy terms of protein-ligand complex, ligand and receptor.

The ligand strain was calculated as follows [53]:

$$LigandStrain = E_{ligand,complex} - E_{ligand} \tag{3.6}$$

where $E_{ligand,complex}$ and E_{ligand} were the energy terms for the ligand from optimized complex and the optimized free ligand, respectively.

The algorithm behind the binding free energy $\Delta\ G_{bind}$ was as follows [72]:

$$\Delta G_{bind} = \Delta H - T\Delta S = \Delta E_{MM} + \Delta G_{sol} - T\Delta S \tag{3.7}$$

$$\Delta E_{MM} = \Delta E_{internal} + \Delta E_{electrostatic} + \Delta E_{vdw} \tag{3.8}$$

$$\Delta G_{sol} = \Delta G_{GB} + \Delta G_{SA} \tag{3.9}$$

where the gas-phase MM energy, the solvation energy, the conformational entropy upon binding were denoted by $\Delta\ E_{MM}$, $\Delta\ G_{sol}$ and TΔS, respectively. $\Delta\ E_{MM}$ consists of the internal energy including bond, angle and dihedral energies, the electrostatic energy and the van der Waals (vdW) energy. $\Delta\ G_{GB}$ is the polar contribution calculated by GB model and $\Delta\ G_{SA}$ is the nonpolar contribution calculated by solvent accessible surface area (SASA) [72].

4. RESULTS AND DISCUSSION

4.1. Docking of the Natural Substrate (SM) to *Bc*-SMases and Human nSMase2

The natural substrate of nSMases is SM which has a long hydrophobic acyl chain. To see the effects of the length of the hydrophobic tail of SM and the water molecules around the active site metal ion, several SM docking simulations were performed on the *Bc*-SMases; 2UYR and 2DDS, and the human nSMase2; 5UVG. To find the optimum length of the hydrophobic tail of SM and the importance of the water molecules in docking, these docking simulations were carried out on the crystal structures of 2UYR, 2DDS and 5UVG.

To see the impact of the water molecules in docking, three structures were prepared for each protein; proteins with only metal bound water kept (i.e. all water except metal bound ones were deleted, denoted by MBW), proteins with only water within 5 Å of the metal ion kept (i.e. all water except the ones within 5 Å of metal ions were deleted, denoted by WW5M), and proteins with all water deleted. Since apo MD simulations conducted on the structures with only metal bound water kept and with only water within 5 Å of the metal ion kept had some conformational differences (see Section 4.2), both cases were analyzed to see whether the additional water molecules in 'WW5M' case were important or not.

The length of the hydrophobic tail of SM may vary generally between C16 to C24. In this study, C16-SM was tried to dock into 2DDS, 2UYR and 5UVG, however due to its long chain, no pose was generated for C16-SM except for 5UVG with only metal bound water molecules kept and with all water deleted structures. Hence by taking this and the suggestion that SM was partially extracted by nSMase2 from PM [1] into account, an analysis on the effect of the length of the hydrophobic tail was carried out. C16-SM was truncated from both tails carbon by carbon. A variety of cropped SM

structures (lengths of tail ends varied between C3 and C16 for fatty acid part, and d5 and d18 for sphingosine backbone) was created (Figure 2.7). The cropping was stopped at C3 and d5 to preserve the head group of SM. C(n)-SM refers to d(n+2):1C(n)-SM (e.g. C9-SM is d11:1C9-SM), where n is the number of carbon atoms in the tail of SM.

When analyzing the docking results, three main aspects were considered; (i) the estimated binding energy; XP GScore, (ii) whether the phosphate moiety of SM was interacting with the active site metal ion or not, and finally (iii) the closeness of the metal ion to the phosphate moiety of SM. The latter two aspects are important since it was proposed that the active site metal ions interacted with the phosphate moiety of SM [1, 2, 30]. The metal ion was assumed to be close to the phosphate moiety of SM if the distance between the metal ion and the phosphorus from phosphate moiety was around 6 Å or lower. This threshold value was determined by analyzing the top poses and the distances between the phosphate moieties of SM and the metal ions that were interacting with them through metal coordination or salt bridge.

The direction of the amino group of SM was also taken into account when analyzing the poses of *Bc*-SMases; 2DDS and 2UYR since the mechanism proposed by Ago *et al.* suggested that this amino group might be pointing towards the aromatic residues; Trp232 and Phe244 [2] (see Figure 2.6).

4.1.1. Docking of SM to 2DDS

The first poses docked into the crystal structure of 2DDS are tabulated in Table 4.1 and Table 4.2. Pose # in these tables indicates the ranking of the stated pose. The poses were sorted out in an ascending order according to their estimated binding affinities; XP GScores. Hence a ligand with a pose ranking of 1 has the best estimated binding affinity. If the first pose of each cropped SM ligand exhibits no interaction between the phosphate moiety of SM and the metal ion, the next pose in the pose ranking list that had an interaction between cobalt ions and phosphate moiety of the cropped SM structures is also provided in Table 4.1 and Table 4.2. The pose generation

was initially observed for C12-cropped SM, hence no pose was generated for C13- to C16-SM.

The top poses of 2DDS MBW mainly interacted with DK Switch residue; Lys131 and the cobalt ions (Co1117 and Co1127). Amino group of SM was directed away from Trp232 and Phe244. The top poses of 2DDS WW5M did not form interactions with cobalt ions. These poses mainly interacted with Lys131, Asp156, HOH1183 and HOH1229. The latter two water molecules were not bound to the metal ion. The top poses belonging to this group have better XP GScores than the 2DDS MBW. However, the phosphate moieties were far apart from cobalt ions, hence no interaction was observed between them.

Table 4.1. Top poses of the cropped SM docked into the crystal structure of 2DDS MBW.

Ligand Pose #	**XP GScore**	**Phosphate Moiety Interacting with Metal Ion**	**Metal Ion Close to Phosphate Moiety**
C3-1	-5.135	Yes	Yes
C9-1	-4.749	No	No
C12-1	-4.628	No	Yes
C5-1	-4.530	Yes	Yes
C9-4	-4.419	Yes	Yes
C10-1	-4.271	No	No
C8-1	-4.131	No	No
C7-1	-3.998	No	No
C12-4	-3.942	Yes	Yes
C6-1	-3.885	Yes	Yes
C4-1	-3.854	Yes	Yes
C7-3	-3.784	Yes	Yes
C10-2	-3.654	Yes	Yes
C11-1	-3.048	Yes	Yes
C13-C16	-		

Two common binding modes were observed among the top poses of each 2DDS group which are given in Table 4.3. The common binding modes are determined if the head groups of SMs (including amino group and phosphate moiety) approximately aligned when the poses were superimposed on each other. These common binding modes of 2DDS are demonstrated in Figure 4.1 by selecting some of the cropped SM ligands presented in Table 4.3 as examples. The binding mode 1 of 2DDS MBW is similar to that of 2DDS WW5M as seen in Figure 4.1a. However, in the binding mode 1, the phosphate moieties of SM were far away from the metal ions.

Table 4.2. Top poses of the cropped SM docked into the crystal structure of 2DDS WW5M.

Ligand Pose #	**XP GScore**	**Phosphate Moiety Interacting with Metal Ion**	**Metal Ion Close to Phosphate Moiety**
C6-1	-6.985	No	No
C10-1	-6.738	No	No
C11-1	-6.286	No	No
C9-1	-6.252	No	No
C7-1	-5.958	No	No
C4-1	-5.804	No	No
C12-1	-5.664	No	No
C3-1	-5.368	No	No
C5-1	-5.119	No	No
C8-1	-4.730	No	No
C13-C16	-		

The second binding mode of 2DDS MBW is not similar to that of 2DDS WW5M. In the second binding mode of 2DDS MBW, the cobalt ion-phosphate moiety interaction was observed. Even though the amino group did not directly face Trp232 and Phe244, it was closer to these residues as seen in Figure 4.1b. Among the binding modes of 2DDS, this second binding mode of 2DDS MBW has the most favorable interactions including the cobalt ion-phosphate moiety interaction. The direction of the amino groups of the cropped SMs also point approximately towards Trp232 and Phe244 in this binding mode. In the second common binding mode of 2DDS WW5M, cobalt

ion-phosphate moiety interaction was not observed since phosphate moiety faced and interacted with DK Switch residue; Lys131 (see Figure 4.1c).

Table 4.3. Cropped SM docked into the crystal structure of 2DDS that have similar binding modes.

Only Metal Bound Water Kept				**Only Water within 5 Å of Metal Kept**			
Binding Mode 1		**Binding Mode 2**		**Binding Mode 1**		**Binding Mode 2**	
Pose #	**XP GScore**	**Pose #**	**XP GScore**	**Pose #**	**XP GScore**	**Pose #**	**XP GScore**
C9-1	-4.749	**C3-1**	-5.135	**C6-1**	-6.985	**C9-1**	-6.252
C12-1	-4.628	**C9-5**	-4.301	**C10-1**	-6.738	**C7-2**	-5.516
C10-1	-4.271	**C6-1**	-3.885	**C7-1**	-5.958	**C5-2**	-4.813
C8-2	-3.917	**C7-3**	-3.784	**C4-1**	-5.804	**C10-6**	-3.951
C3-4	-3.683	**C10-2**	-3.654	**C12-1**	-5.664		
C4-2	-3.649	**C5-2**	-3.636	**C5-1**	-5.119		
C7-4	-3.542	**C4-4**	-3.273	**C8-1**	-4.730		
				C9-2	-4.562		
				C11-2	-4.169		

4.1.2. Docking of SM to 2UYR

The first poses and the top poses that had an interaction between magnesium ion and phosphate moiety of the cropped SM structures docked into the crystal structure of 2UYR are tabulated in Table 4.4 and Table 4.5. No pose was generated for C12- to C16-SM for 2UYR MBW, and C11- to C16-SM for 2UYR WW5M. However, the poses generated for C11-SM docked into 2UYR MBW have XP GScores greater than -5 kcal/mol.

In 2UYR MBW, the amino groups of almost all top poses directed themselves towards Trp232 and Phe244 by forming pi-cation interactions with them. Phosphate moieties of all top poses except for C11-1 (Cropped Ligand-Pose #) were close to magnesium ion. All the top poses of 2UYR MBW formed hydrogen bonding with

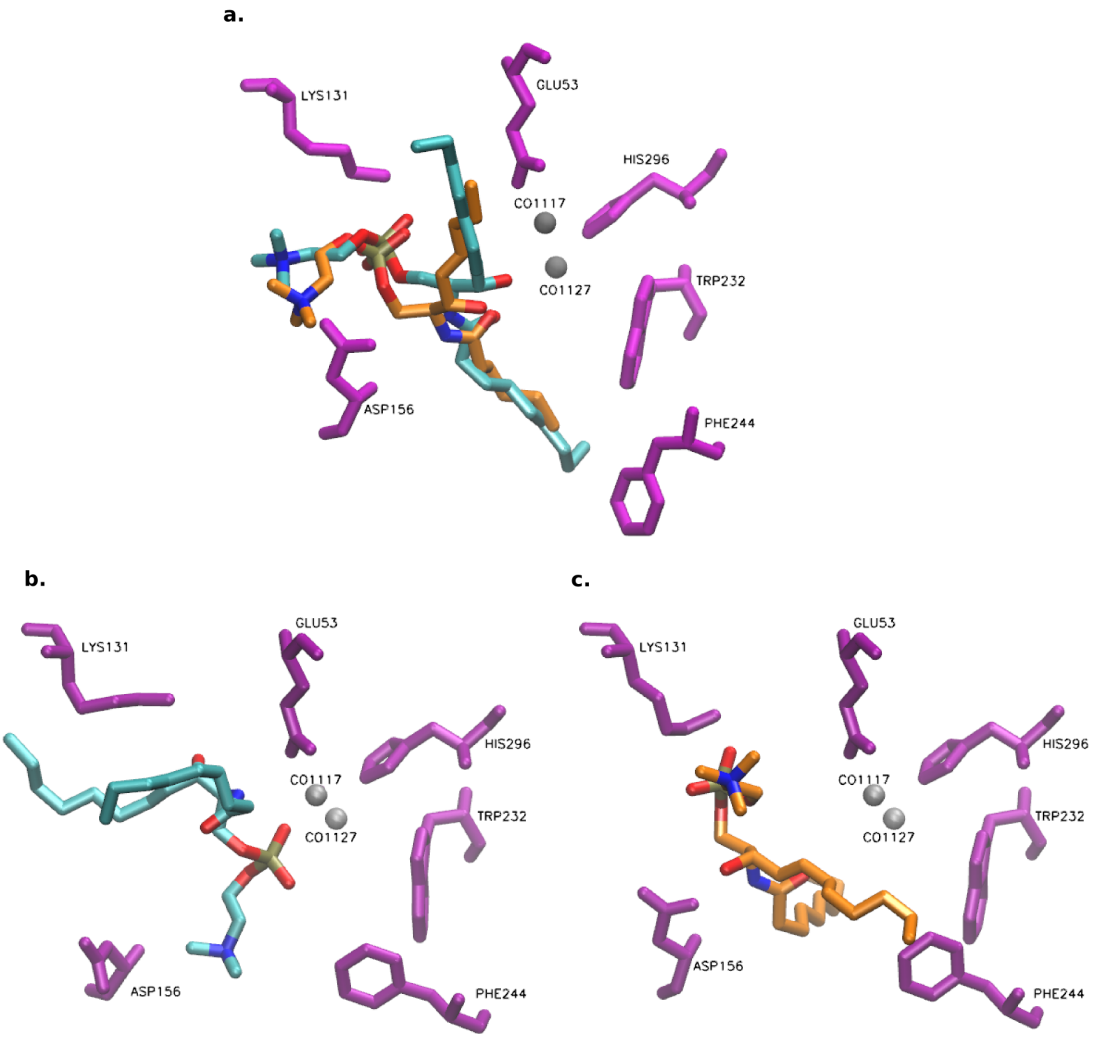

Figure 4.1. Common binding modes of 2DDS. First binding mode; C9-1 (cyan) and C6-1 (orange) docked into 2DDS MBW and WW5M (a). Second binding mode; C9-5 (b) and C9-1 (c) docked into 2DDS MBW and WW5M, respectively.

HOH2010 which was bound to the magnesium ion. For 2UYR WW5M, no interaction between magnesium ion and cropped SMs was seen except for C7-1.

Table 4.4. Top poses of the cropped SM docked into the crystal structure of 2UYR MBW.

Ligand Pose #	**XP GScore**	**Phosphate Moiety Interacting with Metal Ion**	**Metal Ion Close to Phosphate Moiety**
C9-1	-7.538	No	Yes
C4-1	-7.309	No	Yes
C4-3	-6.821	Yes	Yes
C9-2	-6.483	Yes	Yes
C7-1	-6.429	Yes	Yes
C5-1	-6.399	No	Yes
C9-3	-6.370	Yes	Yes
C8-1	-6.323	No	Yes
C3-1	-6.317	No	Yes
C6-1	-6.259	No	Yes
C10-1	-6.078	No	Yes
C6-3	-5.897	Yes	Yes
C5-2	-5.102	No	Yes
C8-2	-4.673	Yes	Yes
C11-1	-4.436	No	No
C11-2	-3.414	Yes	Yes
C12-C16	-		

Only one common binding mode was observed among the top poses of 2UYR MBW structure, while two common binding modes were observed among the top poses of 2UYR WW5M which are given in Table 4.6.

These common binding modes of 2UYR are demonstrated in Figure 4.2 by selecting some cropped SM ligands presented in Table 4.6 as examples. In the first binding mode of 2UYR WW5M, the poses had their hydrophobic tails pointing towards the groove of the active site. However, these tails are expected to point towards the entrance of the active site since SM is embedded in PM and possibly partially extracted

Table 4.5. Top poses of the cropped SM docked into the crystal structure of 2UYR WW5M.

Ligand Pose #	**XP GScore**	**Phosphate Moiety Interacting with Metal Ion**	**Metal Ion Close to Phosphate Moiety**
C6-1	-7.521	No	No
C5-1	-7.217	No	No
C9-1	-6.968	No	No
C7-1	-6.877	Yes	Yes
C8-1	-6.765	No	No
C4-1	-6.632	No	No
C3-1	-6.322	No	No
C10-1	-4.561	No	No
C11-C16	-		

from the PM by SMases (see Figure 2.6). C6-1 and C5-3 docked into this 2UYR structure is shown in Figure 4.2a.

The second binding mode of 2UYR WW5M is similar to the binding mode of 2UYR MBW as seen in Figure 4.2b. These two similar binding modes had more favorable interactions since the amino groups of these poses directed themselves towards Trp232 and Phe244 by forming pi-cation interactions with them and phosphate moieties of these poses were close to the magnesium ion.

4.1.3. Docking of SM to 5UVG

The first poses and the top poses that had an interaction between calcium ion and phosphate moiety of the cropped SM structures docked into the crystal structure of 5UVG are tabulated in Table 4.7 and Table 4.8. Interestingly, a pose for C16-SM docked into 5UVG MBW was generated with an XP GScore of -2.884 kcal/mol. While a salt bridge formation between C16-SM and calcium ion was seen, this score indicates that C16-SM was poorly docked into 5UVG. No pose was generated for C14- to C15-

Table 4.6. Cropped SM docked into the crystal structure of 2UYR that have similar binding modes.

Only Metal Bound Water Kept		**Only Water within 5 Å of Metal Kept**			
Binding Mode		**Binding Mode 1**		**Binding Mode 2**	
Pose #	**XP GScore**	**Pose #**	**XP GScore**	**Pose #**	**XP GScore**
C9-1	-7.538	**C6-1**	-7.521	**C9-1**	-6.968
C4-4	-6.745	**C5-3**	-6.851	**C5-1**	-7.217
C7-1	-6.429	**C7-2**	-6.216	**C3-4**	-4.905
C8-1	-6.323	**C8-2**	-5.749		
C3-1	-6.317	**C4-2**	-5.372		
C6-1	-6.259	**C3-5**	-4.742		
C10-1	-6.078	**C9-2**	-4.137		
C5-2	-5.102				
C11-2	-3.414				

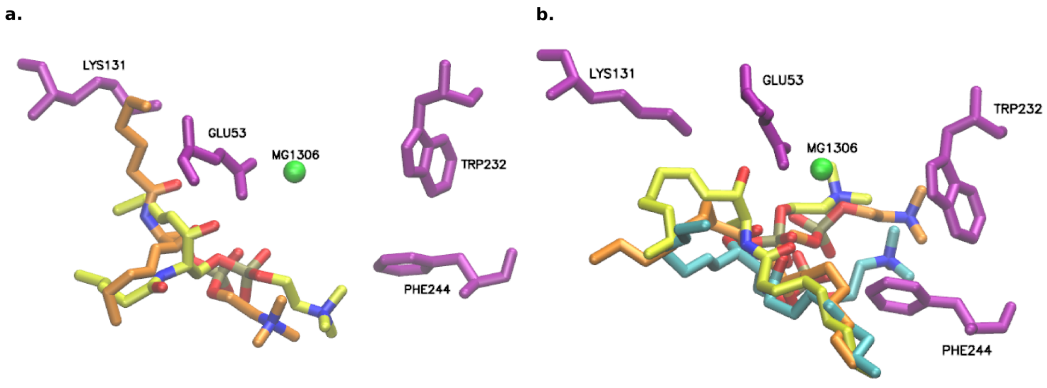

Figure 4.2. Common binding modes of 2UYR structures. (a) First binding mode; C6-1 (orange) and C5-3 (yellow) in 2UYR MBW. (b) Second binding mode; C9-1 (orange) and C9-2 (yellow) in 2UYR MBW, and C9-1 (cyan) in 2UYR WW5M.

SM docked into 5UVG with only metal bound water kept, and C14- to C16-SM docked into 5UVG with only water within 5 Å of metal ion kept.

Table 4.7. Top poses of the cropped SM docked into the crystal structure of 5UVG MBW.

Ligand Pose #	**XP GScore**	**Phosphate Moiety Interacting with Metal Ion**	**Metal Ion Close to Phosphate Moiety**
C10-1	-7.094	No	No
C9-1	-6.981	No	No
C7-1	-6.815	Yes	Yes
C8-1	-6.544	Yes	Yes
C12-1	-6.475	No	No
C9-2	-6.471	Yes	Yes
C3-1	-6.052	No	Yes
C10-2	-5.828	Yes	Yes
C5-1	-5.818	No	Yes
C12-4	-5.663	Yes	Yes
C11-1	-5.596	Yes	Yes
C6-1	-5.306	Yes	Yes
C4-1	-5.222	Yes	Yes
C5-3	-5.101	Yes	Yes
C13-1	-4.292	No	No
C3-15	-3.967	Yes	Yes
C16-1	-2.884	Yes	Yes
C14-C15	-		

Two common binding modes were observed for both 5UVG structures; MBW and WW5M as seen in Table 4.9. In all of the binding modes, the cropped SMs mainly interacted with Glu364 (active site residue), Lys435 (DK residue) and Ca701. However, in the binding mode 1 for both 5UVG, calcium ion interacted with the phosphate moiety of the SM. In the second binding mode of both 5UVG structures, calcium ion interacted mainly with the hydroxyl group of the cropped SMs. These common binding modes of 5UVG are demonstrated in Figure 4.3 by selecting some cropped SM ligands presented

Table 4.8. Top poses of the cropped SM docked into the crystal structure of 5UVG WW5M.

Ligand Pose #	**XP GScore**	**Phosphate Moiety Interacting with Metal Ion**	**Metal Ion Close to Phosphate Moiety**
C12-1	-7.232	No	No
C8-1	-6.851	Yes	Yes
C9-1	-6.577	No	No
C9-2	-6.485	Yes	Yes
C13-1	-6.410	No	No
C8-2	-6.312	Yes	Yes
C9-3	-6.226	Yes	Yes
C7-1	-5.923	Yes	Yes
C3-1	-5.744	No	Yes
C6-1	-5.621	Yes	Yes
C11-1	-5.472	No	No
C5-1	-5.442	Yes	Yes
C11-2	-5.387	Yes	Yes
C5-2	-5.259	Yes	Yes
C4-1	-5.240	No	Yes
C4-2	-5.185	Yes	Yes
C10-1	-5.043	No	No
C3-4	-4.916	Yes	Yes
C13-3	-4.151	Yes	Yes
C12-5	-3.935	Yes	Yes
C14-C16	-		

in Table 4.9 as examples. The phosphate moiety of SM is closer to the calcium ion in the first binding mode as seen in Figure 4.3.

Table 4.9. Cropped SM docked into the crystal structure of 5UVG that have similar binding modes.

Only Metal Bound Water Kept				**Only Water within 5 Å of Metal Kept**			
Binding Mode 1		**Binding Mode 2**		**Binding Mode 1**		**Binding Mode 2**	
Pose #	**XP GScore**	**Pose #**	**XP GScore**	**Pose #**	**XP GScore**	**Pose #**	**XP GScore**
C7-1	-6.815	**C10-1**	-7.094	**C8-1**	-6.581	**C9-1**	-6.577
C8-1	-6.544	**C9-1**	-6.981	**C9-2**	-6.485	**C7-4**	-5.369
C9-2	-6.471	**C7-2**	-5.557	**C7-1**	-5.923	**C3-3**	-5.051
C10-2	-5.828	**C8-6**	-5.099	**C3-1**	-5.744	**C10-1**	-5.043
C12-4	-5.663	**C6-7**	-4.797	**C6-1**	-5.621	**C8-13**	-4.898
C11-1	-5.596	**C4-7**	-4.482	**C5-1**	-5.442	**C4-10**	-4.514
C6-1	-5.306	**C5-10**	-4.410	**C11-2**	-5.387	**C5-6**	-4.372
C4-1	-5.222	**C12-6**	-4.262	**C4-1**	-5.240	**C6-18**	-3.532
C5-3	-5.101	**C11-3**	-3.624	**C13-3**	-4.151		
C13-1	-4.292			**C12-5**	-3.935		
C16-1	-2.844						

The first and second binding modes of 5UVG structures are similar among themselves. The ranges for XP GScore values are approximately the same for all of the binding modes. However, the first binding mode seems to be superior to the second one according to the aforementioned criteria; the closeness of metal ion to the phosphate moiety. As seen in Figure 4.3a, the phosphate moieties of the cropped SM ligands are closer to the calcium ion in the first binding mode, while in the second binding mode, these moieties are far away from the calcium ion (see Figure 4.3b). Since the proposed mechanism of SMases requires the phosphate moiety of SM to be closer to the active site metal [1, 2], the first binding mode is the most probable binding mode of 5UVG compared with its second common binding mode.

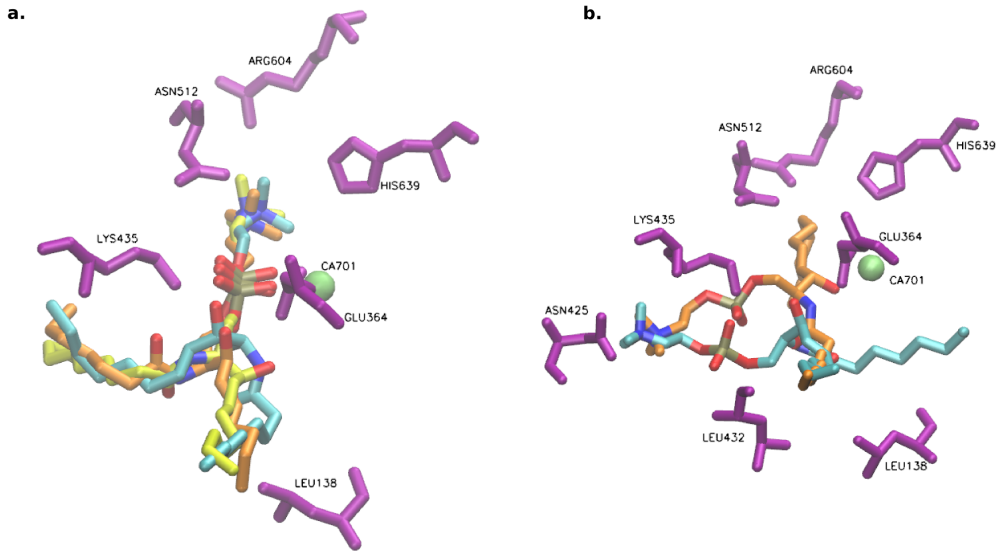

Figure 4.3. Common binding modes of 5UVG. (a) First binding mode; C7-1 (orange) and C9-2 (cyan) in 5UVG MBW, and C9-2 (yellow) in 5UVG WW5M. (b) Second binding mode; C10-1 (orange) in 5UVG MBW, and C9-1 (cyan) in 5UVG WW5M.

4.1.4. Docking of SM to the Proteins with All Water Deleted

The cropped SM ligands were docked into the all water deleted protein structures with better estimate of the binding affinities (see Table 4.10) compared with the other water-kept protein structures (see Table 4.1 to Table 4.9). In Table 4.10, the XP GScore values of 2UYR and 5UVG are sorted according to a common binding mode observed for these structures. The common binding modes observed for 2UYR and 5UVG are similar to those for 2UYR with only metal bound metal kept and first binding modes of 5UVG structures. However, no common binding mode was observed for 2DDS with all water deleted among the top poses, hence only the XP GScores of the first ligand poses are given in Table 4.10 for 2DDS.

The poses generated for all water deleted protein structures showed favorable interactions with the metal ions and the active site residues. This was expected since water molecules occupied a space in the active site, and SM ligand could not enter

the active site fully computationally due to the presence of the water molecules in this region. However, since these water molecules around the metal ions at the active site were reported to be important they should be kept in the prepared structures since their possible role in the catalytic activity might be seen during MD simulations.

Table 4.10. XP GScores of cropped SM docked into the all water deleted structures of 2DDS, 2UYR and 5UVG.

2DDS		**2UYR**		**5UVG**	
Pose #	**XP GScore**	**Pose #**	**XP GScore**	**Pose #**	**XP GScore**
C12-1	-7.010	**C5-1**	-8.549	**C9-1**	-7.130
C10-1	-6.995	**C6-1**	-8.395	**C12-1**	-7.026
C7-1	-6.057	**C7-1**	-8.354	**C6-1**	-6.939
C9-1	-5.988	**C9-1**	-8.045	**C10-2**	-6.652
C6-1	-5.745	**C10-2**	-7.810	**C7-1**	-6.487
C11-1	-5.599	**C3-1**	-7.437	**C16-1**	-6.413
C8-1	-5.373	**C4-1**	-7.118	**C8-2**	-6.288
C3-1	-4.903	**C8-1**	-7.081	**C11-3**	-5.997
C4-1	-4.639	**C11**	-	**C4-1**	-5.588
C5-1	-4.637	**C12**	-	**C5-1**	-5.537
C13	-	**C13**	-	**C13-1**	-5.359
C14	-	**C14**	-	**C3-3**	-4.807
C15	-	**C15**	-	**C14-1**	-4.540
C16	-	**C16**	-	**C15**	-

4.1.5. Comparison of the SM Docking Results

When the most promising binding modes of each protein are taken into account, the docking scores of 2UYR and 5UVG are superior to those of 2DDS, indicating that cropped SM structures docked better into the active *Bc*-SMase, 2UYR and human nSMase2, 5UVG. The common binding modes of 5UVG structures, especially for the first binding mode, showed that the SM ligands were well-aligned even when they were cropped as seen in Figure 4.3. While the alignment of the cropped SMs was also seen

in 2UYR and 2DDS cases, the ligands were not well-aligned like in 5UVG case (see Figure 4.2 and Figure 4.1).

When selecting the proper ligand for the docking analysis, it was important to choose the one that could be docked into all protein structures since they would be comparatively analyzed further by performing MD simulations on these bound complexes. The poses for C16- to C11-SMs were eliminated since these SM structures could not be docked into all protein structures, e.g. pose generation started with C10-SM for 2UYR WW5M. While the starting SM ligand, C16-SM docked into 5UVG MBW was able to generate a pose, it was eliminated due to its insufficient XP GScore.

C10-SM was able to generate poses when docked into all protein structures. However, even though C10-SM docked into 5UVG MBW with a good XP GScore value of -7.094 kcal/mol, C10-1 SM was not among the most favored binding mode (1). Hence it is also eliminated.

C7- to C9-SM poses were good enough for all poses hence the cropped SMs that had a carbon number below 9 in fatty acid tail and 5 in sphingosine backbone (see Figure 2.7), i.e. below C9, were eliminated since the cropped SMs were desired to be kept long enough to be similar to its original structure, C16-SM and short enough to be able to generate a good estimate of the binding affinity with nSMase structures.

Taken together, among the cropped SM ligands, d11:1C9-SM (C9-SM) was the most promising one. It was among the top poses generated for the most favored binding mode of each protein structure. The C9-SM poses selected for each water-kept structure of the proteins are given in Table 4.11. Instead of C9-1 SM, C9-2 was chosen for 2UYR MBW. These two poses have similar binding modes (see Figure 4.2b), however only C9-2 SM forms a salt bridge with magnesium ion. It is important to state that the phosphate moiety of C9-1 SM is closer to the magnesium ion however not close enough to form salt bridge with it. The 2D ligand interaction diagrams of these top selected C9-SM poses are also shown in Figure 4.4, Figure 4.5 and Figure 4.6.

Table 4.11. Most promising C9-SM poses for water-kept protein structures.

PDB ID	Only Metal Bound Water Kept (XP GScore)	Only Water within 5 Å of Metal Ion Kept (XP GScore)
2DDS	C9-5 (-4.301 kcal/mol)	C9-1 (-6.252 kcal/mol)
2UYR	C9-2 (-6.483 kcal/mol)	C9-1 (-6.968 kcal/mol)
5UVG	C9-2 (-6.471 kcal/mol)	C9-2 (-6.485 kcal/mol)

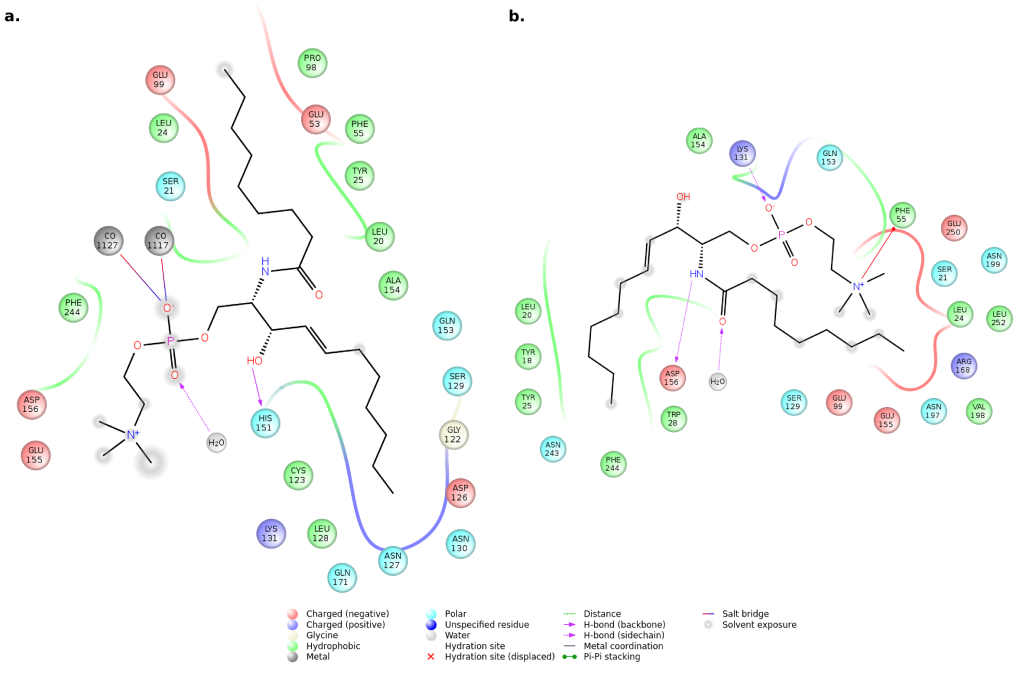

Figure 4.4. 2D interaction diagram for C9-SM docked to 2DDS structures. (a) C9-5 docked into 2DDS MBW. (b) C9-1 docked into 2DDS WW5M.

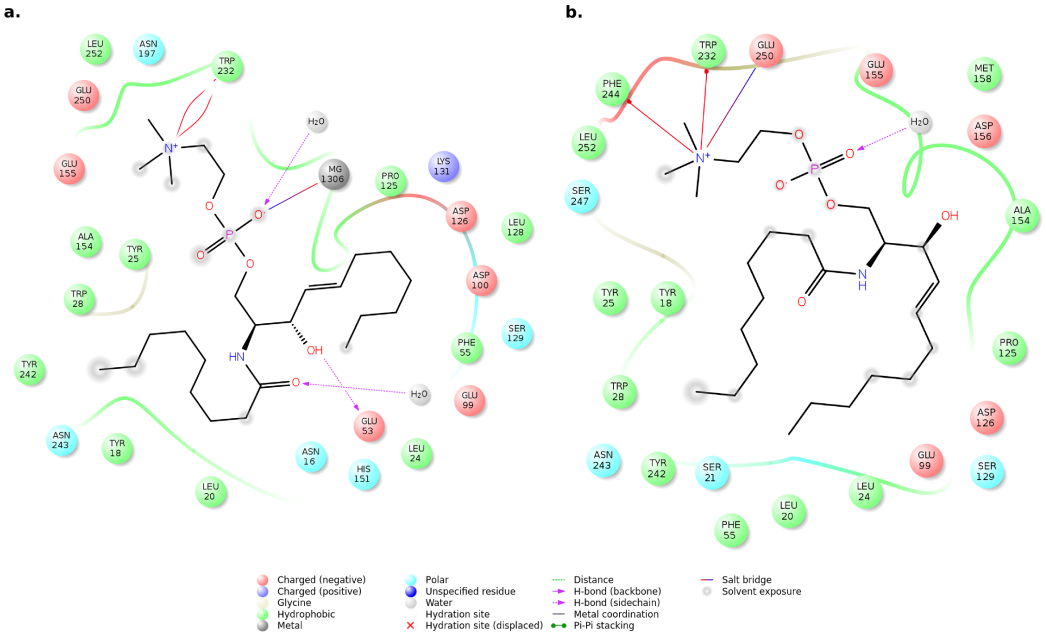

Figure 4.5. 2D interaction diagram for C9-SM docked to 2UYR structures. (a) C9-2 docked into 2UYR MBW. (b) C9-1 docked into 2UYR WW5M.

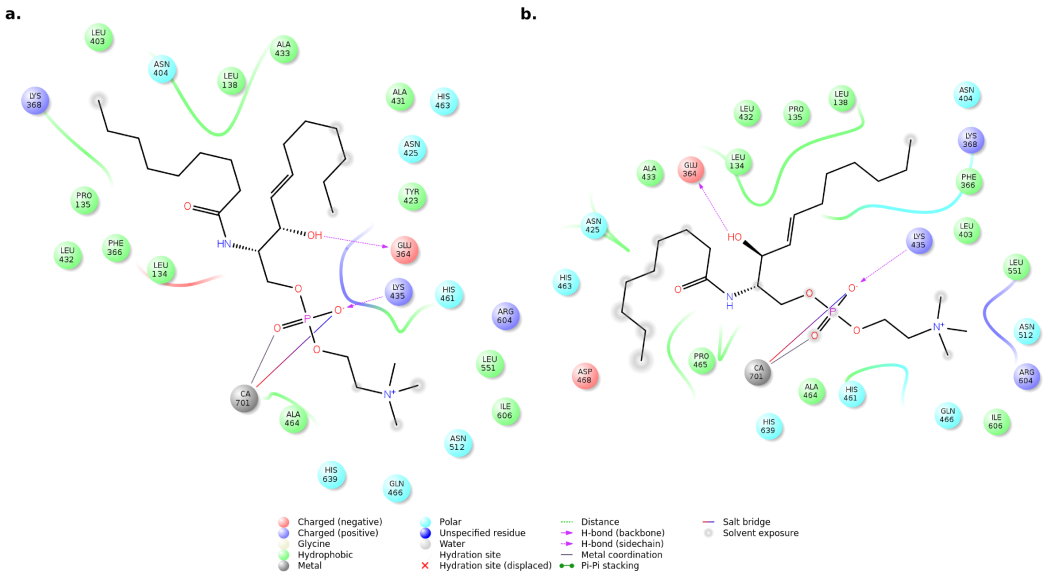

Figure 4.6. 2D interaction diagram for C9-SM docked to 5UVG structures. (a) C9-2 docked into 5UVG MBW. (b) C9-1 docked into 5UVG WW5M.

Table 4.12 shows the residues on 2DDS that are interacting with the cropped C9-SM according to the selected C9-SM poses (given in Table 4.10 and Table 4.11). C9-5 SM formed backbone hydrogen bonding (H(b)) with active site residue, His151 and side chain hydrogen bonding (H(s)) with the metal-bound water, HOH1130 on 2DDS MBW. C9-5 SM also interacted with Co1117 by forming a salt bridge. The phosphate moieties of C9-1 SMs for both 2DDS WW5M and with all water deleted (AWD) were not close enough to form interactions with cobalt ions. In 2DDS WW5M and AWD cases, the phosphate moieties of C9-SMs were 6.90 Å and 9.51 Å away from the Co1117, respectively. The C9-5 SM pose in 2DDS MBW seems superior to the other two poses presented in Table 4.12 due to its interaction with cobalt ion while its XP GScore is high. The stability of the interactions between C9-SM and 2DDS was tested further by performing MD simulations on the selected poses that are shown in Figure 4.4.

Table 4.12. Selected C9-SM poses and the interacting residues on 2DDS. Active site and DK switch residues are underlined. Salt bridge, hydrogen bonding (backbone) and hydrogen bonding (side chain) are denoted by Salt b, H(b) and H(s), respectively.

Structure Pose #	**Interacting Residues**								
	E53	F55	K131	H151	D156	N197	Co 1117	HOH 1229	HOH 1130
MBW C9-5				H(b)			Salt b		H(s)
WW5M C9-1		Pi-cation	H(s)					H(s)	
AWD C9-1	H(s)	Pi-cation	H(s)		H(s)	H(s)			

Table 4.13 shows the residues on 2UYR that are interacting with the cropped C9-SM according to the selected poses of C9 (provided in Table 4.10 and Table 4.11). C9-2 SM formed side chain hydrogen bonding with the active site residue, Glu53, and two metal bound water molecules; HOH2009 and HOH2010 on 2UYR with only metal bound water kept. It also formed pi-cation interaction with Trp232 and interacted with

Mg1306 by forming a salt bridge. The phosphate moiety of C9-1 SM was away from the magnesium ion of 2UYR (active structure) with water within 5 Å of metal ion kept with a distance of 7.21 Å. While both MBW and AWD 2UYR structures interacted with the magnesium ion, MBW 2UYR was opted as the starting structure for the MD simulations due to the aforementioned reason that the water molecules at the active site were important for catalytic activity. The stability of the interactions between C9-SM and 2UYR was tested further by performing MD simulations on the selected poses; which are shown in Figure 4.5.

Table 4.13. Selected C9-SM poses and the interacting residues on 2UYR. Active site residues are underlined. Salt bridge, hydrogen bonding (side chain) and metal coordination are denoted by Salt b, H(s) and metal coor, respectively.

Structure Pose #	**Interacting Residues**									
	E53	H151	N197	W232	F244	E250	D295	Mg 1306	HOH 2009	HOH 2010
MBW C9-2	H(s)			Pi-cation				Salt b	H(s)	H(s)
WW5M C9-1				Pi-cation	Pi-cation	Salt b				
AWD C9-1		H(s)	H(s)	Pi-cation			H(s)	Salt b, Metal coor		

Table 4.14 shows the residues on 5UVG (inactive structure) that are interacting with the cropped C9-SM according to the selected poses of C9 (provided in Table 4.10 and Table 4.11). The three poses presented in Table 4.14 formed the same interactions with the exception of H639 interaction in AWD 5UVG case. C9-SMs formed side chain hydrogen bonding with the active site residue, Glu364 and DK Switch residue, Lys435 in all cases. Metal coordination and salt bridge formation was also observed between calcium ion and C9-SM. 5UVG AWD was eliminated since important water molecules should be preserved during computational studies. Hence the stability of the

interactions between C9-SM and both 5UVG MBW and WW5M was tested further by performing MD simulations on the selected poses; which are shown in Figure 4.6.

Table 4.14. Selected C9-SM poses and the interacting residues on 5UVG. Active site and DK switch residues are underlined. Salt bridge, hydrogen bonding (side chain) and metal coordination are denoted by Salt b, H(s) and metal coor, respectively.

Structure Pose #	**Interacting Residues**			
	E364	K435	H639	Ca 701
MBW C9-2	H(s)	H(s)		Salt b, Metal coor
WW5M C9-2	H(s)	H(s)		Salt b, Metal coor
AWD C9-1	H(s)	H(s)	H(s)	Salt b, Metal coor

Taken together, the cropped SM ligands were docked into 5UVG and 2UYR with better XP GScores (estimated binding affinities) compared to 2DDS. Among the cropped SM ligands, C9-SM was selected for further analysis based on the aforementioned criteria; XP GScores and closeness of the phosphate moiety of SM to the active site metal ion. The poses C9 SM docked into 2DDS (Figure 4.4), C9 SM docked into 2UYR (Figure 4.5) and C9-2 SM docked into 5UVG MBW and WW5M structures (Figure 4.6) were further investigated to test the stability of their ligand-protein interactions by performing MD simulations on them.

4.2. MD Simulations Performed on Apo and Sphingomyelin Docked Forms of *Bc*-SMases and Human nSMase2

MD simulations were performed on the selected SM-docked *Bc*-SMases and human nSMase2 to test the stability of the interactions between SM and the proteins and analyze the conformational changes that the DK switch and the active site regions underwent with the binding of SM. Initially, 100 ns MD simulations were performed on each selected pose of d11:1C9-SM to see whether these selected poses maintained their binding modes or not. Some of the simulations were extended based on their RMSD profiles, i.e. whether the systems reached equilibrium or not.

A 100 ns MD simulation was carried out on the selected pose of d11:1C9-SM docked 2DDS (Figure 4.4a). The estimated binding affinity of the pose (XP GScore: -4.301 kcal/mol) was not good. However, an MD simulation was performed to see whether 2DDS could accommodate SM as it went through conformational changes. The binding mode observed for d11:1C9-SM bound 2DDS WW5M was different from the proposed binding mode by Ago *et al.* [2]. Hence the results for the MD simulation performed on d11:1C9-SM bound 2DDS WW5M were not provided.

Two 100 ns MD simulations were carried out on the selected poses of d11:1C9-SM docked 2UYR (Figure 4.5). Both MBW and WW5M structures were utilized to carry out the MD simulations. The estimated binding affinity of these selected poses (XP GScores: -6.483 and -6.968 kcal/mol) were better compared to 2DDS. These simulations were performed to see the stability of the interactions between SM and 2UYR as time passes. Among these simulations, the simulation conducted on the SM-bound 2UYR WW5M produced promising results hence it was further extended to 300 ns.

Two MD simulations with a duration of 500 ns were carried out on the selected poses of d11:1C9-SM docked 5UVG (Figure 4.6). The estimated binding affinities of these poses (XP GScores: -6.471 and -6.485 kcal/mol) were better compared to 2DDS, and similar to 2UYR. MD simulations were performed to see the stability of the interactions between SM and 5UVG as time passed.

These MD simulations were comparatively investigated with the MD simulations performed on apo (no-ligand-bound) forms of *Bc*-SMases and human nSMase2. A total number of six 500 ns MD simulations of apo structures were conducted; apo 2UYR MBW, apo 2UYR WW5M, apo 2DDS MBW, apo 2DDS WW5M, apo 5UVG MBW and apo 5UVG WW5M.

4.2.1. RMSD and RMSF Profiles of the MD Simulations

The RMSD profiles of the backbone atoms of *Bc*-SMases and human nSMase2 aligned on the first frames (0 ns) of their respective MD trajectories are given in Figure 4.7 and Figure 4.8. RMSD provides information on how much the conformation of a protein deviates from its reference structure [49].

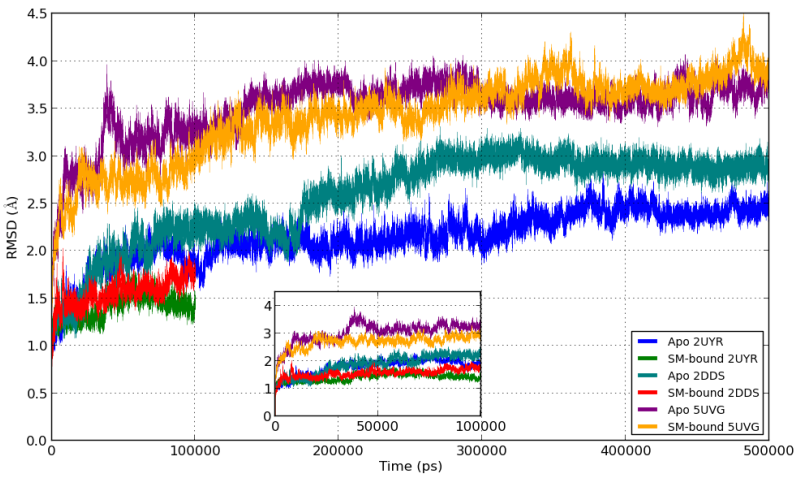

Figure 4.7. RMSD of the backbone atoms of *Bc*-SMases and human nSMase2 MBW throughout the simulations.

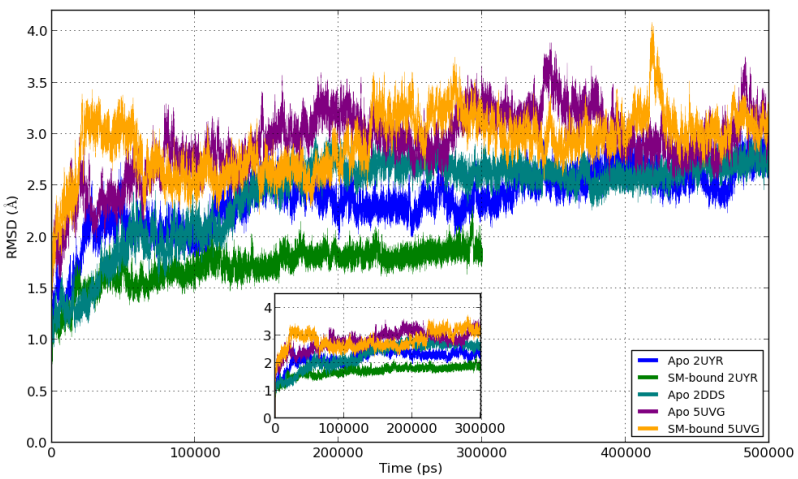

Figure 4.8. RMSD of the backbone atoms of *Bc*-SMases and human nSMase2 WW5M throughout the simulations.

As seen in Figure 4.7 and Figure 4.8, all of the systems seem to be equilibrated according to the RMSD backbone profiles, i.e. RMSD reaches a plateau over time. *Bc*-SMases have similar profiles, and their RMSDs have equilibrated around 1.5-2.0 Å indicating that with SM binding, *Bc*-SMases become more stable in a shorter time and their conformations deviate less from their prepared crystal structures compared to their apo-forms which had RMSDs equilibrated around 2.5-3 Å.

The RMSD backbone atoms of 5UVG MBW and 5UVG WW5M have reached a plateau around 2.5-3 Å. While they seem to deviate more from their prepared crystal structures compared to *Bc*-SMases, their RMSDs indicate that these conformational changes are not drastic. The RMSDs of apo forms 5UVG MBW and 5UVG WW5M reached a plateau around 3.5 Å and 3 Å, respectively. RMSD backbone profiles of apo- and SM-bound forms of human nSMase2 are similar.

The RMSDs of the active site backbone atoms of *Bc*-SMases and human nSMase2 structures aligned on the first frame are shown in Figure 4.9 and Figure 4.10. The selected active site residues for *Bc*-SMases are Asn16, Glu53, His151, Asp195, Asn197, Asp253, Asp295 and His296, and for human nSMase2, Asn130, Glu364, His461, Asp510, Asn512, Asp607, Asp638 and His639. Active site RMSD shows that the active site of all the systems were remained stable and did not go through large conformational changes throughout the simulation. Compared to the other SM-bound systems, the active site of 5UVG MBW has fluctuations in its active site RMSD, however, its RMSD values fluctuate around 1.1 Å after 60 ns, indicating that the conformational change it went through was not significant. The RMSDs of the active site backbone atoms of apo 2UYR WW5M and MBW fluctuate around 1.5 Å, while those of SM-bound 2UYR WW5M and MBW are lower indicating that with SM binding, the active site residues did not deviate much from their reference positions (crystal structure).

The RMSD of the DK switch backbone atoms of *Bc*-SMases and human nSMase2 structures aligned on the first frame are shown in Figure 4.11 and Figure 4.12. The selected DK switch residues for *Bc*-SMases are between Asp126 and Lys131, and for

human nSMase2, Asp430 and Lys435. 2UYR WW5M has the most stable DK switch conformation followed by 2UYR MBW. RMSD profiles of WW5M structures look more stable than those of MBW.

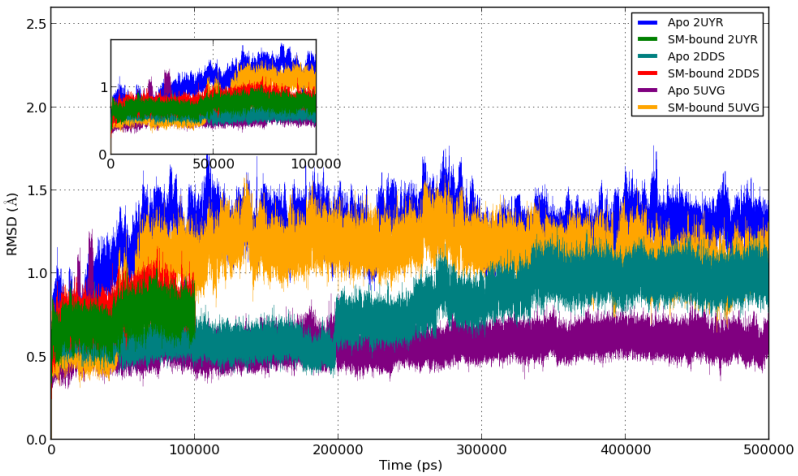

Figure 4.9. RMSD of the active site backbone atoms of *Bc*-SMases and human nSMase2 MBW throughout the simulations.

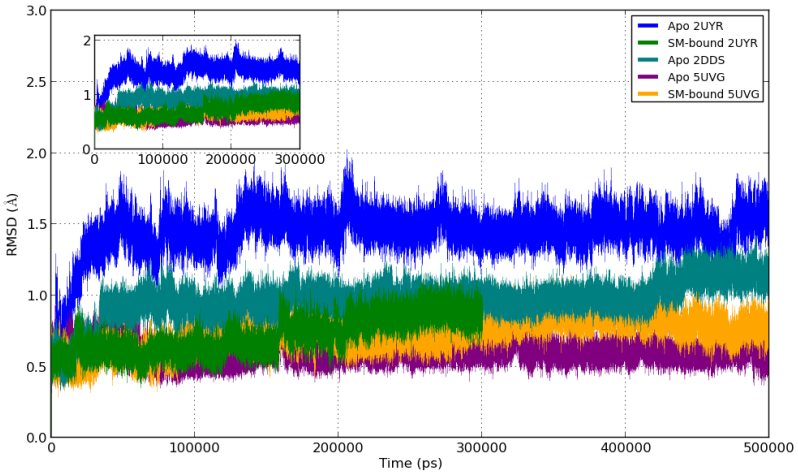

Figure 4.10. RMSD of the active site backbone atoms of *Bc*-SMases and human nSMase2 WW5M throughout the simulations.

Figure 4.13 and Figure 4.14 show the backbone RMSF profiles of *Bc*-SMases WW5M and MBW plotted by taking their respective first frames as the reference frame. RMSF shows the highly mobile regions on the protein throughout the simulation. High

RMSF values indicate that the region is highly mobile. The tails of a protein tend to fluctuate throughout the simulation [49].

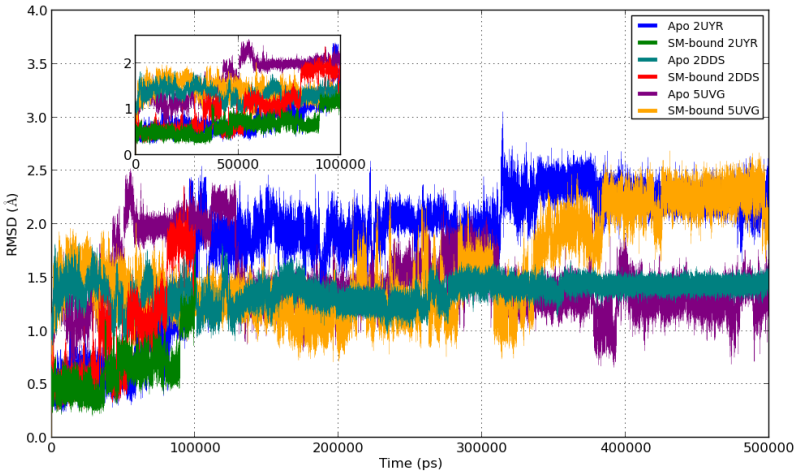

Figure 4.11. RMSD of the DK switch backbone atoms of *Bc*-SMases and human nSMase2 MBW throughout the simulations.

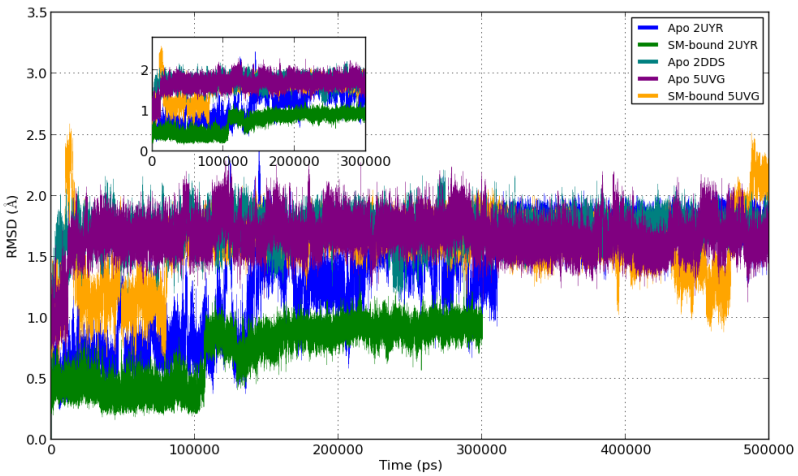

Figure 4.12. RMSD of the DK Switch backbone atoms of *Bc*-SMases and human nSMase2 WW5M throughout the simulations.

The most mobile regions on *Bc*-SMase structures according to RMSF profiles given in Figure 4.13 and Figure 4.14 are tabulated in Table 4.15. RMSF ranges for apo *Bc*-SMases along with those for SM-bound *Bc*-SMases are provided to see whether the mobile regions become stable with SM-binding or not.

The hydrophobic beta-hairpin structure (residues between 281-287) is highly mobile with an RMSF value higher than 2 Å for all *Bc*-SMase structures, and even with SM binding, this region remained mobile. Other regions that are highly mobile for all apo *Bc*-SMases are the residues 21-29, 92-98, 120-130, 155-166, 201-208 and 240-249.

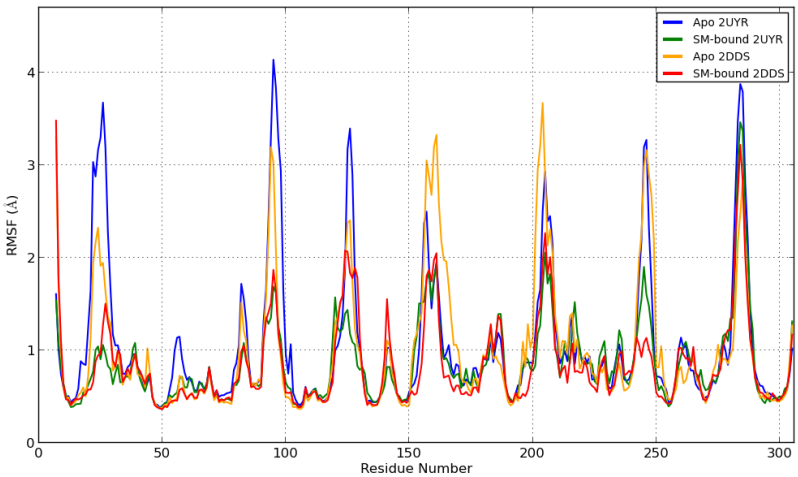

Figure 4.13. Residue-based RMSF profiles of *Bc*-SMases MBW.

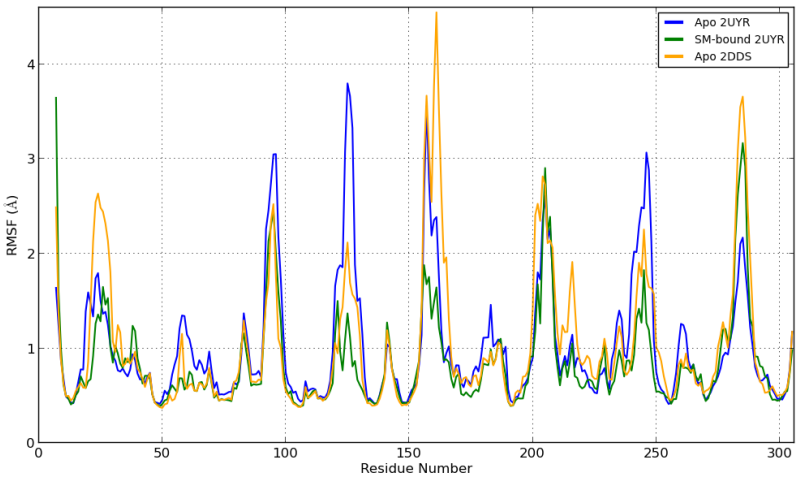

Figure 4.14. Residue-based RMSF profiles of *Bc*-SMases WW5M.

In all *Bc*-SMases, the regions 21-29, 155-166 and 240-249 become less mobile with SM binding indicating that some of the residues in these regions might be interacting with SM. The DK switch region (residues between 119 and 131) is less mobile with SM

binding in both 2UYR cases (MBW and WW5M) indicating that this region does not go through large conformational changes and possible maintained its helical conformation due to interactions with SM. However, in 2DDS case, it remained mobile even when SM was bound. The regions 92-98, which is possibly homologous to the palmitoylation region of human nSMase2, and 201-208 fluctuate more in 2UYR WW5M case. These regions become less mobile with SM binding in both MBW *Bc*-SMases. However, it is important to state that these regions are not close to the active site like the other mobile regions hence it is hard for them to form direct interactions with SM.

Table 4.15. The most mobile regions on *Bc*-SMases based on the RMSF plots. The regions that become less mobile with SM binding are highlighted in yellow.

Region	**Structure**	**Most Mobile Part**	**RMSF**	**RMSF with SM Binding**	**Possible Corresponding Site on 5UVG [1]**
21-29	2UYR WW5M	23-24	1.03-1.79 Å	0.67-1.65 Å	134-146
	2UYR MBW	22-28	1.64-3.67 Å	0.69-1.06 Å	
	2DDS MBW	22-27	1.17-2.32 Å	0.58-1.50 Å	
92-98	2UYR WW5M	93-96	1.72-3.05 Å	1.54-2.29 Å	387-406
	2UYR MBW	93-98	1.65-4.14 Å	1.11-1.69 Å	
	2DDS MBW	93-96	0.95-3.12 Å	0.99-1.87 Å	
120-130	2UYR WW5M	124-127	1.50-3.80 Å	0.61-1.37 Å	424-434
	2UYR MBW	125-127	1.00-3.39 Å	0.79-1.57 Å	
	2DDS MBW	124-126	0.99-2.46 Å	1.09-2.08 Å	
155-166	2UYR WW5M	156-161	0.85-3.56 Å	0.85-1.88 Å	462-470
	2UYR MBW	156-161	0.90-2.50 Å	0.85-1.92 Å	
	2DDS MBW	156-165	1.42-3.31 Å	0.70-2.05 Å	
201-208	2UYR WW5M	202-208	1.38-2.61 Å	1.18-2.90 Å	516-541
	2UYR MBW	202-208	1.17-2.93 Å	0.83-2.05 Å	
	2DDS MBW	201-208	2.10-3.69 Å	1.09-2.26 Å	
240-249	2UYR WW5M	241-248	1.08-3.07 Å	0.69-1.83 Å	546-603
	2UYR MBW	243-248	0.77-3.27 Å	0.75-1.90 Å	
	2DDS MBW	243-249	0.69-3.26 Å	0.75-1.14 Å	
281-287	2UYR WW5M	283-287	1.23-2.17 Å	1.33-3.17 Å	621-637
	2UYR MBW	281-287	1.86-3.87 Å	1.35-3.46 Å	
	2DDS MBW	282-287	0.97-2.77 Å	1.52-3.22 Å	

Figure 4.15 and Figure 4.16 show the backbone RMSF profiles of human nSMase2 MBW and WW5M plotted by taking their respective first frames as the reference frame. The most mobile regions on human nSMase2 structures according to RMSF profiles given in Figure 4.15 and Figure 4.16 are tabulated in Table 4.16. RMSF ranges for apo 5UVG along with those for SM-bound 5UVG are provided to see whether the mobile regions become stable with SM-binding. Interestingly, backbone RMSF profiles for SM-docked 5UVG structures demonstrate that with SM binding human nSMase2 become more mobile when compared with the corresponding apo 5UVG structures. The DK Switch loop residues 424-434 of both 5UVG structures remained mobile throughout the simulation with RMSF values above 2 Å. This region fluctuated more with SM binding.

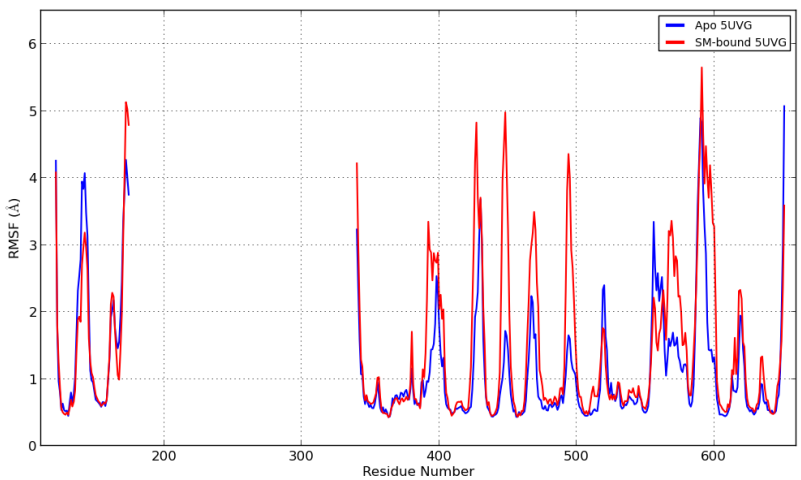

Figure 4.15. Residue-based RMSF profiles of *Bc*-SMases MBW.

Table 4.17 shows the equilibrium RMSD values of the backbone atoms of the proteins with respect to the first frame and SM with respect to ligand and protein. The RMSD plots of the SM atoms with respect to the ligand and protein are given in the Appendix for each protein-ligand complex. Ligand RMSD with respect to protein is measured by aligning the protein-ligand complex on the reference protein backbone. Ligand RMSD provides information about how stable is the ligand with respective to the receptor. If the RMSD of the ligand atoms is considerably higher than the RMSD of the backbone atoms of the protein, the ligand may diffuse away from the

protein [49]. The ligand RMSD with respect to ligand is plotted by aligning the ligand to the reference ligand structure (0 ns). It shows the internal fluctuations of the ligand and provides information about how stable is the ligand with respective to its binding pocket [49].

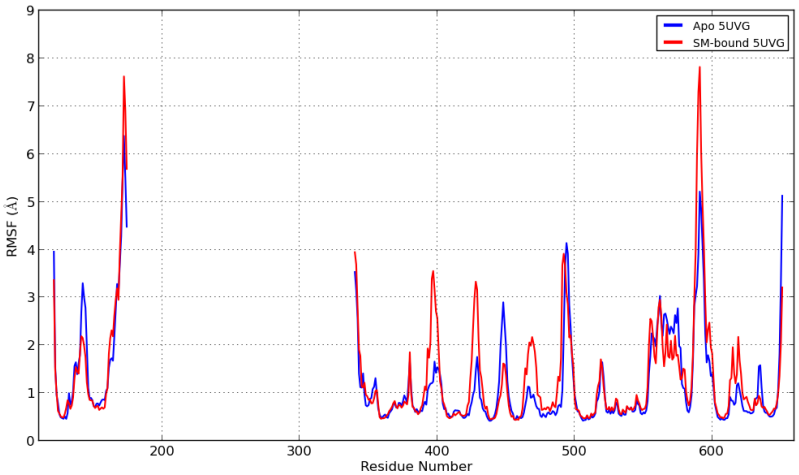

Figure 4.16. Residue-based RMSF profiles of *Bc*-SMases WW5M.

The ligand RMSDs with respect to protein are higher than their respective protein backbone RMSDs, however for 2DDS MBW and 2UYR WW5M, they are not significantly larger indicating that the SMs did not diffuse away from their binding pockets. For 5UVG MBW, 5UVG WW5M and 2UYR MBW (especially for 5UVG structures), SM seems to change its binding mode as the simulations proceeded (see Figure A.1).

The initial SM binding poses of 5UVG MBW, 5UVG WW5M and 2UYR MBW were not preserved according to their ligand RMSD profiles (with respect to ligand). The SM-poses seem to be maintained for 2UYR WW5M and 2DDS MBW since their ligand RMSDs are lower (see Figure A.1).

Table 4.16. The most mobile regions on human nSMase2 according to the RMSF plots. The regions that become less mobile and more mobile with SM binding are highlighted in yellow and red, respectively.

Region	**Structure**	**Most Mobile Part**	**RMSF**	**RMSF with SM Binding**
136-145	5UVG WW5M	141-145	1.40-3.30 Å	1.23-2.19 Å
	5UVG MBW	137-145	1.70-4.07 Å	1.41-3.18 Å
161-342	5UVG WW5M	165-174, 340-342	1.53-6.38 Å	1.82-7.62 Å
	5UVG MBW	161-164, 168-174, 340-342	1.46-4.27 Å	0.99-5.13 Å
391-403	5UVG WW5M	397-398	0.76-1.66 Å	1.06-3.55 Å
	5UVG MBW	397-400	0.96-2.53 Å	1.90-3.35 Å
424-432	5UVG WW5M	429	0.70-1.76 Å	1.30-3.33 Å
	5UVG MBW	427-431	0.84-3.68 Å	2.07-4.83 Å
445-451	5UVG WW5M	446-450	1.24-2.90 Å	0.87-1.62 Å
	5UVG MBW	448	0.89-1.72 Å	1.96-4.98 Å
465-472	5UVG WW5M	467	0.73-1.14 Å	1.39-2.17 Å
	5UVG MBW	466-470	0.74-2.24 Å	1.64-3.49 Å
491-499	5UVG WW5M	492-497	1.055-4.14 Å	1.57-3.92 Å
	5UVG MBW	494-495	0.82-1.65 Å	1.17-4.36 Å
519-520	5UVG WW5M	519-520	1.60-1.65 Å	1.53-1.71 Å
	5UVG MBW	519-520	2.33-2.40 Å	1.73-1.76 Å
554-577	5UVG WW5M	556-575	1.41-3.03 Å	1.55-2.95 Å
	5UVG MBW	555-563	1.05-3.35 Å	1.23-3.36 Å
586-601	5UVG WW5M	588-594	1.12-5.22 Å	1.30-7.82 Å
	5UVG MBW	588-594	1.08-4.90 Å	1.79-4.64 Å
618-620	5UVG WW5M	619	1.05-1.21 Å	1.39-2.18 Å
	5UVG MBW	619-620	1.43-1.94 Å	2.20-2.33 Å

Table 4.17. Backbone and ligand (SM) RMSD values after equilibrium.

Structure	**Time (ns)**	**Equilibrium Reached (ns)**	**RMSD Backbone (Å)**	**Ligand RMSD (wrt Protein, Å)**	**Ligand RMSD (wrt Ligand, Å)**
2UYR MBW	100	10	1.4-1.8	4.8-5.6	2.5-3.0
2UYR WW5M	300	50	1.75-2.0	2.5-3.2	1.6-2.4
2DDS MBW	100	30	1.6-1.8	2.5-3.4	1.9-2.4
5UVG MBW	500	250	3.8-4.0	6.0-7.5	2.5-3.0
5UVG WW5M	500	210	2.8-3.2	7.0-8.0	3.8-4.5

4.2.2. Secondary Structure Analysis

Secondary structure analysis of Schrödinger software shows the secondary structural elements (SSE) maintained or distorted throughout the simulation. The SSE plots are given in the Appendix A (see Figure A.2 to Figure A.4). The regions that were distorted as the simulations proceeded are summarized in Table 4.18 for each protein structure. These regions were investigated in section 4.2.5.

Helix 123-129 (DK switch helix) is present in the crystal structure of 2UYR, while it is a loop in the crystal structure of 2DDS. This helical structure was distorted in apo 2UYR structures, yet almost maintained (slightly distorted) in SM-bound 2UYR structures.

Sheet 279-283 and Sheet 286-290 correspond to the beta hairpin structure of *Bc*-SMases which was reported to take part in membrane binding. This region mainly consists of hydrophobic residues including (F284 and W285) and not directly take part in the catalytic activity. Hence, the distortion in this region is disregarded.

Helix 209-219 and Helix 232-244 regions are distorted in the case of apo *Bc*-SMases, however according to SSE analysis these regions are mainly preserved with

SM binding. Among the distorted regions only Helix 232-244 has high RMSF values, however with SM binding it become stable as seen in Table 4.15.

Table 4.18. Distorted regions according to the SSE analysis. The regions shown with asterisks are slightly distorted compared to the other tabulated regions.

Structure	**Distorted Regions**
Apo 2UYR WW5M	Helix 123-129, Helix 209-219*, Helix 237- 244
Apo 2UYR MBW	Helix 29-39*, Helix 123-129, Helix 209-219*, Helix 237- 244, Helix 253-257*, Sheet 279-283, Sheet 286-290
SM-bound 2UYR WW5M	Helix 123-129*, Sheet 279-283, Sheet 286-290
SM-bound 2UYR MBW	Helix 123-129*, Helix 237-244
Apo 2DDS WW5M	Helix 29-39*, Helix 209-219, Sheet 279-283, Sheet 286-290
Apo 2DDS MBW	Helix 209-219*, Helix 237- 244
SM-bound 2DDS MBW	Helix 209-219*, Helix 237- 244*
Apo 5UVG WW5M	Sheet 346-350*, Helix 388-393, Helix 517-519, Helix 520-525
Apo 5UVG MBW	Helix 146-164*, Helix 388-393, Helix 517-519, Helix 520-525
SM-bound 5UVG WW5M	Sheet 346-350*, Helix 388-393, Helix 517-519, Helix 520-525, Helix 564-573*, Helix 574-582*, Helix 595-599*
SM-bound 5UVG MBW	Helix 146-164*, Helix 388-393, Helix 517-519, Helix 520-525, Helix 527-531*, Helix 564-573, Helix 595-599

According to the SSE analysis conducted on human nSMase2 simulations, in all cases, Helix 388-393, Helix 517-519 and Helix 520-525 are distorted. In WW5M structures of 5UVG, a small helical conformation was observed in the DK switch region. A slight distortion was also observed in the Helix 564-573, Helix 574-582 and Helix 595-599. These distorted regions on 5UVG also have high RMSF values as seen in Table 4.16, and they do not become stable with SM binding.

4.2.3. Binding Free Energies of SM During MD Simulations

The binding free energies between SM and the protein structures were computed by using MM/GBSA tool in Schrödinger Suite. The results are given in Table 4.19 and Table 4.20. Avg_{eq} and $StDev_{eq}$ are the average and standard deviation values calculated after the systems reached equilibrium (see Table 4.17).

2DDS MBW and 2UYR WW5M have the lowest mean binding free energies (after equilibrium) with -64 kcal/mol compared to the other protein structures indicating that SM bound to them tightly. 2UYR MBW follows these structures with a mean binding free energy around -61 kcal/mol. SM bound to 5UVG MBW with a mean binding free energy of -60 kcal/mol, while it bound to 5UVG WW5M with a mean binding free energy of -39 kcal/mol suggesting that SM bound loosely to 5UVG WW5M.

A 100 ns MD simulation was also carried out for d11:1C9-SM bound 2DDS WW5M pose (see Figure 4.4b) to test the stability of this binding mode. However, the binding mode observed for this pose was different from the proposed binding mode by Ago *et al.* [2]. MM/GBSA results also showed that SM did not bind to 2DDS WW5M effectively with a mean binding free energy of -37 kcal/mol in this binding mode.

4.2.4. Protein-Ligand Interactions

4.2.4.1. 2UYR-SM Interactions. The protein-ligand contacts and timeline of these contacts are shown in Figure 4.17 and Figure 4.18. These plots show that d11:1C9-SM forms several interactions with 2UYR WW5M which contribute its stability in the binding pocket.

Glu53 and Mg interactions were seen in both 2UYR MBW and 2UYR WW5M. Asp126, Glu155, Asp156, Asn197, Trp232 and Phe244 mainly interacted with 2UYR WW5M. While DK residue Lys131 formed direct interactions mainly with 2UYR MBW, this residue maintained its salt bridge with Asp126 which in turn formed in-

Table 4.19. Binding free energies computed for WW5M structures. Avg, StDev and eq stand for average, standard deviation and equilibrium, respectively.

2UYR (300 ns)		**2DDS (100 ns)**		**5UVG (500 ns)**	
Frame	**ΔG (kcal/mol)**	**Frame**	**ΔG (kcal/mol)**	**Frame**	**ΔG (kcal/mol)**
0	-62.86	0	-60.77	0	-81.12
2400	-54.06	800	-42.10	4000	-44.54
4800	-57.87	1600	-41.61	8000	-43.48
7200	-70.82	2400	-54.59	12000	-50.02
9600	-64.38	3200	-29.88	16000	-54.03
12000	-55.72	4000	-36.80	20000	-38.11
14400	-61.40	4800	-37.59	24000	-42.64
16800	-61.94	5600	-39.85	28000	-42.26
19200	-58.41	6400	-56.36	32000	-32.04
21600	-62.73	7200	-45.03	36000	-39.23
24000	-57.94	8000	-19.29	40000	-52.43
26400	-55.10	8800	-46.68	44000	-42.78
28800	-56.75	9600	-36.38	48000	-41.43
31200	-57.32	10400	-44.98	52000	-19.02
33600	-78.34	11200	-19.68	56000	-35.78
36000	-43.32	12000	-52.48	60000	-47.39
38400	-71.31	12800	-43.86	64000	-50.06
40800	-44.66	13600	-49.01	68000	-36.33
43200	-70.55	14400	-30.76	72000	-33.54
45600	-70.06	15200	-41.83	76000	-29.92
48000	-68.73	16000	-20.94	80000	-47.27
50400	-79.76	16800	-32.13	84000	-49.03
52800	-41.18	17600	-33.03	88000	-45.93
55200	-72.61	18400	-18.91	92000	-36.66
57600	-58.58	19200	-23.83	96000	-27.45
60000	-83.24	20000	-44.29	100000	-41.00
62400	-64.55	20800	-39.32	104000	-43.96
Avg	-62.38	Avg	-38.59	Avg	-42.50
StDev	10.46	StDev	11.56	StDev	11.13
Avg_{eq}	-64.59	Avg_{eq}	-36.96	Avg_{eq}	-38.98
$StDev_{eq}$	13.72	$StDev_{eq}$	11.33	$StDev_{eq}$	8.91

Table 4.20. Binding free energies computed for MBW structures. Avg, StDev and eq stand for average, standard deviation and equilibrium, respectively.

2UYR (100 ns)		**2DDS (100 ns)**		**5UVG (500 ns)**	
Frame	**ΔG (kcal/mol)**	**Frame**	**ΔG (kcal/mol)**	**Frame**	**ΔG (kcal/mol)**
0	-68.52	0	-61.78	0	-87.64
800	-79.76	800	-64.31	4000	-59.88
1600	-63.69	1600	-76.50	8000	-67.18
2400	-64.59	2400	-66.50	12000	-43.27
3200	-71.33	3200	-69.12	16000	-56.14
4000	-57.74	4000	-73.93	20000	-59.94
4800	-64.02	4800	-76.56	24000	-46.89
5600	-61.69	5600	-78.40	28000	-62.79
6400	-60.95	6400	-70.71	32000	-67.84
7200	-44.95	7200	-68.14	36000	-62.18
8000	-47.99	8000	-69.54	40000	-32.94
8800	-49.00	8800	-67.11	44000	-51.07
9600	-51.13	9600	-65.31	48000	-46.35
10400	-70.61	10400	-61.27	52000	-50.01
11200	-61.08	11200	-61.52	56000	-35.67
12000	-63.99	12000	-51.67	60000	-61.36
12800	-64.72	12800	-66.31	64000	-63.49
13600	-65.33	13600	-65.56	68000	-62.44
14400	-53.73	14400	-68.82	72000	-69.96
15200	-85.17	15200	-59.88	76000	-56.50
16000	-56.96	16000	-60.09	80000	-31.16
16800	-62.75	16800	-53.80	84000	-64.01
17600	-54.97	17600	-61.65	88000	-67.77
18400	-68.62	18400	-64.32	92000	-76.93
19200	-70.04	19200	-68.59	96000	-72.34
20000	-72.00	20000	-84.14	100000	-73.54
20800	-52.75	20800	-60.71	104000	-63.59
Avg	-62.52	Avg	-66.53	Avg	-59.00
StDev	9.44	StDev	7.25	StDev	13.44
Avg_{eq}	-61.50	Avg_{eq}	-64.69	Avg_{eq}	-60.63
$StDev_{eq}$	9.22	$StDev_{eq}$	6.96	$StDev_{eq}$	13.48

teractions with SM in the active site of 2UYR WW5M. These results supports the putative role of the helical conformation of DK Switch and Asp 126 in the catalysis suggested by Airola *et al.* [1].

The binding mode of d11:1C9-SM is preserved throughout the 100 ns simulation for 2UYR WW5M while it is slightly distorted for 2UYR MBW as seen in Figure 4.19. The helical conformation of DK Switch region is maintained throughout in 2UYR WW5M case as seen in Figure 4.20. This helical conformation began to be distorted towards the end of the 2UYR MBW MD simulation, i.e. Asp126 started to move away from Lys131 (see Figure 14.21). In apo 2UYR MD simulations, the helical conformation of the DK Switch region was distorted after 100 ns. Hence to test whether this helical conformation was preserved in SM-bound 2UYR WW5M case, the simulation was extended to 300 ns.

DK switch residues and other important residues of 2UYR MBW and 2UYR WW5M that take part in SM binding are shown in Figure 14 and Figure 15, respectively. The initial binding mode of d11:1C9-SM is mainly preserved throughout the simulation of 2UYR WW5M as seen in Figure 4.20. In contrast to 2UYR MBW case, in 2UYR WW5M, the helical conformation of the DK Switch loop is preserved, and Asp126 maintains its interaction with Lys131 and takes part in SM-binding. Phe244 also forms and preserves pi-cation interactions with the amino group of SM.

The initial binding mode of d11:1C9-SM docked 2UYR MBW changes as time passes as seen in Figure 4.21, and Asp126 starts to move away from Lys131 towards the end of the simulation. Asp126 does not participate in SM binding. The side chain of Phe244 also moves away the active site and breaks its pi-cation interaction with the amino group of SM towards the end of the simulation (see Figure 4.21).

4.2.4.2. 2DDS-SM Interactions. The protein-ligand contacts and timeline of the contacts are shown in Figure 4.22 and Figure 4.23. These plots indicate that the active site residues Glu53, Asp195, Asn197 and Asp295, the cobalt ion and the DK Switch

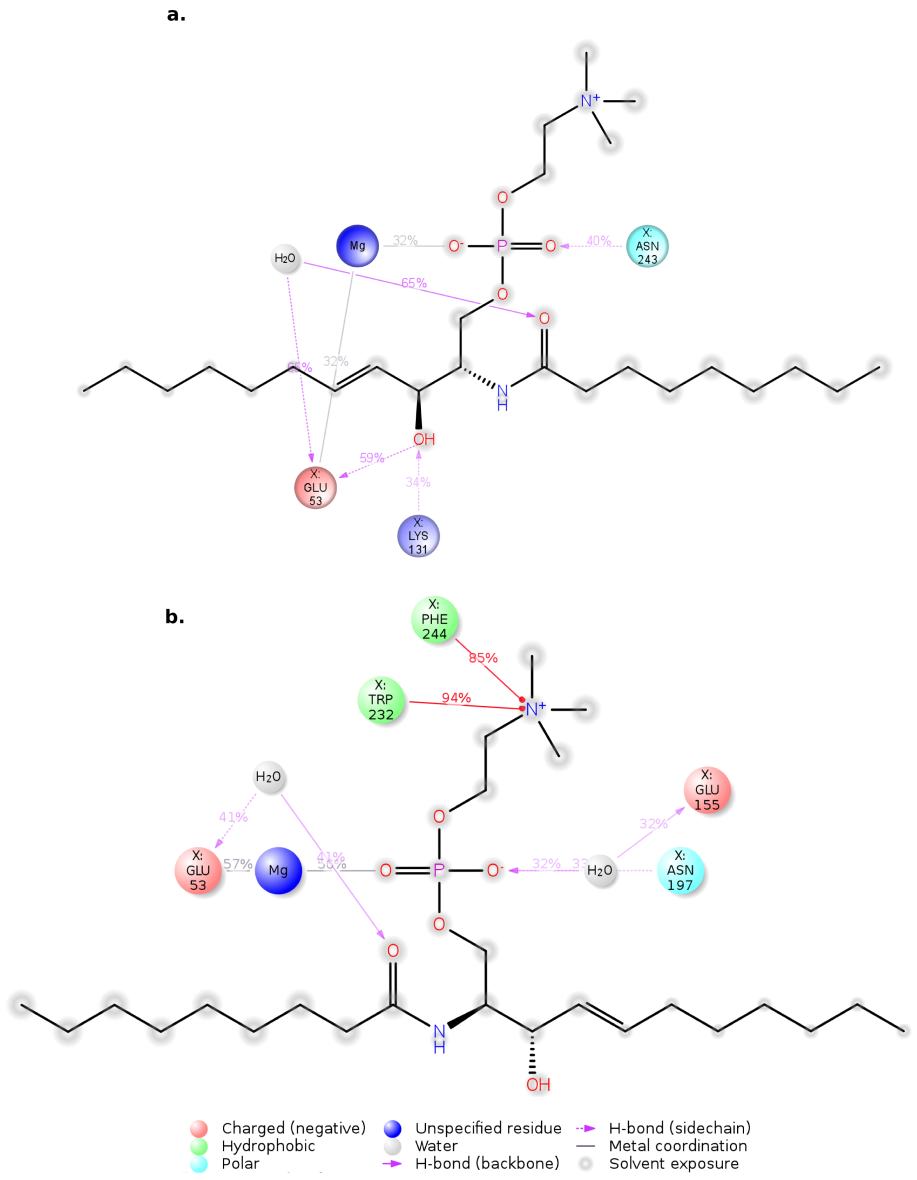

Figure 4.17. Protein-ligand interaction map of protein-ligand interactions of SM-docked 2UYR MBW (a) and SM-docked 2UYR WW5M (b). Only the interactions that occurred more than 30% of the simulation time are depicted.

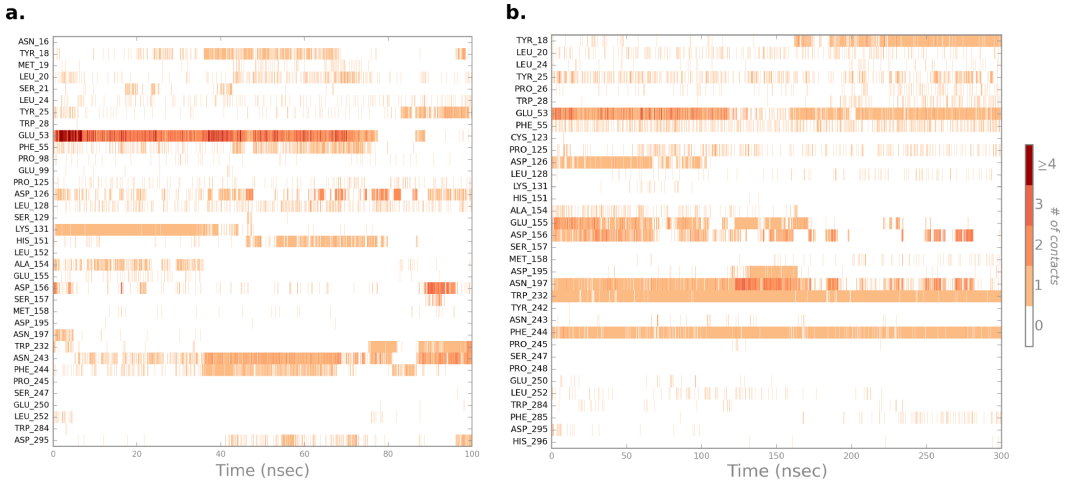

Figure 4.18. Protein-ligand interaction timeline of SM-docked 2UYR MBW (a) and SM-docked 2UYR WW5M (b).

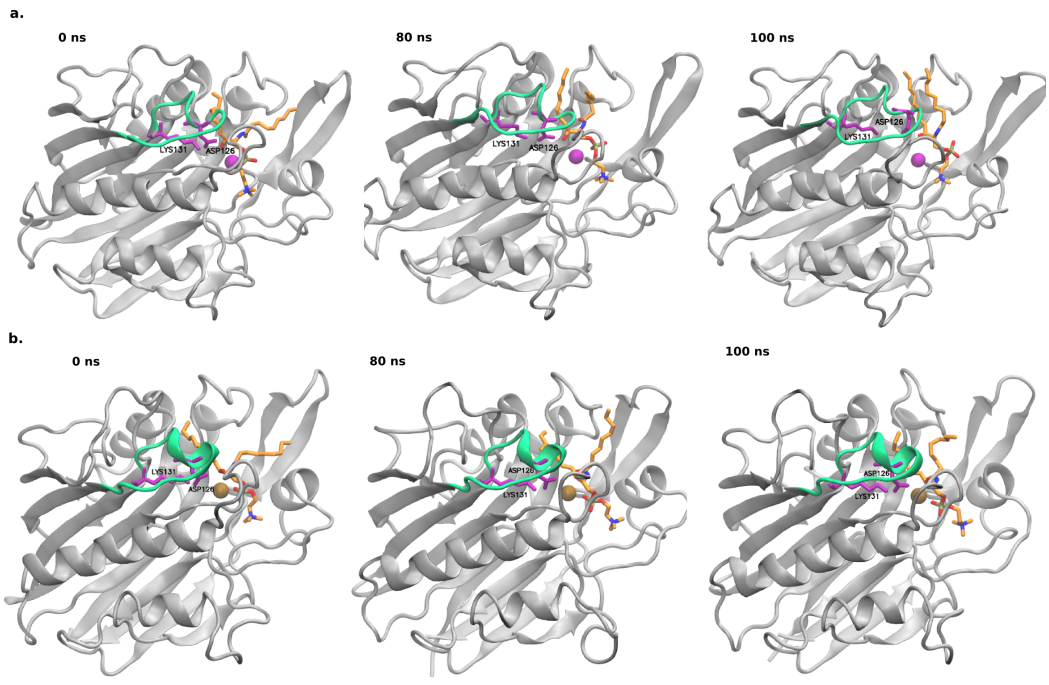

Figure 4.19. Snapshots of SM-docked 2UYR MBW (a) and WW5M (b) simulations taken at 0 ns, 80 ns and 100 ns. DK switch (residues 119-131) is colored in green. C9-SM and DK residues are shown in orange and purple licorice forms, respectively.

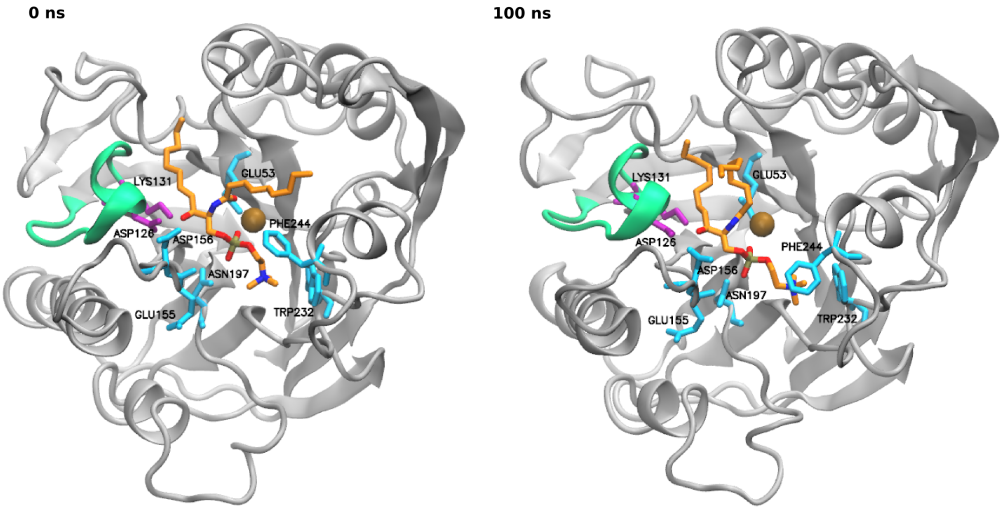

Figure 4.20. Snapshots of SM-bound 2UYR WW5M simulation at 0 ns and 100 ns. DK switch loop, magnesium, C9-SM, DK residues and some of the important residues for SM binding are colored in green, brown, orange, purple and cyan, respectively.

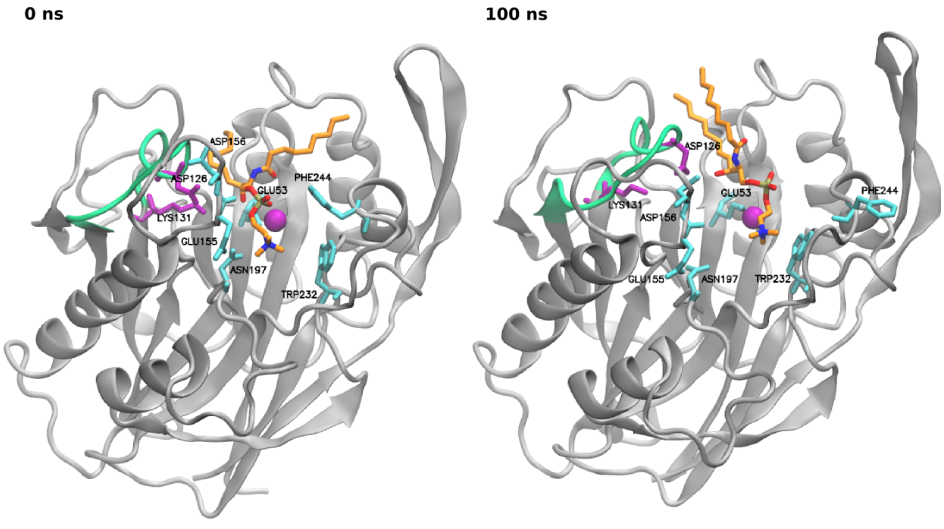

Figure 4.21. Snapshots of SM-bound 2UYR MBW simulation at 0 ns and 100 ns. DK switch loop, C9-SM, DK residues and some of the important residues for SM binding are colored in green, orange, purple and cyan, respectively.

residue Lys131 play an important role in SM binding for 2DDS MBW. However, as seen in Figure 4.23, Lys131 and Asn197 contacts seem to be lost towards the end of the simulation. The loss of contact of Lys131 can also be seen in Figure 4.24. According to the timeline of the contacts, Leu20, His151 and Leu152 also form interactions with SM as the simulation proceeded. The binding mode of d11:1C9-SM is preserved throughout the simulation and no helical conformation is observed in DK Switch region as seen in Figure 4.24.

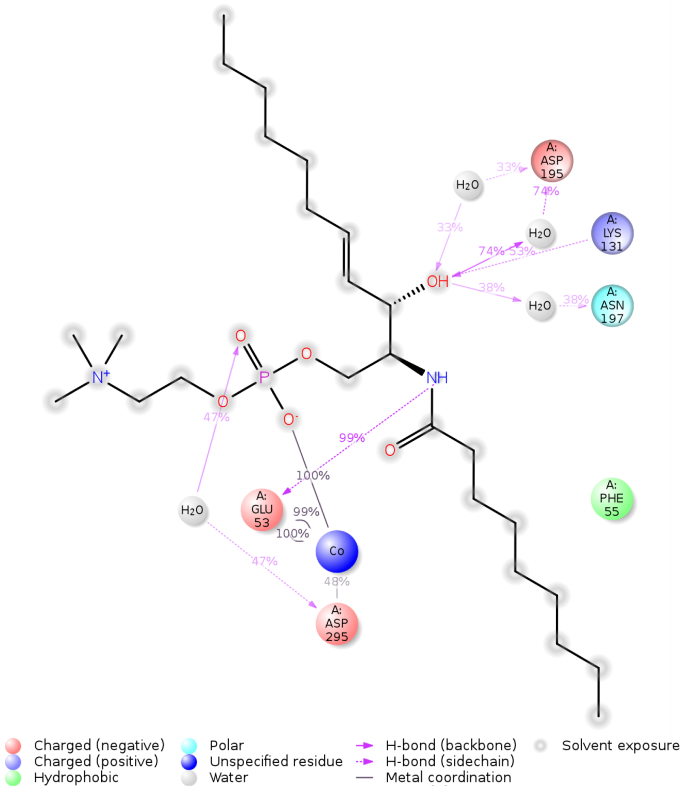

Figure 4.22. Protein-ligand interaction map of 2DDS MBW. Only the interactions that occurred more than 30% of the simulation time are depicted.

4.2.4.3. 5UVG-SM Interactions. SM ligand mainly interacted with Ca701, Glu364 and Asp638 (correspond to Glu53 and Asp295 in *Bc*-SMases) on 5UVG MBW and MMW5 structures as seen Figure 4.25 to Figure 4.26. Glu53 interaction was also observed in the MD simulations of the *Bc*-SMases. Both 5UVG structures mainly interacted with the phosphate moiety of SM, hence SM ligand was mobile throughout the simulation

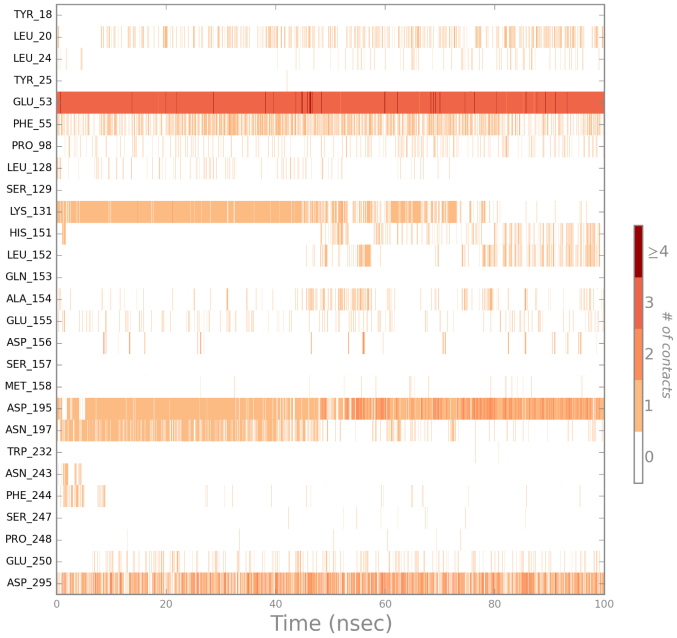

Figure 4.23. Protein-ligand interaction timeline of SM-docked 2DDS MBW. The number of contacts includes h-bond, hydrophobic, water-bridge and ionic interactions.

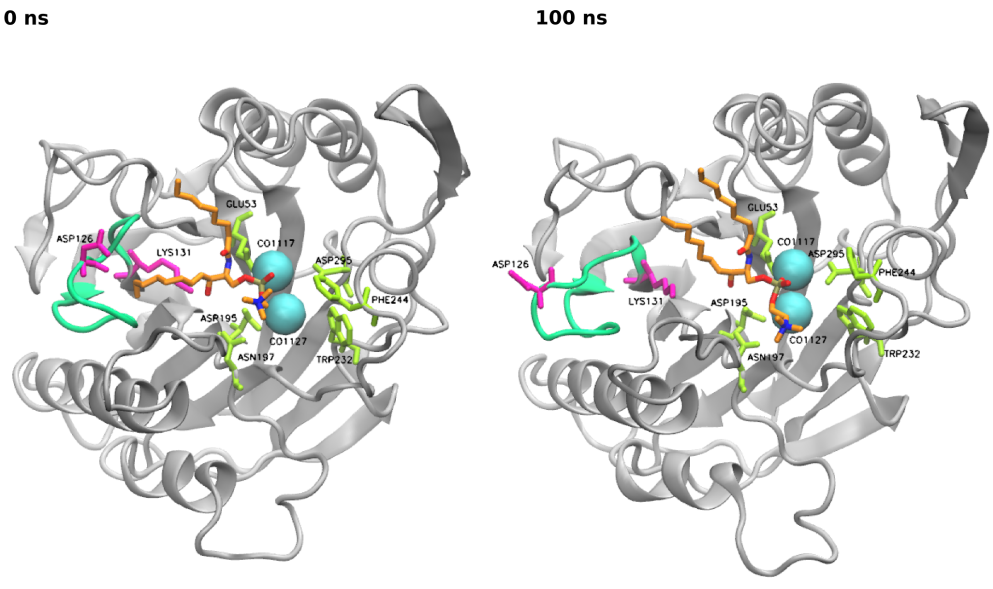

Figure 4.24. Snapshots of SM-bound 2DDS MBW simulation at 0 ns and 100 ns. DK switch loop, cobalt ions, C9-SM, DK residues and some of the important residues for SM binding are colored in green, cyan, orange, magenta and lime, respectively.

but it did not diffuse away from the protein due to the metal coordination of the phosphate moiety as seen in Figure 4.27.

The initial binding mode of d11:1C9-SM in 5UVG MBW and 5UVG WW5M observed in the docking simulations is not maintained in the MD simulations carried out on these poses (see Figure 4.27). Asp430 did not form interactions with Lys435 in both 5UVG MD simulations.

4.2.4.4. Comparison of Protein-SM Interactions for *Bc*-SMases and Human nSMase2. Taken together, the binding mode between SM and the structures; 2DDS MBW and 2UYR WW5M seem to be maintained throughout the simulation. In the MD simulation of 2UYR WW5M, the helical conformation of the DK Switch region was maintained throughout the simulation, and Asp126 participated in SM binding. However, this was not observed in the MD simulation of SM-docked 2UYR MBW.

In 5UVG case, for both structures, especially for 5UVG WW5M, d11:1C9-SM did not maintain its initial binding mode. Many of the protein-ligand contacts were lost as the simulation proceeded. However, MM/GBSA results indicate that SM bound to 5UVG MBW better than 5UVG WW5M.

The protein-ligand interactions observed are summarized in Table A.1. The residues on 5UVG that are homologous to the tabulated *Bc*-SMase residues are written across their corresponding *Bc*-SMase residues.

4.2.5. Comparative Conformational Analysis of Apo and SM-Bound *Bc*-SMases and Human nSMase2

4.2.5.1. Apo and SM-Bound 2UYR. MD simulations performed on 2UYR were analyzed by paying special attention to the regions and the residues presented in Table 4.15, Table 4.18, Figure 4.17 and Figure 4.18. In 2UYR WW5M case, the regions 21-29, 120-130, 155-166 and 240-249 were stabilized with SM binding, indicating that

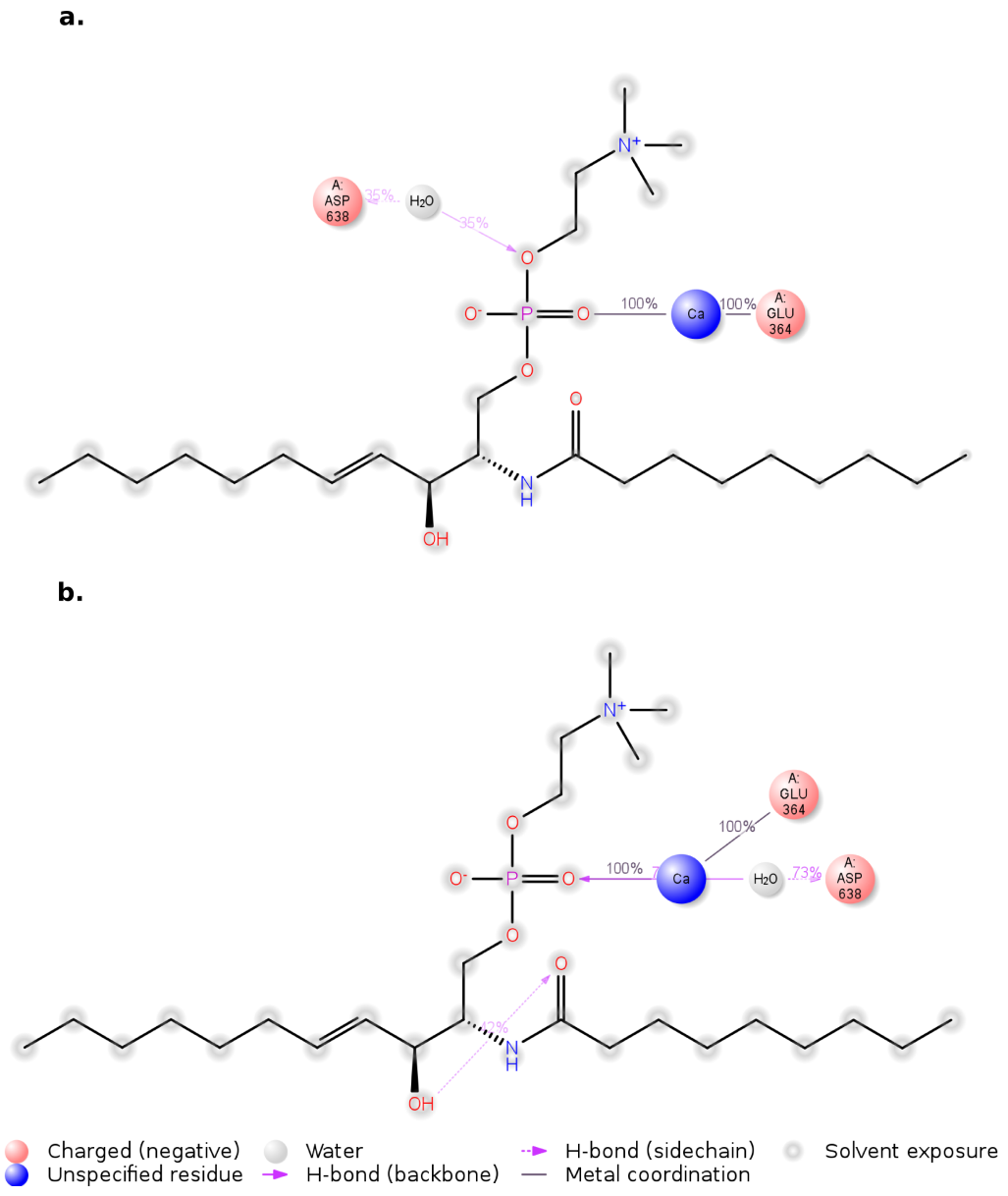

Figure 4.25. Protein-ligand interaction map of SM-docked 5UVG MBW (a) and SM-docked 5UVG WW5M (b). Only the interactions that occurred more than 30% of the simulation time are depicted.

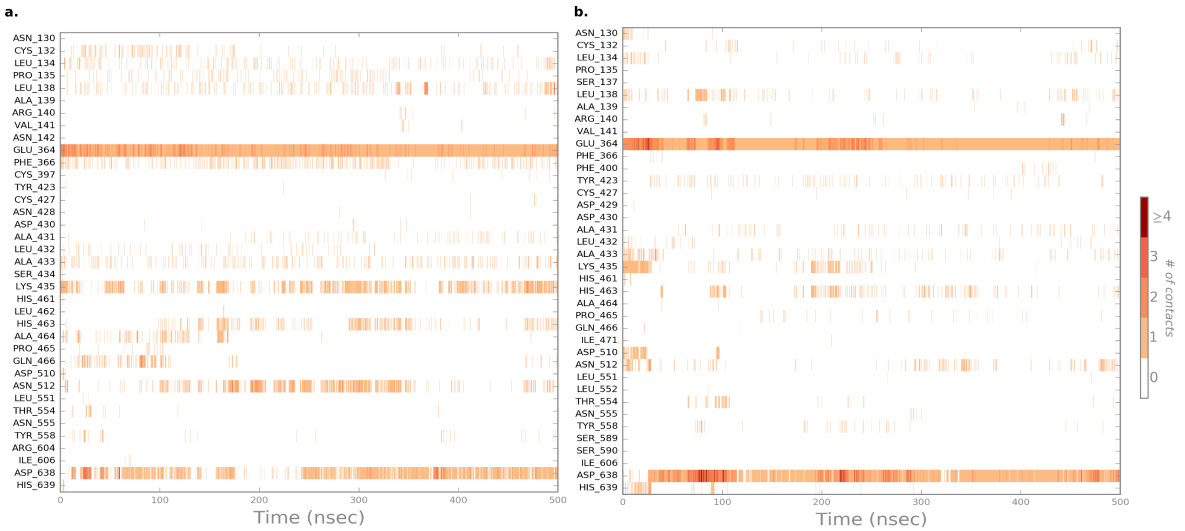

Figure 4.26. Protein-ligand interaction timeline of SM-docked 5UVG MBW (a) and SM-docked 5UVG WW5M (b).

some of the residues in these regions were possibly taking part in the binding of SM to 2UYR. To find these residues, the protein-ligand interaction diagrams were analyzed (see Figure 4.17 and Figure 4.18). First frames and last frames of the MD simulations of the apo and SM-bound 2UYR WW5M were aligned among themselves in Figure 4.28 to depict the conformational changes that some of the important regions surrounding the active site underwent.

According to Figure 4.18 and Figure 4.23, Ser21-Gly29 loop become stable through the hydrophobic interactions made by Tyr18, Leu20 and Tyr25 with SM. This loop was closer to the active site in SM-bound structure, while it remained mobile and distant from the active site in apo case (see Figure 4.28).

Phe119-Lys131 is in helical conformation in the crystal structure of 2UYR, and it is known as the DK switch loop. As stated before, this region was suggested to take part in the catalytic mechanism [1], and this hypothesis required a further validation. Hence, in this study, this region was analyzed carefully. In apo 2UYR simulation, DK Switch lost its helical conformation and Asp126(D)-Lys131(K) interaction was broken in 115

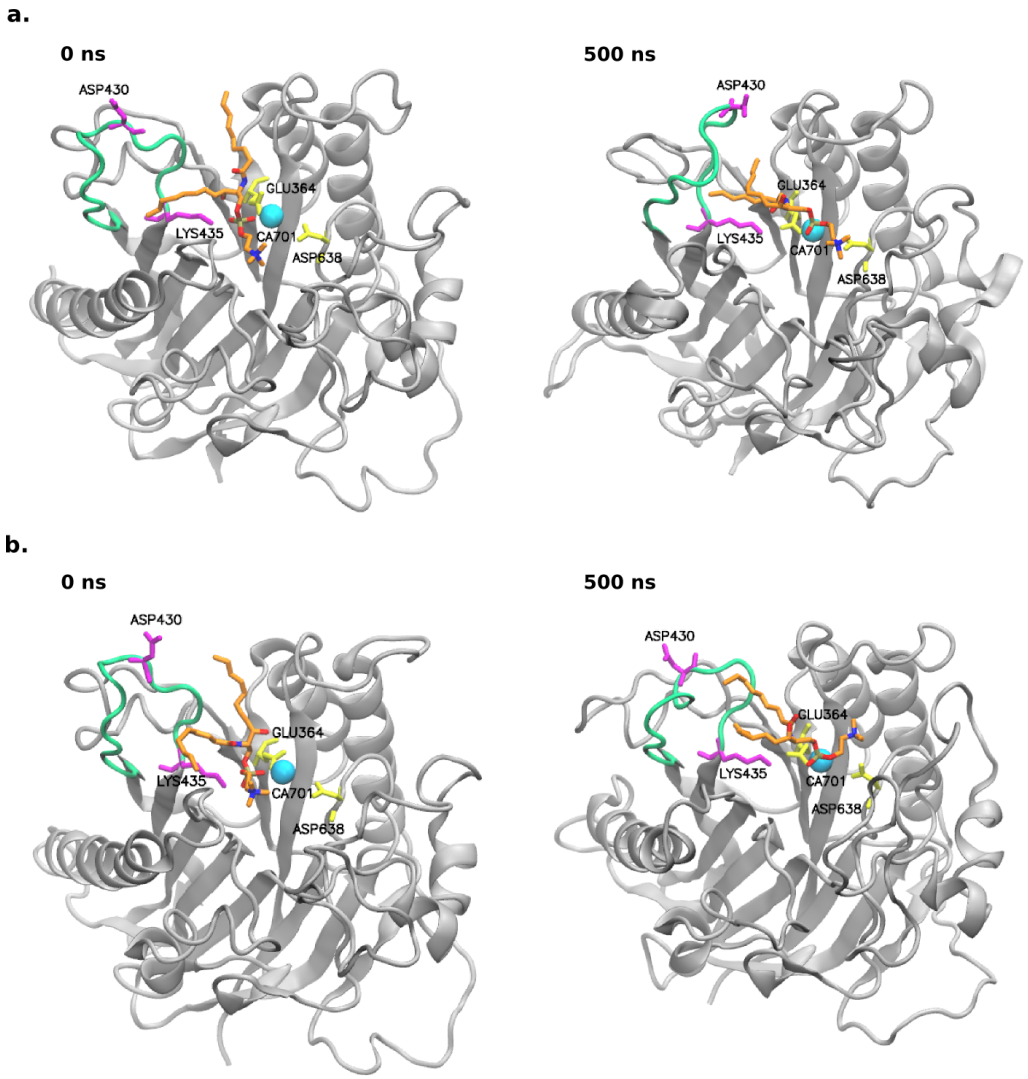

Figure 4.27. Snapshots of SM-bound 5UVG MBW (**a**) and SM-bound 5UVG WW5M (**b**) simulations taken at 0 ns and 500 ns. DK switch loop is colored in green.

ns and Asp126 directed itself away from the active site as seen in Figure 4.29. However, in SM-bound 2UYR WW5M case, the helical structure was maintained throughout the simulation and Asp126 formed salt bridge with Lys131 and hydrogen bonding with SM (see Figure 4.29). However, Asp126-SM interaction was broken down after 105 ns, while Asp126-Lys131 salt bridge maintained throughout the simulation. According to the catalytic mechanism proposed by Ago *et al.* [2] (see Figure 2.6), Lys131 formed interactions with SM, but this interaction was not seen in SM-bound 2UYR WW5M. SM formed hydrophobic interactions with Pro125 throughout the simulation.

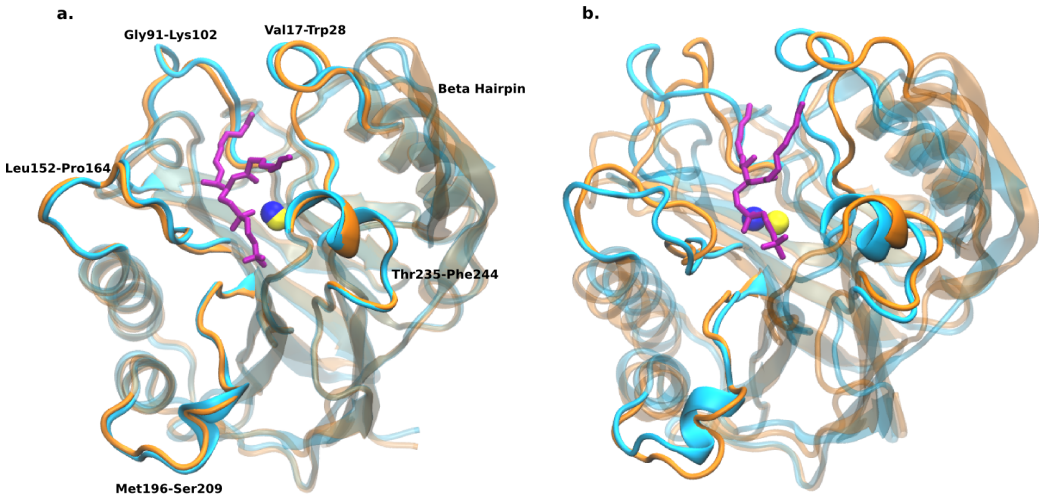

Figure 4.28. Alignment of the first frames (a) and last frames (b) of the simulations of apo (orange) and SM-bound (cyan) 2UYR WW5M with a focus on the active site. Magnesium ions of apo and SM-bound structures are shown in blue and yellow.

Glu155-Ser166 loop is an interesting region. This region has Glu155 and Asp156 residues which interact with SM through water-bridge interactions. Asp156 was coordinated by the magnesium ion at the active site in the apo case, hence the loop shifted towards the active site because of this metal coordination. However, when SM was bound to 2UYR, this loop did not shift towards the active site like seen in the apo case, since it formed interactions with SM instead of being coordinated by the magnesium ion. As seen in Figure 4.28, this loop is closer to the active site in the case of apo 2UYR WW5M (orange). The metal coordination of Asp156 in apo 2UYR can be seen in Figure 4.30.

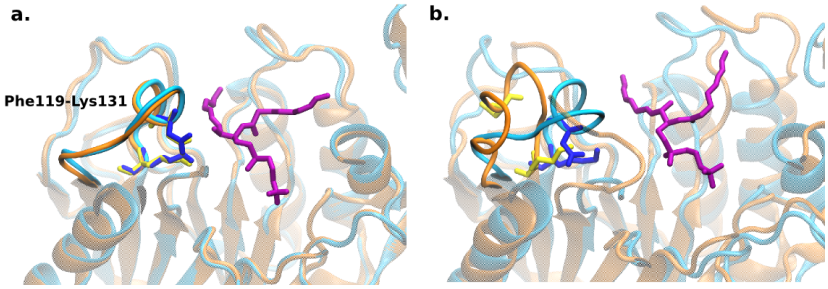

Figure 4.29. Alignment of the first frames (a) and last frames (b) of the simulations of apo (orange) and SM-bound (cyan) 2UYR WW5M with a focus on the DK switch. The residues of apo and SM-bound 2UYR WW5M are shown in yellow and blue.

Ala240-Ala249 region also become stable with SM binding possibly due to the pi-cation interactions between Phe244 and amino group of SM. Trp232 and Phe244 seem to be important for the binding of SM especially the amino group of SM. In apo case, helix Asn237-Phe244 moves away from the active site and become distorted, hence this region was highly mobile. This was not seen in SM-bound 2UYR. As seen in Figure 4.30, Phe244 interacted with SM, whereas it directed itself away from the active site in apo case. Hence this residue seems to be important for the stability of the helix Asn237-Phe244.

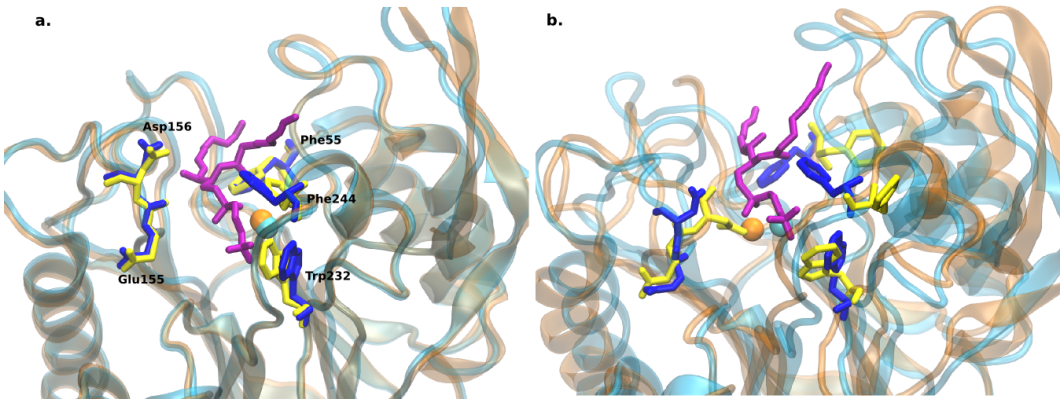

Figure 4.30. Alignment of the first (a) and last (b) frames of the simulations of apo (orange) and SM-bound (cyan) 2UYR WW5M focusing on the important residues. The residues of apo and SM-bound structures are shown in yellow and blue.

The active site residues are shown in Figure 4.31 for 0 ns and the last frame of each MD simulation. As it can be seen, His151 looks towards SM whereas in apo case its side chain directs itself away from the active site. Interestingly, protein-ligand contacts show that His151 did not form interactions with SM ligand. The active site residues are more compact, i.e. close to each other, in SM-bound case.

Phe55 is not named under active site residues, but it is one of the highly conserved residues that seems to be important for SM binding. As seen in His151, Phe55 also directs itself away from the active site in apo case. However, it becomes stable and formed hydrophobic interactions with SM in SM-bound case as seen in Figure 4.30.

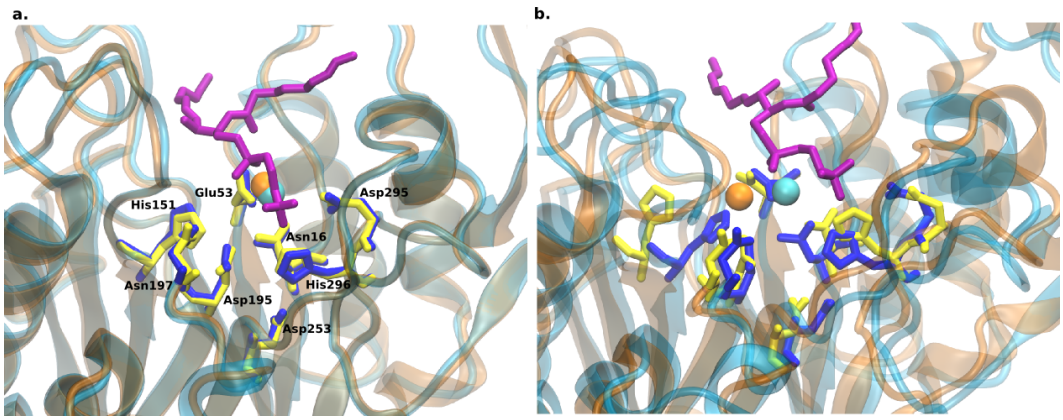

Figure 4.31. Alignment of the first (a) and last (b) frames of the simulations of apo (orange) and SM-bound (cyan) 2UYR WW5M focusing on the active site residues. The residues of apo and SM-bound structures are shown in yellow and blue.

MD simulations results show that among the active site residues, Glu53 and Mg1306 are crucial for SM binding. They interacted with the phosphate moiety of SM as seen in Figure 4.17. The importance of Glu53 and the active site metal ion in SM binding was also mentioned in the literature [1, 2]. Hence the contributions of these residues were also seen in the MD simulations that were performed in this study.

The active site residue, Asn197 plays an important role in SM binding. It formed hydrogen-bonding and water-bridge with the phosphate moiety of SM. When the apo and SM-bound MD simulations were compared, it was seen that Asp195 and Asn197

almost maintained their positions and remained stable in both MD simulations, while Asp295 and His296 was stabilized with SM binding.

Asn92-Pro98, Ile201-Asp208 and Val281-Lys287 regions remained mobile even when SM was bound to 2UYR WW5M. These regions were not close to the active site compared to the other aforementioned regions. Asn92-Pro98 and Val281-Lys287 were suggested to be involved in the binding of the protein to the membrane [2]. Hence they possibly do not affect the catalytic mechanism directly. Val281-Lys287 corresponds to the beta-hairpin region. The region mainly consists of hydrophobic residues and it was distorted especially during SM-bound simulation. However, this was disregarded since the focus of this study was on the active site and this region did not directly take part in the catalytic mechanism.

A small helix was formed in Ile201-Ser209 region in SM-bound 2UYR WW5M, and this was not seen in apo case (see Figure 4.28). However, this region is not close to the active site hence it is likely that this region does not affect the catalytic mechanism directly. Even though it formed a helical conformation, it remained mobile throughout the simulation.

MD simulation results for SM-bound 2UYR MBW were similar to those for SM-bound 2UYR WW5M. Ser21-Gly29, Phe119-Lys131, Glu155-Ser166 and Ala240-Ala249 regions were stabilized with SM binding through similar SM interactions. Val281-Lys287 region was also highly mobile in SM-bound 2UYR MBW case. However, there were also differences between these simulations. The most notable difference was the loss of Glu53-SM interaction towards 80 ns and with the loss of this interaction, SM slightly shifted towards Glu155-Ser166 loop. In addition, Ala240-Ala249 region become mobile towards the end of the simulation due to the loss of Phe244-SM interaction. Amino group of SM become also mobile since Phe244 moved away from the active site. The loss of these interactions caused SM to lose its initial binding mode.

Asp126-Lys131 salt bridge was also broken down at the end of the simulation of SM-bound 2UYR MBW. Hence the helical conformation of DK switch loop preserved until the last nanosecond. Lys131 formed interactions with SM at the beginning of the simulation, however this interaction was lost after 50 ns. Asp126 formed transient interactions with SM throughout the simulation, this interaction also appeared to be lost towards the end of the simulation, especially after the loss of interaction between Glu53 and SM. In apo 2UYR MBW simulation, Asp126-Lys131 salt bridge was also broken down after 95 ns.

Ile201-Ser209 of SM-bound 2UYR MBW did not form a small helix as seen in the simulation of SM-bound 2UYR WW5M. However, it was more stable in SM-bound 2UYR MBW compared to SM-bound 2UYR WW5M.

Taken together, MD simulations results for SM-bound 2UYR WW5M were better than those for SM-bound 2UYR MBW. The binding free energy was also better for SM-bound 2UYR WW5M (see Table 4.20 and Table 4.19). The protein-ligand contacts were in accordance with the literature in the case of 2UYR WW5M.

4.2.5.2. Apo and SM-Bound 2DDS. MD simulations performed on 2DDS were analyzed by paying special attention to the regions and the residues presented in Table 4.15, Table 4.18, Figure 4.22 and Figure 4.23. In 2DDS case, the regions 21-29, 92-98, 155-166, 201-208 and 240-249 were stabilized with SM binding, indicating that some of the residues in these regions were possibly taking part in the binding of SM to 2DDS. To find these residues, the protein-ligand interactions shown in Figure 4.22 and Figure 4.23 were analyzed. First frames and last frames of the MD simulations of the apo and SM-bound 2DDS MBW were aligned among themselves in Figure 4.32 to depict the conformational changes that some of these important regions surrounding the active site underwent.

Ser21-Gly29 loop become stable possibly through the hydrophobic interactions made by Leu20 with SM. This loop was closer to the active site in SM-bound structure,

while it remained mobile and distant from the active site in apo case hence become distorted (see Figure 4.32).

The loop region Asn92-Pro98 become less mobile with SM binding, and it did not go through large conformational changes in SM-bound case as seen in Figure 4.32. This is possibly due to the hydrophobic interactions formed between Pro98 and the tails of SM. However, the tails of SM are normally embedded in PM and to what extent it is extracted from PM is still not known. Hence the stabilization of this loop might not be related with the catalytic activity of SMases. This interaction was also not seen in the case of 2UYR WW5M.

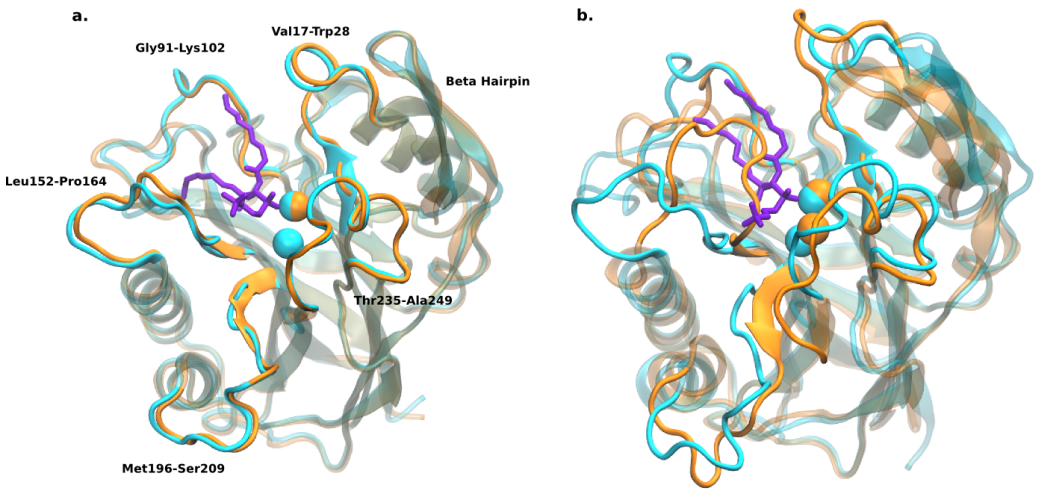

Figure 4.32. Alignment of the first frames (a) and last frames (b) of the simulations of apo (orange) and SM-bound (cyan) 2DDS MBW with a focus on the region surrounding the active site.

Phe119-Lys131 loop remained mobile in both apo and SM-bound cases. No salt bridge was formed between Asp126 and Lys131, hence no helical conformation was observed in this region of 2DDS. Asp126 did not direct itself towards the active site throughout the simulation. Lys131 formed hydrogen-bonding with SM, however this interaction was broken after 80 ns. The DK switch regions of apo and SM-bound 2DDS are seen in Figure 4.33.

Glu155-Ser166 loop is an interesting region. This region has His151, Leu152 and Glu155 residues interacting with SM through water-bridge interactions. Glu155 was coordinated by the active site metal ion (cobalt) at the active site in the apo case (see Figure 4.34), hence the loop shifted towards the active site because of this metal coordination. When SM was bound to 2DDS, this loop did not shift towards the active site like seen in the apo case. This observation was in accordance with the findings of Sergellius *et al.* [30]. They also reported that this loop region adjusted its conformation to accommodate SM [30]. When apo and SM-bound structures are aligned, it can be seen that this loop overlaps the space occupied by SM as seen in Figure 4.32. In apo 2UYR WW5M case, Asp156 was coordinated by the active site metal ion, magnesium.

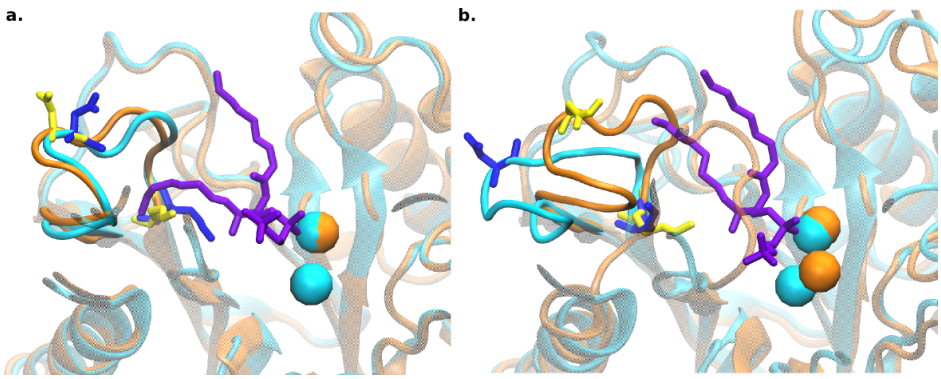

Figure 4.33. Alignment of the first frames (a) and last frames (b) of the simulations of apo (orange) and SM-bound (cyan) 2DDS MBW with a focus on the DK switch. The residues of apo and SM-bound 2DDS MBW are shown in yellow and blue.

The pi-cation interactions formed between the residues; Trp232 and Phe244 and the amino group of SM were transient in 2DDS. These pi-cation interactions were important for the stabilization of the amino group of SM ligand in the binding site of 2UYR.

Glu53 and active site cobalt ions were important for the binding of SM to the active site of 2DDS. The importance of Glu53 and the active site ion was also seen in the 2UYR case. In addition to Glu53, the active site residues Asp195, Asn197 and Asp295 and the highly conserved residue Phe55 also take part in the binding of SM.

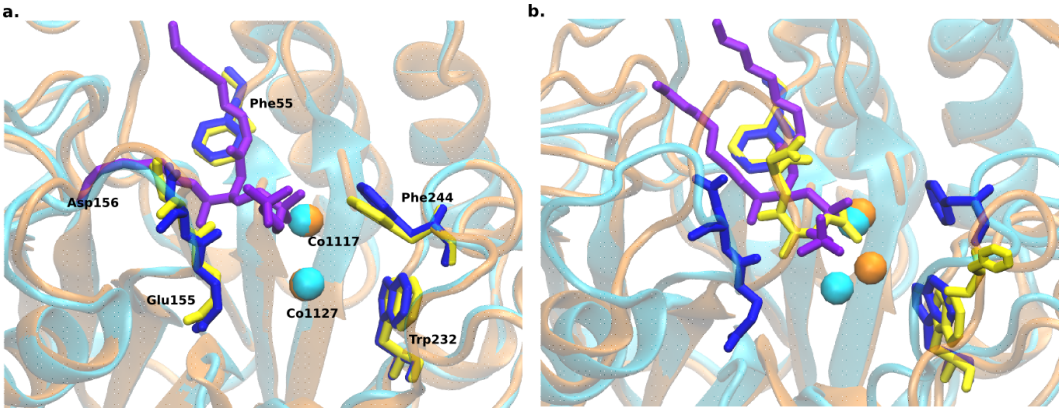

Figure 4.34. Alignment of the first (a) and last (b) frames of the simulations of apo (orange) and SM-bound (cyan) 2DDS MBW focusing on the important residues. The residues of apo and SM-bound structures are shown in yellow and blue.

The active site residue His151 directs itself towards the active site with SM binding (see Figure 4.35) which was also seen in the case of 2UYR.

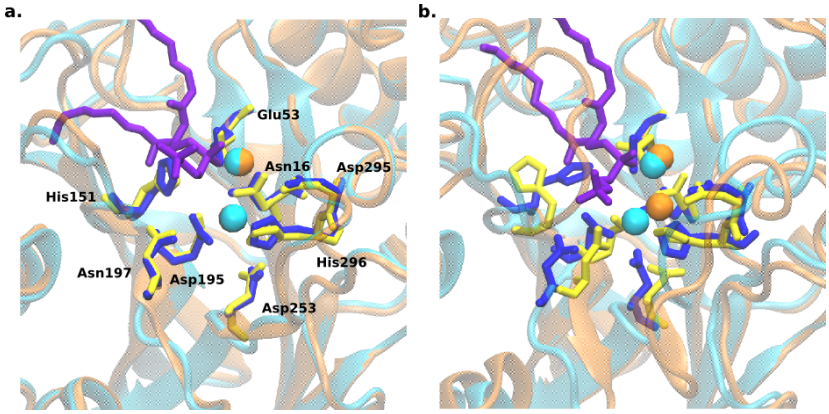

Figure 4.35. Alignment of the first (a) and last (b) frames of the simulations of apo (orange) and SM-bound (cyan) 2DDS MBW focusing on the active site residues. The residues of apo and SM-bound structures are shown in yellow and blue.

One of the most notable conformational change observed in apo 2DDS MBW and WW5M is the closing motion observed in the loops region around the active site. These loops, especially Leu20-Gly29 and Leu152-Ser166 move towards each other and blocks the entrance of the active site in the apo 2DDS case (see Figure 4.32). This movement of the loops was not seen in apo 2UYR and SM-bound 2DDS and 2UYR

cases. This closing motion might be due to the crystal contact. Another possible explanation is the presence of two cobalt ions at the active site coordinating the residue Glu155. Hence Leu152-Ser166 loop region overlaps the active site due to this metal coordination. While the metal coordination of Asp156 was seen in apo 2UYR case, the closing motion of the loops was not seen. The reason behind this might be the difference in the metal ions at their active sites. 2UYR has one magnesium ion, while 2DDS has two cobalt ions at their respective active sites.

Among the MD simulations performed on SM-bound 2DDS structures, only the SM-bound 2DDS MBW was analyzed carefully since docking simulations conducted on SM-bound 2DDS WW5M did not generate a pose that was in agreement with the proposed binding modes in the literature [2]. This was possibly due to the water molecules kept around the third cobalt ion present near Asn92-Gly102 loop. Since SM is a large molecule, its tails cannot be accommodated by 2DDS due to presence of additional waters around the third cobalt ion.

Taken together, Glu53 and the active site metal ion are crucial for SM binding. The helical conformation observed in 2UYR case was not seen in 2DDS case suggesting that this difference in their conformations might be due to crystal contact. Glu155-Ser166 loop in both 2UYR and 2DDS overlapped the active site in apo cases due to metal coordination, while it did not move towards active site and formed interactions with SM in SM-bound cases. The regions 21-29, 155-166 and 240-249 were stabilized with SM binding in both 2UYR and 2DDS. Asp156 and Glu155 in Leu152-Ser166 loop were coordinated by the active site metal ions of apo 2UYR and 2DDS, respectively but with SM binding this interaction was not seen, hence this loop did not overlap the active site.

4.2.5.3. Apo and SM-Bound 5UVG. As seen in Table 4.16, both 5UVG MBW and WW5M structures become mobile with SM binding. Also many regions on 5UVG become distorted with SM binding. This might be due to the absence of the membrane-associated NTD of human nSMase2 on its crystal structure. NTD contains the palmi-

toylation, calcineurin, phosphoserine sites and APL which are important for the regulation of the activity and stability of the protein [1]. Unfortunately, these regions are not present on the crystal structure. Hence the MD simulation results show the importance of the membrane domain for the stability of the protein. Some of the loop regions around the active site of 5UVG are shown in Figure 4.36. Frames of 0, 300 and 500 ns of the simulations of apo and SM-bound 5UVG are aligned to observe the conformational differences between apo and SM-bound structures.

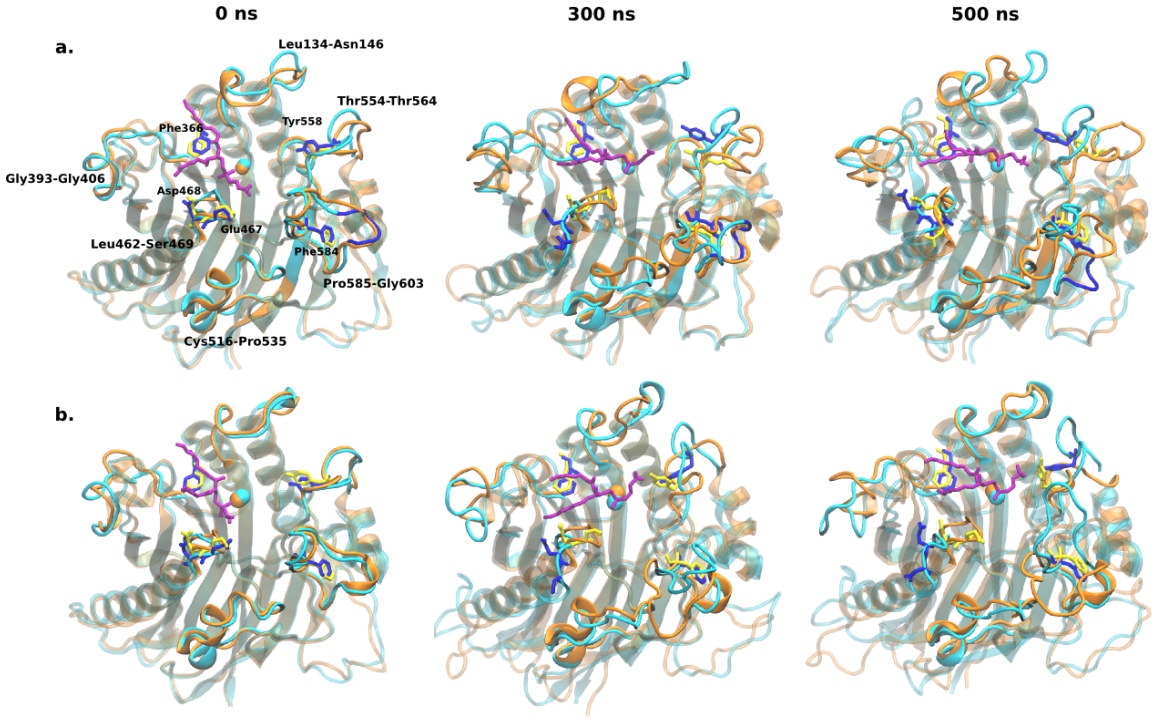

Figure 4.36. Loops around the active site of 5UVG MBW (a) and WW5M (b). Frames of 0, 300 and 500 ns of the simulations of apo (orange) and SM-bound (cyan) 5UVG are aligned. The residues of apo and SM-bound 5UVG are shown in yellow and blue.

The missing residues that were filled by Schrödinger Suite; Cys394-Lys401, Ser493-Asn497, Gly556-Asp561 were highly mobile throughout the simulation. Except for Ser493-Asn497, these regions were close to the active site. Cys394-Lys401 is one of the important regions that contains palmitoylation residues (Cys397 and Cys398). This region is important for the regulation of the activity and the stability of the protein [1].

The binding free energies of SM-5UVG (see Table 4.19 and Table 4.20) indicates that SM bound to 5UVG MBW tightly compared to 5UVG WW5M. When the simulations were analyzed, it was seen that SM remained highly mobile in the binding pocket of 5UVG WW5M compared to 5UVG MBW.

In both 5UVG WW5M and MBW cases, the residues Glu364 and Asp638 and the active site calcium ion took part in SM binding (see Figure 4.25). These interactions were also consistent with *Bc*-SMase MD simulations results. The SM-Phe366 interaction was seen in 5UVG MBW, while it was not seen for 5UVG WW5M. This interaction was also seen in *Bc*-SMase as SM-Phe55 interaction.

The amino group of SM transiently interacted with Tyr558. In the MD simulations of *Bc*-SMases, Trp232 and Phe244 were important for the binding of the amino group of SM and formed pi-cation interactions with the amino group of SM. The closest aromatic residues to the amino group of SM were Tyr558 and Phe584 in 5UVG. Hence these residues were expected to be important for the binding of the amino group of SM. However, only Tyr558 formed transient interactions with SM. Tyr558 was also mobile and away from the active site in MD simulations of apo 5UVG, while less mobile and directed towards the active site in SM-bound simulations possibly forming pi-cation interactions with the amino group of SM. Phe584 directed its side chain away from the active site (see Figure 4.36). While the residues Tyr558 and Phe584 are not homologous to the *Bc*-SMase residues Trp232 and Phe244 according to the sequence alignment results [1], these residues might be important for the binding of the amino group of SM to the human nSMase2. It is also important to state that Gly556-Glu560 residues were missing residues in the crystal structure that were filled by the software. Hence this missing region in the crystal structure might play a role in the binding of the amino group of SM.

Tyr423-Lys435 region (DK switch loop) remained as a loop in both SM-bound 5UVG MBW and WW5M cases as seen in Figure 4.37. Asp430 and Lys435 did not form salt bridge with each other. They also did not form any interaction with SM.

Interestingly, a small helical conformation was seen in the DK switch loop of apo 5UVG WW5M. However, this was not due to a salt bridge formation between Asp430 and Lys435. It was due to a salt bridge interaction between Asp430 and Lys426, and hydrogen bonding of Asn425 and Asp430 with Cys427.

It is important to state that SM did not bind to 5UVG structures tightly like in the case of *Bc*-SMase. However, while SM ligand remained mobile except for its phosphate moiety, it did not diffuse away from the protein due to Glu364, Asp638 and calcium ion interactions (see Figure 4.25 and Figure 4.27). The loop regions around the active site did not move closer to or away from the active site to accommodate SM as seen in Figure 4.36. Co^{2+} and Mg^{2+}-bound *Bc*-SMases were reported to have higher catalytic activity, while Ca^{2+} had much lower catalytic activity. This might be due to the Lewis acid strengths of these metal ions [2]. Hence if Mg^{2+} was present at the active site of 5UVG instead of Ca^{2+}, SM might have bound to 5UVG tightly.

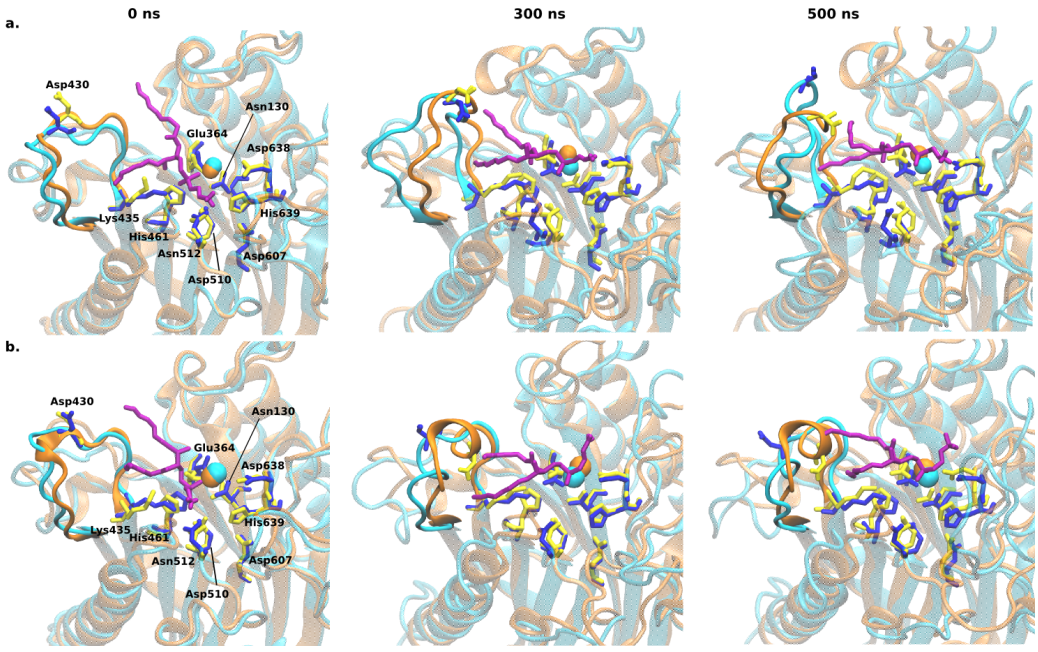

Figure 4.37. Active site and DK switch of 5UVG MBW (a) and WW5M (b). Frames of 0, 300 and 500 ns of the simulations of apo (orange) and SM-bound (cyan) 5UVG are aligned. The residues of apo and SM-bound 5UVG are shown in yellow and blue.

Leu462-Ser469 loop (possibly corresponding to the Leu152-Ser166 loop in *Bc*-SMases was closer to the active site in apo cases of 5UVG compared to their SM-bound structures. The closeness of this loop was maintained in apo 5UVG WW5M, but lost towards the end of the MBW simulation (see Figure 4.36). However, this closeness was possibly not due to the coordination of this loop by the calcium ion at the active site. It might due to the hydrogen bonding interaction between Gln466 and Asp520. This interaction was broken down in apo 5UVG MBW case, and not seen for SM-bound 5UVG cases. While Leu462-Ser469 loop contains Glu and Asp residues at position 467 and 468, these residues were not coordinated by the calcium ion. Interestingly, Ala464 directed itself towards the calcium ion in both apo 5UVG cases. However, the active site calcium ion is not close enough to Ala464, Glu467 or Asp468 to coordinate these residues. If there were two magnesium ions present at the active site of human nSMase2, these residues might have been coordinated by these metal ions. However, it is important to state that according to the sequence alignment of Airola *et al.*, Glu467 and Asp468, as well as Glu155 and Asp156 in *Bc*-SMase, are not named under universally conserved or homologous residues. Ala464 is the homologous residue of Ala154 in *Bc*-SMase [1].

Taken together, the membrane-associated NTD is important for the stability and the regulation of the activity of human nSMase2. Without this domain, many regions on 5UVG got distorted. Glu364, Asp638 and the active site calcium ion are important for SM binding. Even though SM did not bind to human nSMase2 like it bound to *Bc*-SMases, these interactions did not let SM to diffuse away from the protein. Asp430 and Lys435 did not form salt bridge with each other hence DK switch loop did not attain a helical conformation in both apo and SM-bound human nSMase2. It is important to state that JX region of nSMase2 which was suggested to be important for the regulation of DK switch activity, is also missing in the crystal structure of human nSMase2 [1]. Hence this missing part might be crucial to see the putative functional conformational change in DK switch.

4.3. Finding the Possible Binding Sites on *Bc*-SMases and Human nSMase2 with SiteMap

A SiteMap analysis was conducted on *Bc*-SMases and human nSMase2 to find the possible binding sites on these structures [42–44]. This was done to find the potential binding site of GW4869 on these structures. While the binding site of the natural substrate is known, the binding site of this noncompetitive inhibitor is not exactly known. However, it was suggested that this inhibitor might interfere with the involvement of DK switch in the catalytic mechanism [1]. Hence its binding site might contain DK switch residues.

The possible binding sites on *Bc*-SMases (2DDS and 2UYR) and human nSMase2 (5UVG) proposed by the software are given in Table 4.21, Table 4.22 and Table 4.23. The scores tabulated in these tables have average or threshold values computed by SiteMap by taking a large number of tight-binding (binding affinity ≤ 1 μM) sites of an extensive set of proteins available in literature into account [42].

Five possible binding sites were identified for 2UYR as tabulated and shown in Table 4.21 and Figure 4.38. The front and back views of the protein are provided to visualize these binding sites in Figure 4.38. The residues present at Site 1 and Site 2 are depicted in licorice forms colored in green and red, respectively (Figure 4.38a). Site 3, Site 4 and Site 5 are colored in yellow, white and violet, respectively (Figure 4.38). Magnesium ion is colored in orange.

The latter three sites were eliminated due to their lower site scores. The first binding site contains the active site and DK switch residues, while the second binding site mainly contains the DK switch residues. Even though the score of the second binding site is not very promising, this site was also utilized for GW4869 docking since it contains mainly the DK switch residues.

The calibration value for SiteScore is 1.0, hence if the SiteScore of a binding site is greater than 1, it indicates that it is a very promising site [42]. For a SiteScore, a value of 0.80 is defined as the threshold level for distinguishing between drug-binding and non-drugbinding sites. Hence according to the SiteScores in Table 4.21, only the first binding site is the possible drug-binding site. However, with a SiteScore of 0.741, Site 2 can also be a possible drug-binding site since its SiteScore is close to 0.80.

Table 4.21. Possible binding sites found on the crystal structure of 2UYR and their SiteMap scores. All of the italic residues are conserved residues, and the residues marked with asterisks are active site or DK switch residues.

Site	**Site Score**	**Dscore**	**Volume**	**Enclosure**	**Philic**	**Residues**
Site 1	0.998	1.025	545.713	0.682	0.994	Chain X: 128,129,*131**,240,243,201,244,202, 203,247,209,250,*53**,*295**,98,252, 55,99,210,*296**,211,*16**,18,*151**, *195**,*197**,154,20,198,155,21,199, 24,25,125,168,*126**,232
Site 2	0.881	0.741	91.581	0.767	1.373	Chain X: *126**,127,118,129,119,171,92,94, 130,120,*131**,153,121,97,122
Site 3	0.667	0.521	85.064	0.562	1.371	Chain X: 11,45,47,7,8,305,9,108,109,140,141,143
Site 4	0.609	0.461	81.977	0.662	1.246	Chain X: 25,26,27,28,290,281,283,284,242,243
Site 5	0.603	0.561	95.011	0.55	0.897	Chain X: 22,55,99,56,57,79,80,130,95,97,100,21

Three possible binding sites were suggested for 2DDS as seen in Table 4.22 and Figure 4.39. In Figure 4.39, the residues present at Site 1 are depicted in licorice colored in green. Site 2 and Site 3 are shown in transparent 'surf' forms colored in red and violet, respectively. Cobalt ions, which are at the active site are colored in orange.

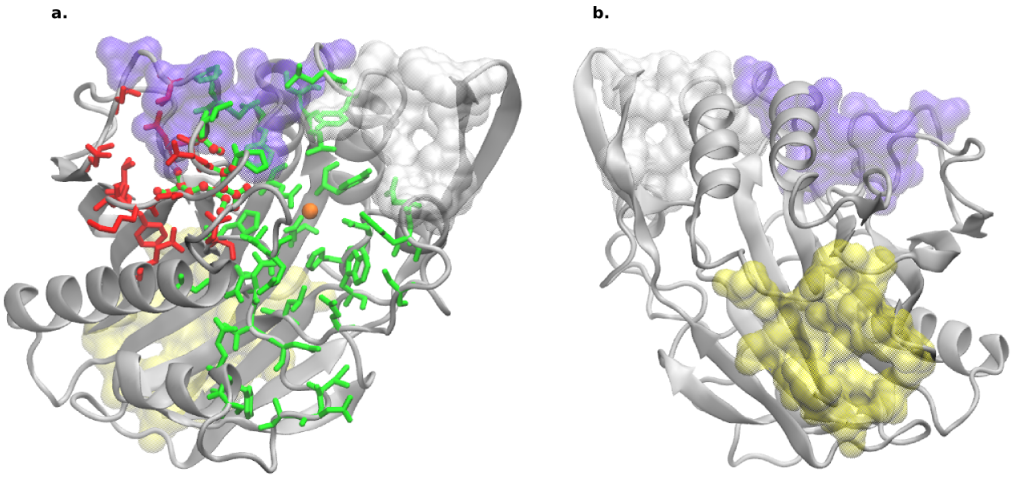

Figure 4.38. Five possible binding sites found on the crystal structure of 2UYR. The front (a) and back (b) views of 2UYR are provided. Site 1, Site 2, Site 3, Site 4 and Site 5 are colored in green, red, yellow, white and violet, respectively.

The last two sites are eliminated due to their lower scores. The top possible binding site contains the residues present in the active site and the loop regions surrounding the active site including the DK switch region. The SiteScore and Dscores of this site are promising indicating that it is suitable for ligand (drug) binding. The first possible binding site of 2DDS contains almost the same residues present in that of 2UYR.

The top 5 possible binding sites determined by SiteMap on the crystal structure of human nSMase2, 5UVG are tabulated and shown in Table 4.23 and Figure 4.40, respectively. When the results are sorted based on the overall SiteScores, which is defined as the most important property produced by SiteMap [42], it is seen that Site 3 has the highest SiteScore, followed by Site 2 and Site 1, respectively. These top three sites are located in the loop region surrounding the active site as seen in Figure 4.40a.

According to the SiteScores in Table 4.23, the first four sites are possible drug-binding sites since their SiteScores are higher than the defined threshold level, 0.80. However, with a SiteScore of 0.789, Site 5 can also be named under possible drug-binding sites since its SiteScore is close to this threshold value, 0.80.

Table 4.22. Possible binding sites found on the crystal structure of 2DDS and their SiteMap scores. All of the italic residues are conserved residues, and the residues marked with asterisks are active site or DK switch residues.

Site	**Site Score**	**Dscore**	**Volume**	**Enclosure**	**Philic**	**Residues**
Site 1	0.99	0.978	571.095	0.684	1.141	Chain A: 128,129,170,171,130,*131**,240,243, 244,92,*53**,250,55,252,295,210, *296**,*16**,18,*151**,*195**,152,153, *197**,154,20,155,198,156,199,159,118, 119,160,161,162,120,121,122,123, 166,124,167,125,168,*126**,232,127
Site 2	0.749	0.537	92.61	0.668	1.558	Chain A: 24,25,26,27,28,290,281,283, 284,242,243,288
Site 3	0.613	0.564	100.842	0.523	1.055	Chain A: 55,99,23,56,24,57,79,58, 80,95,97,100,21,98

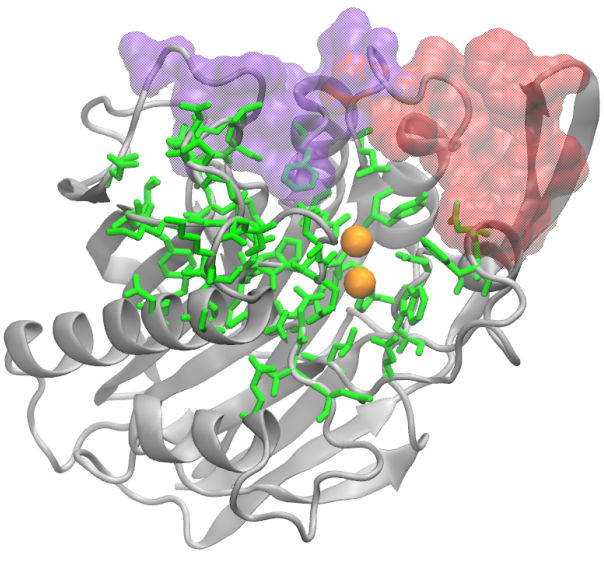

Figure 4.39. Three possible binding sites found on the crystal structure of 2DDS. The residues present at Site 1 are depicted in licorice forms colored in green. Site 2 and Site 3 are shown in transparent 'surf' forms colored in red and violet, respectively.

Table 4.23. Possible binding sites on 5UVG and their SiteMap scores. The italic residues are conserved residues with the active site or DK switch residues marked with asterisks. The underlined residues are the missing residues filled by the software.

Site	**Site Score**	**Dscore**	**Volume**	**Enclosure**	**Philic**	**Residues**
Site 1	0.967	0.951	353.29	0.649	1.16	Chain A: 553,555,556,557,558,*510**,580,*639**, *512**,581,513,514,583,584,585,517, *130**,586,518,587,519,588,*461**,464, 466,520,467,469,592,593,604,596, 606,472,551
Site 2	1.001	1.034	318.304	0.673	0.95	Chain A: 397,*475*,398,399,431,432, 433,434,*435**,134,135,463,464,465, 138,*364**,366,420,422,390,424,400, 425,402,403,404,395,429,405,396
Site 3	1.006	0.949	219.52	0.746	1.242	Chain A: 147,554,635,558,636,559,637,*638**, *150*,132,134,136,139,140,141,143, 144,145,146
Site 4	0.881	0.775	149.205	0.686	1.334	Chain A: 350,351,352,353,354,355,356,643, 645,569,626,161,628,164,165,166, 348,167,168
Site 5	0.789	0.803	137.2	0.633	0.569	Chain A: 487,531,532,456,457,458,612,614, 439,505,615,506,480,483,440,484, 486

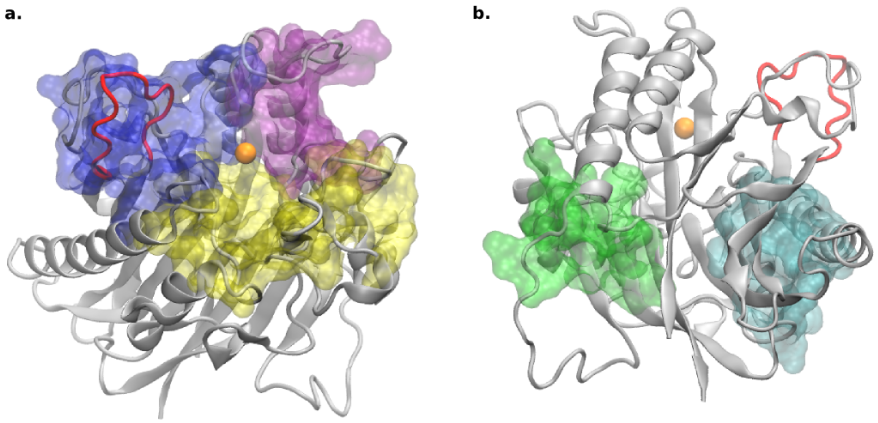

Figure 4.40. Possible binding sites on 5UVG. Top 3 (a) and last 2 (b) binding sites are depicted; Site 1, Site 2 and Site 3 are shown in yellow, blue and purple (a) and Site 4 and Site 5 are shown in green and cyan, respectively (b). DK switch is colored in red.

Site 3 and Site 2 are very promising since their SiteScores are higher than 1.0. While Site 3 has the highest SiteScore, Site 2 has the highest Dscore. The SiteScore and Dscore of Site 2 are both higher than 1, indicating that it is a very promising 'druggable' binding site. This is due its low hydrophilic score compared to that of Site 3 and Site 1 (see Table 4.23).

Enclosure is a measure of how open the site is to solvent. It evaluates whether the ligand can be enclosed by the protein or not. The higher this score, the better it is. An average value of 0.78 is determined for a tight-binding (binding affinity ≤ 1 μM) site [42]. Site 3 has the highest enclosure score with 0.746.

The top three binding sites according to the SiteScore results for 5UVG are mainly the loop regions surrounding the active site (see Figure 4.40a). Site 1 contains some of the active site residues; Asn130, His461, Asp510, Asn512 and His639. The binding site, Site 2 encompasses the DK switch region (Asp430-Lys435, colored red in Figure 4.40) which has been reported as an important region for the catalytic activity of human nSMase2 by Airola *et al.* [1], and this site also contains two palmitoylation cysteine residues; Cys397 and Cys398. However, it is important to restate that these two residues are normally missing in the crystal structure of 5UVG, and they are filled

by the software; Schrödinger. Site 3 contains two conserved residues; Arg150 and an active site residue, Asp638. These top three binding sites surround the active site. The last two binding sites are away from the active site (see Figure 4.40b) and their SiteScores are lower than and not as promising as the top three binding sites.

Taken together, among these putative binding sites, Site 2 is the most suitable one for drug binding with a Dscore of 1.034, and it contains the DK switch residues. Site 2 is followed by Site 1 and Site 3 for their potential to be drug-binding sites. These three binding sites are located at the loop region surrounding the active site (Figure 4.40a), while Site 4 and Site 5 are far away from the active site as seen in Figure 4.40b. Among the five possible binding sites found on 5UVG by SiteMap analysis, the top three binding sites were utilized for GW4869 docking analysis since their scores especially their Dscores (Table 4.23) indicated that these sites were the most suitable ones for drug-binding.

GW4869 was suggested as a PS-competitive inhibitor for nSMase2 [1]. Hence the closeness of this inhibitor to the membrane region might also be important for its inhibitory effect on nSMase2. The selected top three binding sites are also around the active site region and closer to the membrane, while the last two sites are far away from the membrane.

4.4. Docking of the nSMase2 Inhibitor GW4869 to *Bc*-SMases and Human nSMase2

The non-competitive inhibitor of nSMase2, GW4869 was docked into the possible binding sites/regions of *Bc*-SMases and human nSMase2 to find the binding region for GW4869 on nSMase2. The possible binding sites were found by using Schrödinger's tool SiteMap [42]. The most suitable sites for GW4869 were utilized as docking sites to find the binding site for GW4869 on nSMase2. Possible geometric isomers of GW4869 were also generated (see Figure 3.1) and docked into these possible binding sites to see which isomeric form of GW4869 possibly binds effectively/efficiently to nSMase2.

The stability of the interactions between GW4869 and nSMase2 was further tested by carrying out MD simulations on these ligand-bound structures.

Three criteria were taken into account when analyzing the results; i. docking scores and the binding free energies, ii. closeness of GW4869 to the DK switch region (Airola *et al.* suggested that GW4869 might interfere with the role of DK switch in catalytic activity [1]), and iii. closeness of GW4869 to the active site (GW4869 is a noncompetitive inhibitor for SM binding [1]). Hence when analyzing the potential binding residues of this inhibitor whether it formed interactions with DK switch region or not was also taken into account.

4.4.1. Docking of GW4869 to 2UYR

GW4869 was docked into the first two possible binding sites of 2UYR (see Table 4.21), and the docking scores and the binding free energies of the top selected poses that have similar binding modes are tabulated in Table 4.24 to Table 4.27, and the common binding mode observed for Site 1 is shown in Figure 4.41. The poses that are similar and have similar binding pockets are named under the common binding mode.

Table 4.24. Docking scores for GW4869 docked into the Site 1 of 2UYR MBW.

Isomer Pose #	**XP GScore**	**Docking Score**	**Ligand Energy (kcal/mol)**	**ΔG (kcal/mol)**	**Ligand Strain (kcal/mol)**
TT 3	-6.733	-0.665	-67.303	-83.116	9.458
TC 2	-4.287	-4.287	-51.883	-85.610	3.533
CT 21	-4.221	-4.221	-51.576	-94.895	3.468
CC 2	-7.714	-7.714	-44.001	-96.642	7.187

The poses generated at Site 1 of 2UYR are promising in terms of both binding mode (see Figure 4.41) and docking scores (Table 4.24 and Table 4.25). They form interactions with DK switch region (residues 119-131). The poses are in a binding pocket adjacent to but not overlapping with the SM-binding site.

Table 4.25. Docking scores for GW4869 docked into the Site 1 of 2UYR WW5M.

Isomer Pose #	**XP GScore**	**Docking Score**	**Ligand Energy (kcal/mol)**	**ΔG (kcal/mol)**	**Ligand Strain (kcal/mol)**
TT 1	-6.888	-0.82	-70.482	-79.576	4.626
TC 1	-6.969	-6.969	-52.162	-86.542	4.091
CT 7	-5.321	-5.321	-51.809	-84.978	6.504
CC 2	-6.469	-6.469	-47.027	-88.149	8.087

Table 4.26. Docking scores for GW4869 docked into the Site 2 of 2UYR MBW.

Isomer Pose #	**XP GScore**	**Docking Score**	**Ligand Energy (kcal/mol)**	**ΔG (kcal/mol)**	**Ligand Strain (kcal/mol)**
TT 1	-5.592	0.475	-70.82	-80.333	11.281
TC 3	-5.106	-5.106	-51.542	-89.182	5.427
CT 1	-4.914	-4.914	-48.644	-90.602	7.389

Table 4.27. Docking scores for GW4869 docked into the Site 2 of 2UYR WW5M.

Isomer Pose #	**XP GScore**	**Docking Score**	**Ligand Energy (kcal/mol)**	**ΔG (kcal/mol)**	**Ligand Strain (kcal/mol)**
TT 3	-5.389	0.679	-67.612	-92.474	13.061
TC 8	-3.243	-3.243	-55.297	-81.786	8.014
CT 6	-3.261	-3.261	-48.768	-84.903	14.618

According to the docking results for Site 2, GW4869 binds to the DK switch region of 2UYR from outside (see Figure 4.42). No pose of CC isomer of GW4869 at Site 2 belonged to the common binding mode group. Even though the binding free energies calculated at Site 1 and Site 2 are similar, the ligand strain energies at Site 2 are much higher than those at Site 1 (see Table 4.24 to Table 4.27). Hence Site 1 seems to be the most promising binding site for GW4869 on 2UYR.

Normally XP GScores and the docking scores are the same [45]. However, as seen in Table 4.24 to Table 4.27, they are different for some poses. Nevertheless, these scores can be different if a penalty is applied [45]. The difference between XP

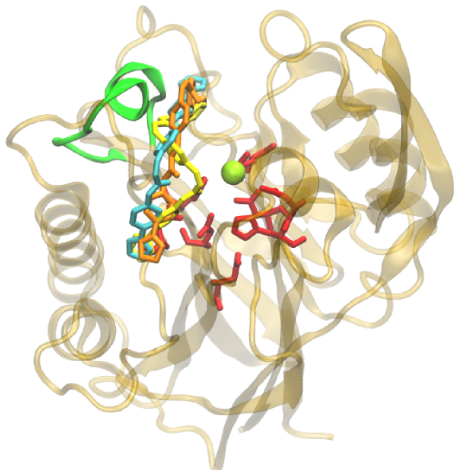

Figure 4.41. Binding mode observed for GW4869 at Site 1 of 2UYR. TC isomer at 2UYR MBW, and CT and CC isomers at 2UYR WW5M are colored in cyan, orange and yellow, respectively. DK switch and active site residues are in green and red.

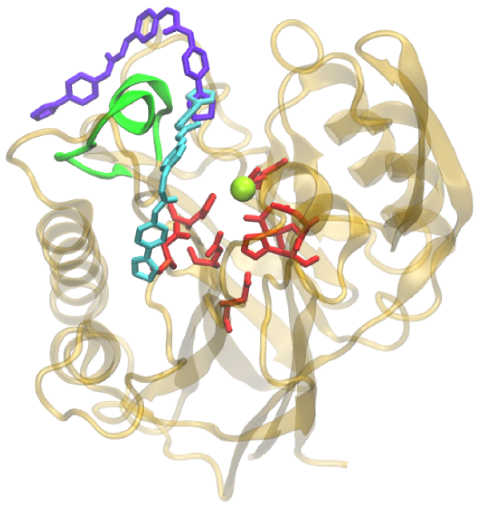

Figure 4.42. Common binding modes observed for GW4869 at Site 1 and Site 2 of 2UYR. TC isomers at Site 1 of 2UYR MBW and Site 2 of 2UYR WW5M are shown in cyan and violet, respectively. DK switch is colored in green.

GScore and docking scores is due to the metal-binding state penalty which is about 6.0678 kcal/mol [41, 45]. As stated before, when preparing GW4869, three ionization states were generated with two of them being the metal binding state where the amine groups had a negative charge as seen in Figure 3.1. These metal-binding states are assigned with a penalty by the software, and this penalty is reflected on the docking score, not on the XP GScore. Hence in the poses in which the docking score is higher than the XP GScore, the metal binding state of GW4869 binds to the protein. If the difference between XP GScore and docking score is about 6 kcal/mol, this means that the metal-binding state of GW4869 does not interact with the metal ion hence the penalty (6.0678 kcal/mol) is fully reflected on the docking score. However, if the difference is lower than 6 kcal/mol (as will be seen in the first pose of TC isomer of 2DDS MBW in the first binding mode group (see Table 4.28), it indicates that the metal-binding state of GW4869 interacted with a metal ion, and the penalty was lowered due to that interaction.

4.4.2. Docking of GW4869 to 2DDS

GW4869 was docked into the first binding site of 2DDS suggested by SiteMap (see Table 4.22). The docking scores and the binding free energies of the top selected poses that have similar binding modes are tabulated in Table 4.28 and Table 4.28. Compared to the common binding mode of GW4869 poses docked into 2UYR, the common binding mode observed for 2DDS is closer to the active site (see Figure 4.43), and in some poses GW4869 formed interactions with the active site cobalt ions. While this binding mode is similar to that of the poses at Site 1 of 2UYR, the common binding mode observed in 2UYR is closer to the DK switch region when compared with the results of 2DDS.

As stated before, only one promising binding site was found on 2DDS by SiteMap. This binding site is similar to the first binding site of 2UYR (see Table 4.21 and Table 4.22). Even though 2DDS and 2UYR are both *Bc*-SMases with minor differences, the second binding site of 2UYR was not suggested as a possible binding site for 2DDS.

This was possibly due to the conformational differences in their DK switch regions. The second binding site suggested for 2UYR was also utilized as a possible binding site for GW4869 on 2DDS to see if this inhibitor binds to this site or not. The docking scores and the binding free energies of the top selected poses that have similar binding modes at this site of 2DDS are tabulated in Table 4.26 and Table 4.27.

Table 4.28. Docking scores for GW4869 docked into the Site 1 of 2DDS MBW.

Isomer Pose #	**XP GScore**	**Docking Score**	**Ligand Energy (kcal/mol)**	**ΔG (kcal/mol)**	**Ligand Strain (kcal/mol)**
TT 2	-5.562	0.215	-66.574	-60.218	9.858
TC 1	-8.403	-6.387	-63.339	-101.49	9.380
CT 1	-7.999	-5.983	-63.509	-96.227	11.271
CC 1	-8.514	-6.498	-55.622	-98.689	5.450

Table 4.29. Docking scores for GW4869 docked into the Site 1 of 2DDS WW5M.

Isomer Pose #	**XP GScore**	**Docking Score**	**Ligand Energy (kcal/mol)**	**ΔG (kcal/mol)**	**Ligand Strain (kcal/mol)**
TT 1	-8.395	-2.327	-70.648	-67.137	3.492
TC 10	-5.093	-5.093	-51.655	-69.893	5.443
CT 5	-6.133	-6.133	-51.734	-98.881	7.845
CC 5	-6.370	-6.370	-47.138	-54.279	10.794

Table 4.30. Docking scores for GW4869 docked into the 2UYR's Site 2 of 2DDS MBW.

Isomer Pose #	**XP GScore**	**Docking Score**	**Ligand Energy (kcal/mol)**	**ΔG (kcal/mol)**	**Ligand Strain (kcal/mol)**
TT 11	-6.985	-0.828	-71.035	-91.660	7.596
TC 2	-7.830	-7.830	-51.724	-103.944	5.033
CT 3	-7.060	-7.060	-48.066	-102.733	4.216
CC 6	-6.767	-6.767	-43.905	-89.335	4.168

Table 4.31. Docking scores for GW4869 docked into the 2UYR's Site 2 of 2DDS WW5M.

Isomer Pose #	**XP GScore**	**Docking Score**	**Ligand Energy (kcal/mol)**	**ΔG (kcal/mol)**	**Ligand Strain (kcal/mol)**
TT 1	-11.430	-5.362	-70.618	-83.198	7.886
TC 10	-7.693	-7.693	-51.617	-98.414	5.653
CT 5	-7.974	-7.974	-51.558	-98.619	5.524
CC 5	-7.635	-7.635	-43.515	-80.999	6.213

Site 1 of 2DDS actually contains most of the residues present in the Site 2 of 2UYR. Prior to docking, a receptor grid box is defined in which the poses are generated. The center of this grid box is defined as the centroid of the selected residues. Since the content of the residues are not the same for Site 1 of 2DDS and Site 2 of 2UYR, the centroid of the selected will be different, hence the grid box defined will not be entirely the same.

The binding mode observed for 2DDS docked into this second binding site is shown in Figure 4.43. This common binding mode of GW4869 docked into 2DDS was different from that of GW4869 docked into 2UYR. GW4869 surrounded DK switch of 2UYR from outside (see Figure 4.42), while it bound DK switch of 2DDS from inside (see Figure 4.43). The docking scores tabulated for GW4869 poses at this site of 2DDS are more promising compared to those tabulated for 2UYR. However, these poses were not enclosed by the protein and the inhibitor was exposed more to the solvent when compared with the GW4869 poses at Site 1 of 2DDS and 2UYR so the poses generated at Site 2 of 2DDS were not selected as the potential binding mode of GW4869 on 2DDS.

4.4.3. Docking of GW4869 to 5UVG

The four GW4869 isomers were docked into the top three binding sites of 5UVG. The docking and MM/GBSA results for 5UVG are tabulated in Table 4.32 to Table 4.36. Among these binding sites, Site 2, which contained the DK switch residues, was

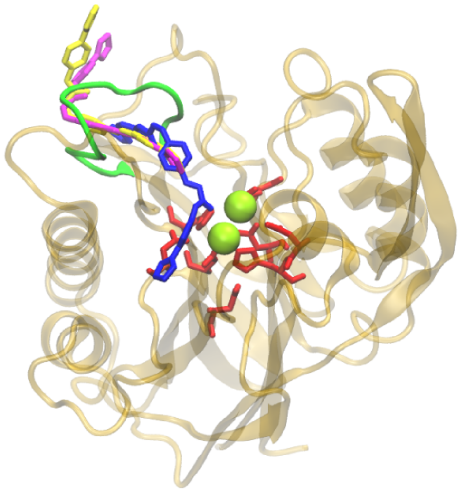

Figure 4.43. Common binding modes observed for GW4869 at Site 1 and Site 2 of 2DDS. CT isomers at Site 1 and Site 2 of 2DDS MBW and at Site 2 of 2DDS WW5M are shown in blue, magenta and yellow, respectively.

the most promising binding site for GW4869 according to the docking results. As stated before, Site 2 was also the most suitable site for drug-binding according to its Dscore (Table 4.23).

The docking results for Site 1 are given in Table 4.32. Compared to the results of GW4869 docked into the Site 2 and Site 3 of human nSMase2, Site 1 is not the binding site for GW4869 due to its lower docking scores. No common binding mode was observed in Site 1 of 5UVG hence the first poses based on the XP GScores are given in Table 4.32. Since these results are not as good as the results of Site 2 and Site 3, MM/GBSA analysis was not conducted on the poses at Site 1. GW4869 was not expected to bind to the Site 1 since Site 1 contained some of the active site residues as seen in Table 4.23, and GW4869 is known as a non-competitive inhibitor for SM-binding.

The docking scores of GW4869 docked into Site 2 and Site 3 are both promising with Site 3 slightly having better docking scores as seen in Table 4.33 to Table 4.36. While both sites surround the active site, only Site 2 contains the DK switch residues, and it was suggested that GW4869 might interfere with the catalytic mechanism of

Table 4.32. Docking scores for GW4869 docked into the Site 1 of 5UVG.

5UVG MBW			**5UVG WW5M**		
Isomer	**XP GScore**	**Docking Score**	**Isomer**	**XP GScore**	**Docking Score**
TT	-5.801	0.267	TT	-5.992	0.076
TC	-6.126	-4.110	TC	-4.280	-4.280
CT	-4.127	-4.127	CT	-3.989	-3.989
CC	-6.734	-6.734	CC	-6.573	-6.573

nSMase2 through DK switch [1]. Hence in addition to the docking scores, the binding free energies calculated by MM/GBSA and the common binding modes observed at each site were also compared to see which site was more appropriate for GW4869 binding.

Table 4.33. Docking scores for GW4869 docked into the Site 2 of 5UVG MBW.

Binding Mode	**Isomer Pose #**	**XP GScore**	**Docking Score**	**Ligand Energy (kcal/mol)**	**ΔG (kcal/mol)**	**Ligand Strain (kcal/mol)**
1	TT 1	-7.956	-1.888	-70.745	-56.968	14.315
	TC 1	-9.164	-3.069	-60.903	-73.631	14.110
	CT 1	-8.433	-2.365	-60.736	-77.867	12.512
	CC 7	-7.303	-7.303	-43.969	-116.950	3.244
2	TC 11	-6.794	-6.794	-48.556	-88.583	2.628
	CT 12	-6.527	-6.527	-48.645	-89.116	2.760
	CC 6	-7.498	-7.498	-43.351	-110.504	7.361
3	TC 30	-4.696	-4.696	-48.469	-73.498	7.871
	CT 32	-4.612	-4.612	-48.698	-69.543	7.340
4	TT 13	-5.819	-0.248	-70.328	-73.430	7.418
	CC 5	-7.670	-7.670	-43.690	-102.194	9.624

The binding free energies calculated for the GW4869 poses at Site 2 and Site 3 are closer to each other. However, when their ligand strain energies are compared, some of the GW4869 poses at Site 2 had lower ligand strain energies as seen in Table

Table 4.34. Docking scores for GW4869 docked into the Site 2 of 5UVG WW5M.

Binding Mode	**Isomer Pose #**	**XP GScore**	**Docking Score**	**Ligand Energy (kcal/mol)**	**ΔG (kcal/mol)**	**Ligand Strain (kcal/mol)**
1	TT 2	-6.977	-0.910	-70.602	-67.936	8.932
	TC 1	-9.058	-2.990	-63.073	-71.908	6.876
	CT 1	-9.076	-3.008	-62.928	-77.608	7.499
	CC 4	-7.058	-7.058	-43.885	-113.515	3.070
2	TC 24	-5.854	-5.854	-51.717	-93.366	4.954
	CT 26	-5.668	-5.668	-51.703	-93.945	3.756
	CC 3	-7.520	-7.520	-43.395	-105.293	6.414
3	TC 25	-5.822	-5.822	-48.916	-83.380	3.330
	CT 24	-6.000	-6.000	-51.368	-80.078	3.144
4	TT 1	-7.670	-1.602	-66.489	-82.835	12.890
	CC 2	-8.301	-8.301	-43.705	-112.808	5.24

Table 4.35. Docking scores for GW4869 docked into the Site 3 of 5UVG MBW.

Isomer Pose #	**XP GScore**	**Docking Score**	**Ligand Energy (kcal/mol)**	**ΔG (kcal/mol)**	**Ligand Strain (kcal/mol)**
TT 3	-8.460	-2.392	-71.675	-69.431	7.212
TC 7	-6.886	-6.886	-51.656	-105.959	6.207
CT 5	-6.878	-6.878	-51.651	-106.169	6.030
CC 1	-10.545	-10.545	-43.469	-137.454	7.562

Table 4.36. Docking scores for GW4869 docked into the Site 3 of 5UVG WW5M.

Isomer Pose #	**XP GScore**	**Docking Score**	**Ligand Energy (kcal/mol)**	**ΔG (kcal/mol)**	**Ligand Strain (kcal/mol)**
TT 3	-8.927	-2.859	-71.893	-77.647	6.116
TC 14	-5.456	-5.456	-48.585	-84.331	7.764
CT 18	-5.145	-5.145	-51.670	-78.743	12.180
CC 3	-9.242	-9.242	-44.103	-122.128	9.439

4.33 to Table 4.36. Four common binding modes were observed for GW4869 at Site 2, while no common binding mode was observed for GW4869 at Site 3 of 5UVG. These results indicate that Site 2 which contained DK switch residues might be the possible binding site of GW4869 as suggested by Airola *et al.* [1].

The poses in the first and second common binding modes of 5UVG at Site 2 are in a binding pocket adjacent to but not overlapping with the SM-binding site as seen in Figure 4.44 and Figure 4.45, respectively. The third common binding mode is similar to the second common binding mode as seen in Figure 4.45 and Figure 4.46. To compare these binding modes easily, the top three common binding modes are all shown on the same figure as seen in Figure 4.47.

A fourth common binding mode was also observed for GW4869 at Site 2 (see Figure 4.48). However, in this binding mode, GW4869 was not enclosed by the protein. It was only seen for TT and CC isomers of GW4869 at Site 2, and the poses of GW4869 were not as well-aligned as seen in other common binding modes (see Figure 4.47).

4.4.4. Comparison of the GW4869 Docking Results

As stated before GW4869 is a non-competitive (for SM binding) inhibitor so it possibly does not bind to the active site. The poses that lay directly on the active site were all eliminated and the poses that were closer to the DK switch were selected for analysis. However, almost in all common binding modes, the binding pocket of GW4869 is close to the active site especially in 2DDS case (see Figure 4.43). While in 5UVG and 2UYR cases, GW4869 is not interacting with the active site residues, in 2DDS case, some of the poses were interacting with the active site cobalt ions.

4.4.4.1. Selection of the Isomeric Form of GW4869. As stated before, there are four possible isomers for GW4869 (see Figure 3.1), and in which isomeric state GW4869 binds to nSMase2 is not known. Hence all the possible geometric isomers of GW4869

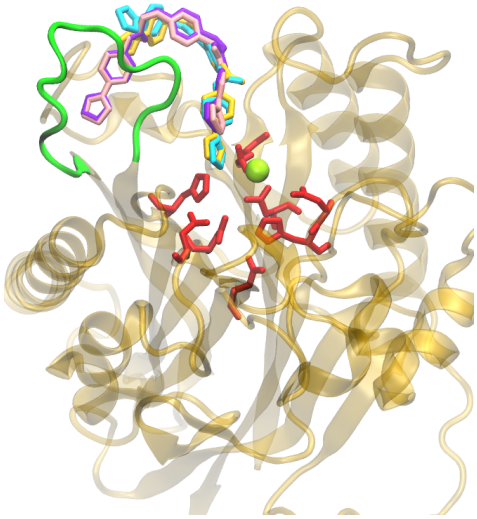

Figure 4.44. First common binding mode observed for GW4869 at Site 2 of 5UVG. TT and CC isomers at 5UVG MBW and at 5UVG WW5M are shown in orange, violet, cyan and pink, respectively. DK switch region is colored in green.

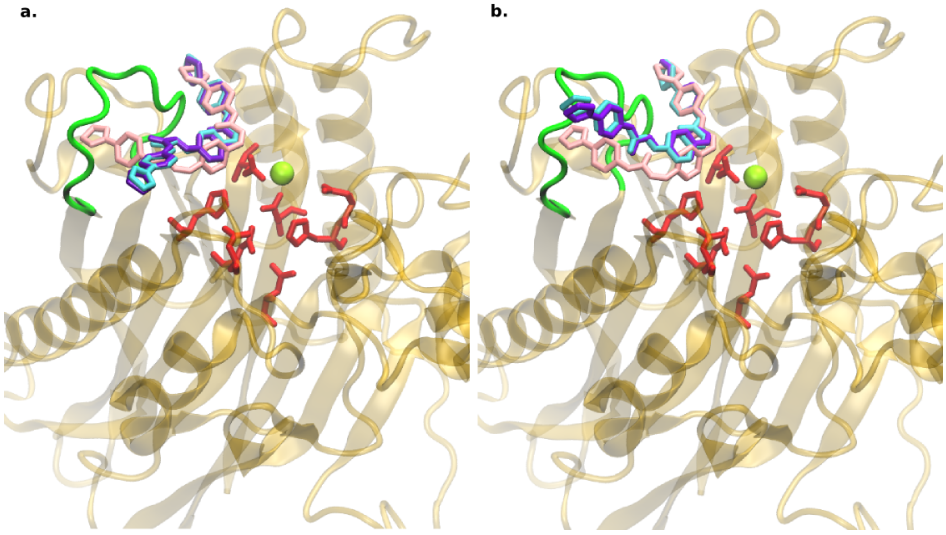

Figure 4.45. Second common binding mode observed for GW4869 at Site 2 of 5UVG. TC, CT and CC isomers at 5UVG MBW (a) and at 5UVG WW5M (b) are shown in cyan, violet and pink, respectively. DK switch region is colored in green.

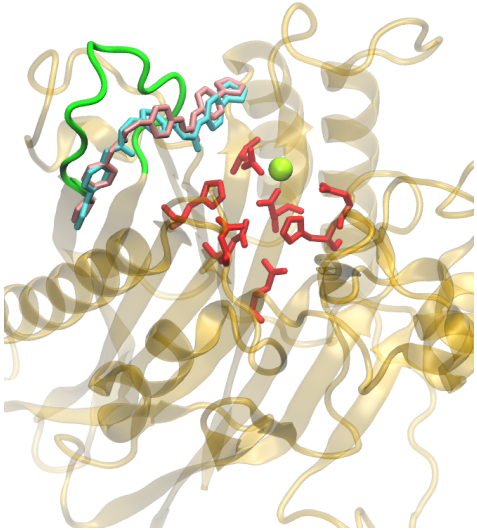

Figure 4.46. Third common binding mode observed for GW4869 at Site 2 of 5UVG. TC isomer at 5UVG MBW and at 5UVG WW5M are shown in cyan and pink, respectively. DK switch region is colored in green.

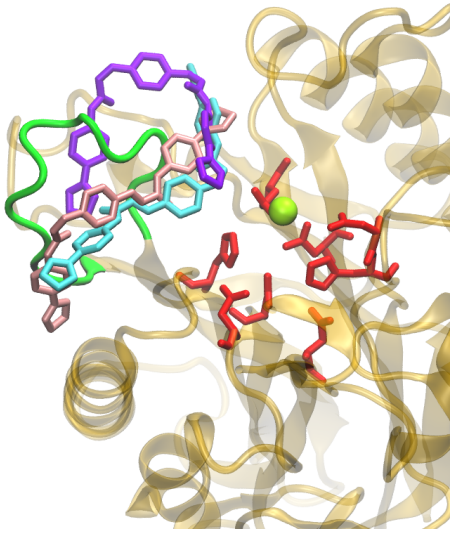

Figure 4.47. Top three common binding modes observed for GW4869 at Site 2 of 5UVG. The first, second and third binding modes at Site 2 are shown in violet, cyan and pink, respectively. DK switch region is colored in green.

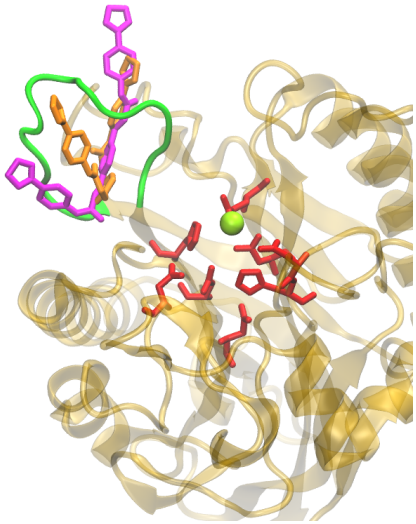

Figure 4.48. Fourth common binding mode observed for GW4869 at Site 2 of 5UVG. TT isomer at 5UVG MBW, and CC isomer at 5UVG WW5M are shown in magenta and orange, respectively. DK switch region is colored in green.

were generated and docked into *Bc*-SMases and human nSMase2 to find the best isomeric form of GW4869 that could be accommodated by nSMase2.

As expected, TT isomer of GW4869 has the lowest optimized free ligand energy with around -70 kcal/mol. However it only bound to the *Bc*-SMases and human nSMase2 in its metal-binding states. The normal ionization state of TT isomer of GW4869 (see Figure 3.1a) was not able to generate poses at the possible binding sites of the protein structures. It was seen that the software applied a state penalty to the poses that were in metal-binding state since the ligand required energy to attain that state, and this penalty was lowered when the GW4869 at the metal-binding state bound to a metal ion. Hence the poses that were in metal-binding state and did not interact with the metal ions were all eliminated. Because of this, TT isomer of GW4869 was not selected as the possible isomeric form for *Bc*-SMases and human nSMase2.

The metal ions present at the active site are known to interact with SM (the natural ligand/substrate), and the nSMase2 inhibitor GW4869 is non-competitive for SM binding so that it was expected not to interact with the active site metal ions. Hence the poses that were in metal-binding state and interacted with the metal ions were also eliminated. However, in 2DDS MBW case, the poses that have similar binding modes were all interacting with the metal ion.

The poses generated for TC and CT isomers of GW4869 are highly similar in terms of both binding modes and binding affinities (please refer Table 4.24, Table 4.25, Table 4.28, Table 4.29, Table 4.33 and Table 4.34). This was expected since GW4869 is a symmetrical dihydroimidazolo-amide compound. The optimized ligand free energies are at around -50 kcal/mol for TC and CT isomers, which are higher than the optimized ligand free energy of TT isomer. Hence in a solvent, the free ligand will be in its TT isomeric form as expected. However, the ligand binding free energies of the TC and CT isomers indicate that with favorable interactions with the protein, GW4869 can attain these isomeric forms when bound to the protein. This also applies for CC isomer of GW4869, which has an optimized ligand free energy around -43 kcal/mol and forms favorable interactions with the protein.

When selecting the most appropriate isomer of GW4869 for nSMase2 binding, the binding free energies were also considered in addition to the ligand strain energies. CC isomer of GW4869 bound to 5UVG have the most promising binding free energy values (Table 4.33 and Table 4.34). Hence CC isomer was selected as the isomeric form of GW4869.

4.4.4.2. Selection of the Binding Mode. Initially, among the common binding modes of 5UVG, the second common binding mode at Site 2 seemed to be the most promising one (see Figure 4.47). While the first common binding mode of 5UVG had good docking results especially for the CC isomer of GW4869 (Table 4.33 and 4.34), this binding mode was not seen in 2DDS. The common binding mode of GW4869 at Site 2 of 2UYR (Figure 4.42) was actually similar to the first common binding mode of 5UVG.

While the poses belonging to these common binding mode group (the first common binding mode of 5UVG at Site 2 and the common binding mode of GW4869 of 2UYR at Site 2) were mainly interacting with the DK switch region and far away from the active site, the ligand strain energies observed in this binding mode were higher for 2UYR. Hence the second common binding mode of 5UVG was selected as the binding mode of GW4869 on nSMase2. According to this, the common binding modes observed at Site 1 of 2UYR (see Figure 4.42) and 2DDS (see Figure 4.43) were selected as the binding mode of GW4869 on *Bc*-SMases since they were similar to the second common binding mode of 5UVG. However, in 2DDS case, GW4869 was closer to the active site compared to the poses seen in 2UYR and 5UVG cases.

To test the stability of the selected poses, 100 ns MD simulations were performed on the poses from the second binding mode of 5UVG MBW and WW5M. In this binding mode, GW4869 diffused away from the protein in 100 ns. The first binding mode of 5UVG was also tested by carrying out 100 ns MD simulations, however GW4869 again diffused away from the protein. Finally, the fourth binding mode was tested with 100 ns MD simulations. In 100 ns, GW4869 did not diffuse away from the protein, and bound tightly to 5UVG. Hence the possible binding mode of GW4869 at Site 2 is the fourth binding mode which is shown in Figure 4.48.

This binding mode was not observed in *Bc*-SMases. It is experimentally shown that GW4869 bound to and inhibit human nSMase2. Since the fourth binding mode was not seen in *Bc*-SMases, MD simulations were not performed on GW4869-bound *Bc*-SMases.

4.4.5. Docking of GW4869 into SM-Bound Human nSMase2

The fourth binding mode was also tested to see whether it blocked the binding of the natural substrate, SM. For this purpose, cis-cis form of GW4869 was docked into SM-bound 5UVG MBW and WW5M. C9- to C6-SM-bound 5UVG were utilized for this docking because the long hydrophobic tail of SM hindered the binding of GW4869

and these tails are embedded in PM hence in reality, they do not point towards the DK switch region. When GW4869 was docked into C8-SM and C6-SM bound structures, the fourth common binding mode was observed indicating that in this binding mode, it could bind to human nSMase2 without hindering the binding of SM. The binding free energies of the selected poses belonging to fourth common binding mode are given in Table 4.37.

Table 4.37. Docking scores of the selected GW4869 poses in the Site 2 of SM-bound 5UVG.

SM	**Structure**	**Pose #**	**ΔG of GW4869 (kcal/mol)**	**ΔG of SM (kcal/mol)**
C8	WW5M	3	-52.311	-73.959
C6	WW5M	2	-100.496	-78.018
C6	WW5M	3	-110.072	-69.672
C6	WW5M	4	-108.113	-77.711
C6	WW5M	5	-111.336	-74.949
C6	WW5M	7	-107.604	-67.659
C6	MBW	1	-95.969	-73.126
C6	MBW	2	-104.680	-71.564

According to GW4869 and SM binding free energies, the fourth pose of GW4869 docked into C6-SM-bound 5UVG WW5M (GW/SM-bound 5UVG WW5M) and the second pose of GW4869 docked into C6-SM bound 5UVG MBW (GW/SM-bound 5UVG MBW) were selected. Both of these poses interacted with DK residue, Asp430 (see Figure 4.49). MD simulations were carried out on these selected GW4869-C6-SM-bound structures. Both GW4869 and C6-SM did not diffuse away from the protein according to these simulations. Hence the fourth binding mode at Site 2 (DK switch region) of human nSMase2 can be the possible binding mode of GW4869 at DK Switch region.

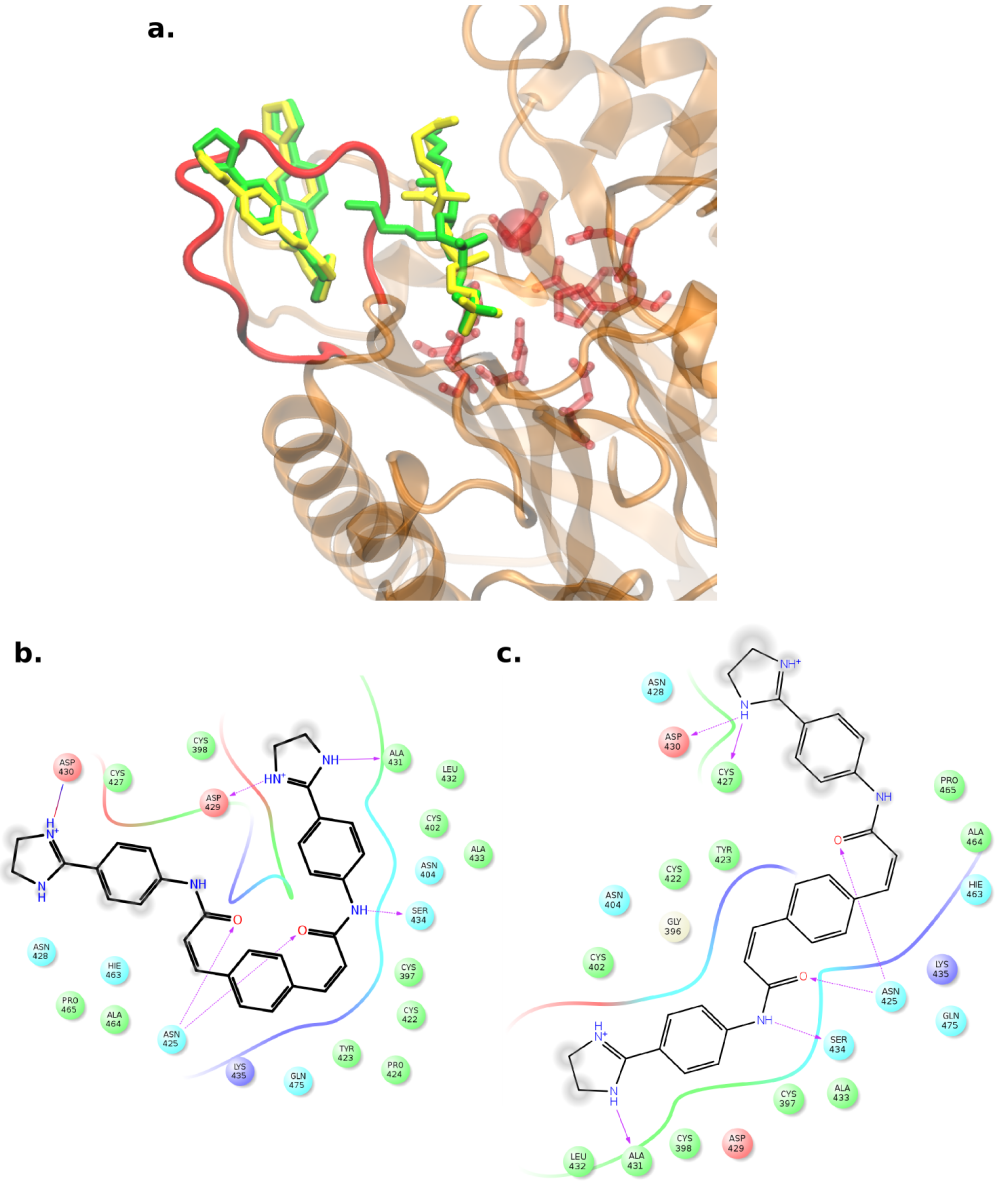

Figure 4.49. GW4869 docked to SM-bound 5UVG WW5M (ligands in green) and SM-bound 5UVG MBW (ligands in yellow) (a). 2D interaction diagrams of GW/SM-bound 5UVG WW5M (b) and MBW (c).

4.5. MD Simulation Results of GW4869-Bound Human nSMase2

4.5.1. RMSD and RMSF Profiles of the GW4869 MD Simulations

The RMSD profiles of the backbone atoms of GW-bound and GW/SM-bound human nSMase2 aligned on the first frames (0 ns) of their corresponding MD trajectories are given in Figure 4.50. According to these plots, all of the structures except for GW/SM-bound 5UVG MBW seem to reach equilibrium in 50 ns within an RMSD value around 2.5-3.0 Å. RMSD of the backbone atoms of GW/SM-bound 5UVG MBW reached a plateau around 3.5 Å after 85 ns.

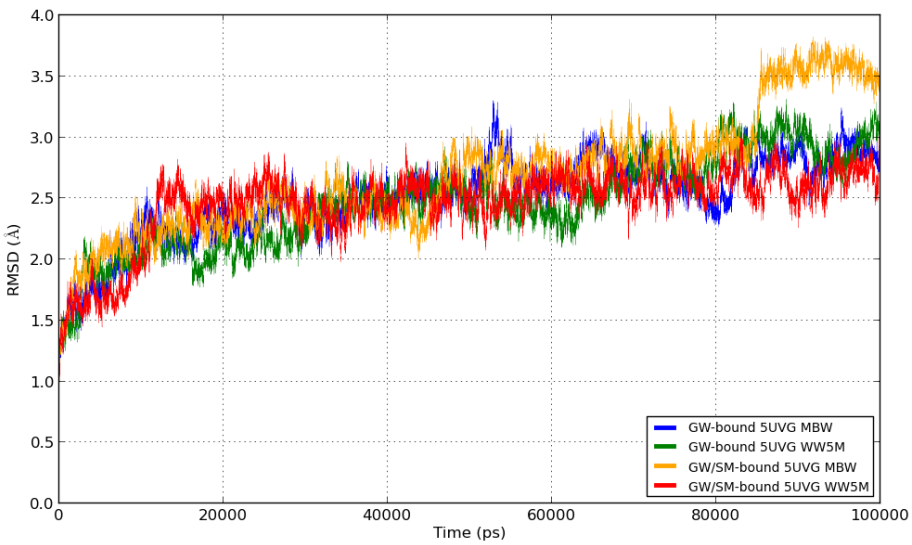

Figure 4.50. RMSD of the backbone atoms of GW-bound and GW/SM-bound 5UVG simulations.

RMSD profiles of the active site and the DK switch backbone atoms are given in Figure 4.51 and Figure 4.52, respectively. Compared to apo and SM-bound 5UVG RMSD profiles (see Figure 4.9 to Figure 4.12), RMSD values of the active site and DK switch of GW-bound and GW/SM-bound 5UVG were lower and reached plateau much faster. As seen in Figure 4.51, GW-bound structures underwent some fluctuations before it reached equilibrium, while GW/SM-bound structures had a stable profile throughout the simulation. This is possibly due to the presence of SM which stabilizes

the active site. However, after 60 ns, all of the structures reached equilibrium around 0.5-1 Å indicating that the active site did not undergo large conformational changes. DK switch regions of GW-bound and GW/SM-bound 5UVG were more stable compared to the apo and SM-bound structures (see Figure 4.11 and Figure 4.12) suggesting that GW4869 bound to and stabilized the DK loop region of 5UVG. Taken together, these RMSD profiles indicate that GW-bound and GW/SM-bound 5UVG structures did not go through large conformational changes.

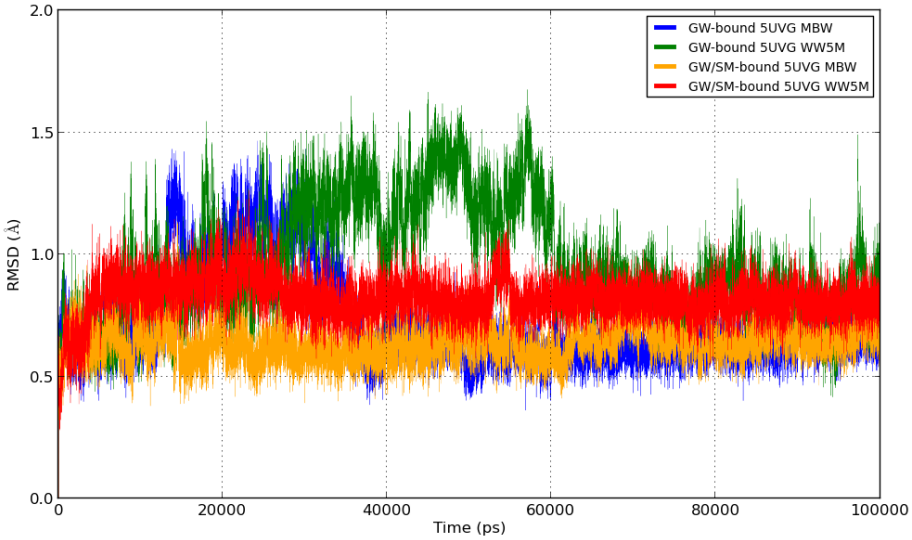

Figure 4.51. RMSD of the active site backbone atoms of GW-bound and GW/SM-bound 5UVG simulations.

RMSF profiles of GW-bound and GW/SM-bound 5UVG are shown in Figure 4.53. According to this RMSF plot, the highly mobile regions on GW-bound and GW/SM-bound 5UVG structures are similar. Ser137-Leu144, Pro165-Pro174, His340-Asp342, Pro448, Gln449, Ser492-Pro498, Glu560-Cys563, Ser587-Leu598, Asp619 and Trp620 are mobile in all GW- and GW/SM-bound 5UVG structures. Gly393-Lys401 loop region is less mobile in GW/SM-bound structures whereas it is highly mobile in other structures. It is important to restate that Cys394-Lys401, Ser493-Asn497 and Gly556-Asp561 were the missing residues in the crystal structure that were filled by the software. DK loop region was also less mobile in GW/SM-bound 5UVG WW5M indicating that GW4869 bound tightly to this structure. Interestingly, loop 464-470 was

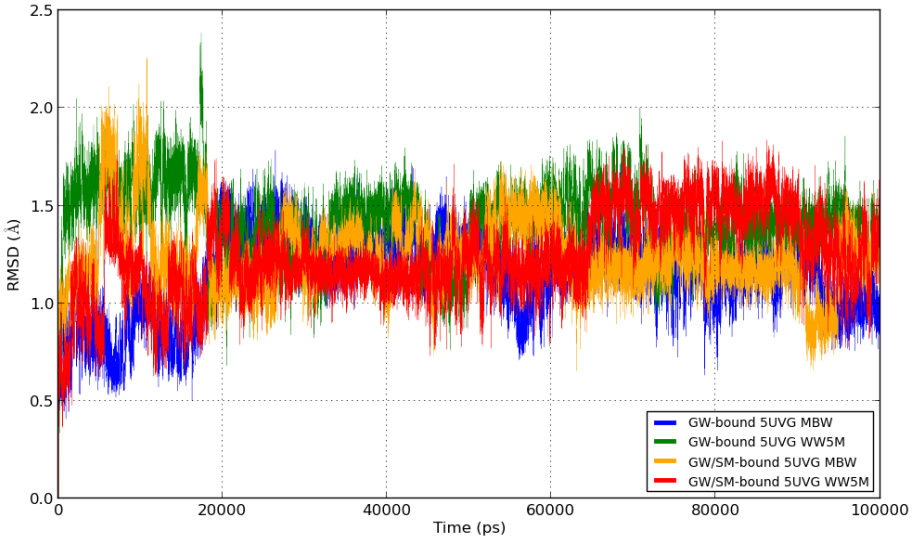

Figure 4.52. RMSD of the DK switch backbone atoms of GW-bound and GW/SM-bound 5UVG simulations.

less mobile in WW5M structures, while mobile in MBW structures. Asp519-Asp520 residues become less mobile in all GW- and GW/SM-bound 5UVG structures compared to apo and SM-bound structures. Asn555-Asp559 become less mobile in GW- and GW/SM-bound 5UVG structures except for GW/SM-bound 5UVG MBW. Among the GW- and GW/SM-bound 5UVG structures, GW/SM-bound 5UVG WW5M showed the most stable profile in terms of RMSF values.

4.5.2. Binding Free Energies of GW4869 During MD Simulations

The binding free energies of GW-bound and GW/SM-bound 5UVG are given in Table 4.38 along with the averages and standard deviations of the overall and after-equilibrium (eq) binding free energies. These binding free energies tabulated in Table 4.38 for GW-bound and GW/SM-bound 5UVG shows that GW4869 bound to DK switch region of 5UVG tightly in both MBW and WW5M cases. Its binding free energy is even better than that of the natural substrate, SM. The binding free energies of the SM ligand in GW/SM-bound 5UVG were calculated to see whether GW4869

affected the binding of SM, it was seen that they are close to the energy values provided in Table 4.20 and 4.19 indicating that SM bound to 5UVG efficiently.

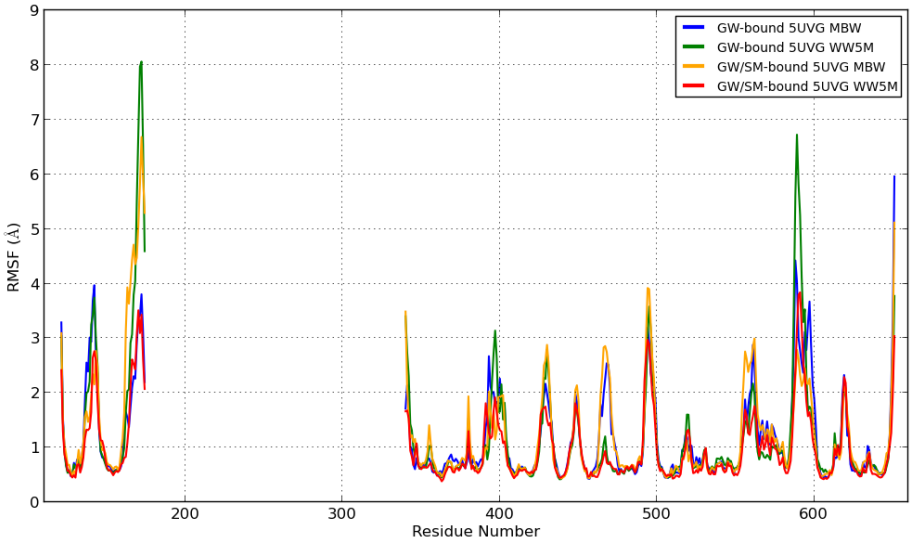

Figure 4.53. Residue-based RMSF profiles of GW-bound and GW/SM-bound 5UVG.

4.5.3. Protein-Ligand Interactions

GW4869-5UVG interactions are shown in Figure 4.54. According to these figures, the most important interaction for the binding of GW4869 is the hydrogen bonding with Asn425 for all GW-bound and GW/SM-bound 5UVG structures (see Figure 4.55). Asp430, Ala431, Leu432 and Ala433 interactions are also important for the GW-bound 5UVG MBW and GW/SM-bound 5UVG WW5M which had better binding free energies (around -100 kcal/mol as seen in Table 4.38) compared to the other two MD simulations. The dominance of these Asp430-Ala433 interactions in the simulations with better binding free energies suggesting that these residues might be important for the tight binding of GW4869 into DK switch region of 5UVG. The timeline graph of these protein-ligand interaction are given in Figure A.5.

Table 4.38. Binding free energies computed for GW-bound and GW/SM-bound 5UVG.

Frames	**GW-bound 5UVG MBW**	**GW-bound 5UVG WW5M**	**GW/SM-bound 5UVG MBW**		**GW/SM-bound 5UVG WW5M**	
	GW	**GW**	**GW**	**SM**	**GW**	**SM**
0	-96.598	-94.874	-103.826	-62.950	-103.058	-77.986
800	-106.368	-102.415	-102.760	-65.116	-108.642	-67.158
1600	-94.314	-88.928	-108.402	-56.502	-112.401	-59.253
2400	-87.831	-84.100	-86.352	-27.398	-88.685	-60.359
3200	-91.384	-91.687	-107.472	-40.687	-100.342	-56.799
4000	-85.982	-87.115	-106.490	-37.510	-102.122	-47.025
4800	-100.403	-85.231	-100.583	-68.905	-101.428	-57.802
5600	-95.664	-86.600	-103.416	-49.592	-106.631	-42.997
6400	-94.861	-82.921	-92.873	-49.379	-100.019	-57.056
7200	-92.802	-89.650	-92.632	-35.041	-105.642	-55.410
8000	-98.972	-93.976	-88.689	-48.338	-104.469	-48.211
8800	-106.720	-84.275	-84.082	-36.926	-88.933	-56.792
9600	-101.984	-84.176	-111.736	-40.949	-108.201	-53.061
10400	-103.346	-79.142	-106.918	-44.787	-104.679	-49.567
11200	-106.693	-80.524	-108.544	-49.102	-100.417	-47.890
12000	-109.133	-79.478	-120.821	-43.436	-112.751	-57.774
12800	-103.596	-93.734	-96.892	-59.236	-111.564	-48.598
13600	-106.539	-73.453	-104.501	-48.872	-98.330	-51.520
14400	-105.422	-83.033	-83.254	-47.422	-94.344	-60.023
15200	-104.626	-78.124	-104.499	-50.807	-101.438	-52.826
16000	-104.107	-108.436	-105.785	-55.586	-93.741	-54.006
16800	-108.206	-90.802	-77.628	-39.901	-93.117	-51.862
17600	-104.156	-89.712	-76.966	-45.213	-104.023	-58.513
18400	-109.845	-93.004	-73.762	-47.818	-97.323	-56.237
19200	-112.280	-94.435	-79.010	-52.521	-100.903	-51.914
20000	-97.495	-95.217	-98.528	-45.341	-103.352	-60.063
20800	-97.398	-100.244	-95.736	-47.800	-104.813	-46.698
Avg	-100.990	-88.714	-97.117	-48.042	-101.903	-55.089
StDev	6.884	7.805	12.228	9.374	6.612	7.067
Avg_{eq}	-105.203	-88.524	-84.800	-47.738	-101.485	-53.392
StDev_{eq}	4.198	9.871	11.454	2.958	6.009	4.501
Eq Time	50 ns	50 ns	85 ns		50 ns	

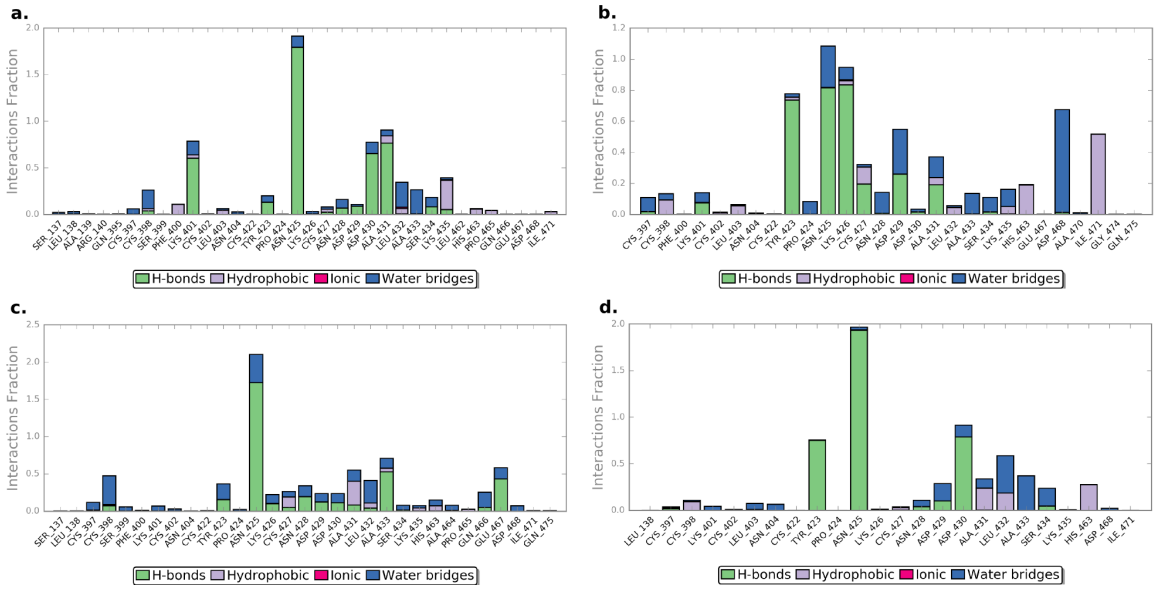

Figure 4.54. GW4869 interactions with GW-bound 5UVG MBW (a) and WW5M (b), and GW/SM-bound 5UVG MBW (c) and WW5M (d).

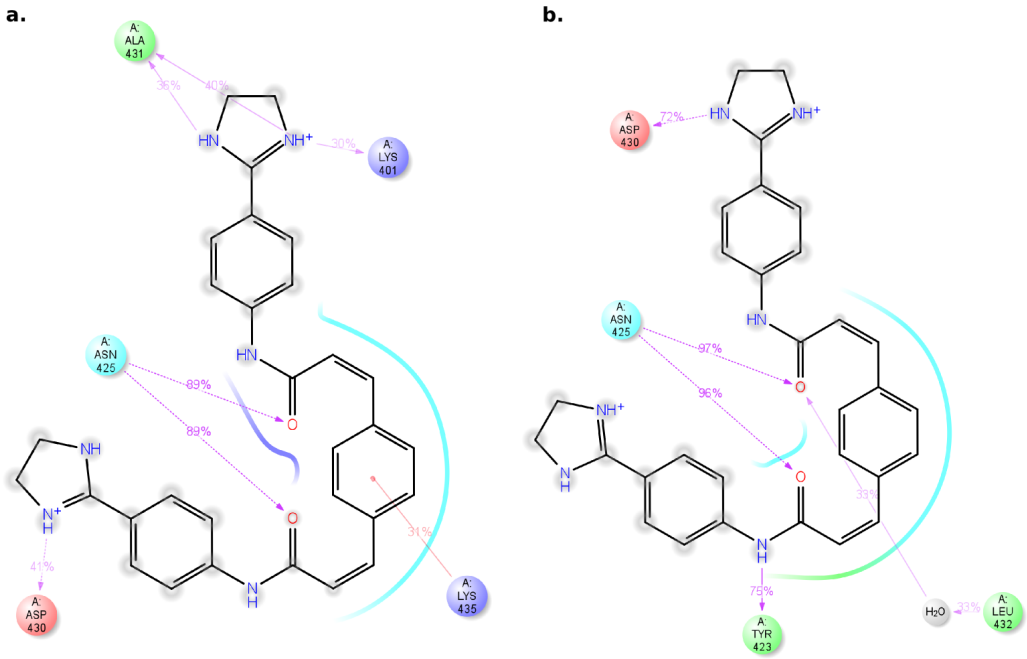

Figure 4.55. Schematic diagrams of the protein-ligand interactions of GW-bound 5UVG MBW (a) and GW/SM-bound 5UVG WW5M (b). Only the interactions that occurred more than 30% of the simulation time are depicted.

4.5.4. Analysis of the Binding Mode of GW4869 in GW- and GW/SM-Bound MD Simulations

The conformational analysis of the MD simulations show that GW4869 preserved its binding mode in the cases of GW-bound 5UVG MBW and GW/SM-bound 5UVG WW5M, most notably the latter one. GW4869 did not preserve its binding mode in the cases of GW-bound 5UVG WW5M and GW/SM-bound 5UVG MBW as seen in Figure 4.56. It is important to state that even GW4869 changed its binding mode, it did not diffuse away from these proteins and remained bound to them.

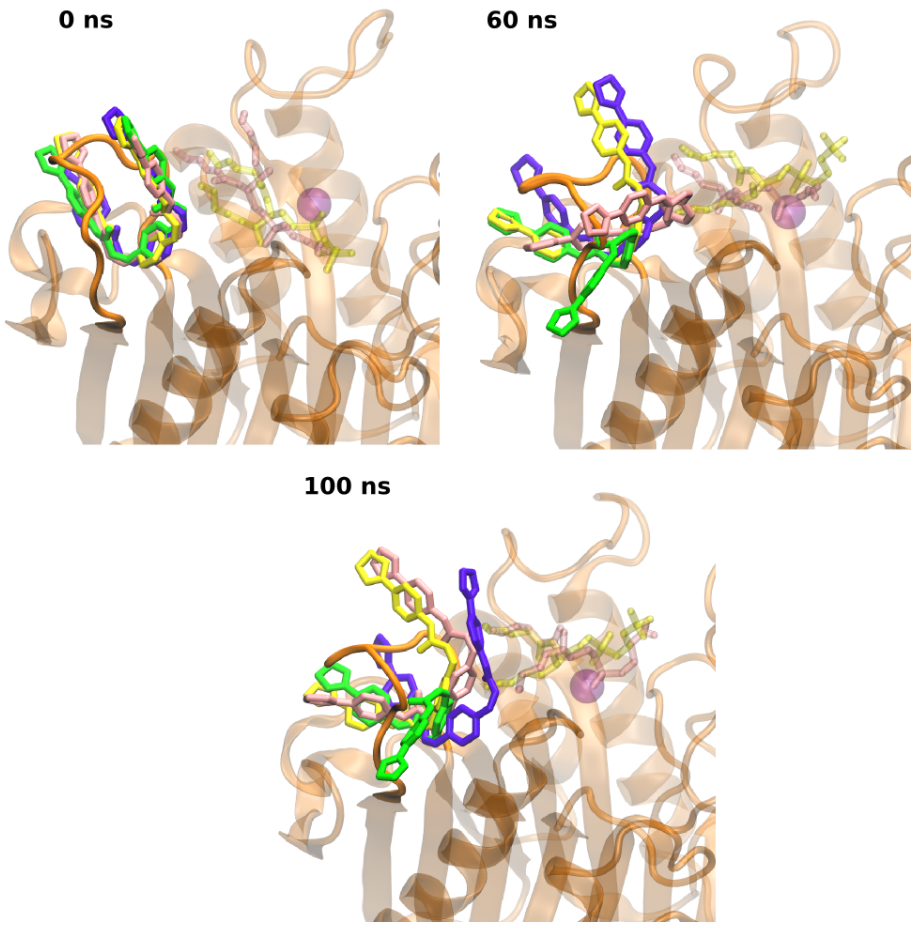

Figure 4.56. Binding mode of GW4869 through 100 ns MD simulations. GW4869 ligands are shown in yellow, pink, green and purple for GW/SM-bound 5UVG WW5M and MBW, GW-bound 5UVG WW5M and MBW structures, respectively.

Asn425 and Asp430 interactions of GW/SM-bound 5UVG WW5M with GW4869 are shown in Figure 4.57. It can be seen that the interaction between Asn425 and 5UVG was present throughout the simulation, while hydrogen bonding with Asp430 was formed later. Once an interaction was formed between GW4869 and Asp430, this interaction was maintained. Even though a salt bridge formation was not observed between Asp430 and Lys435 in the aforementioned SM-bound 5UVG simulations (hence no helical conformation was seen in DK switch), the conserved DK motif in reality might take part in the catalysis as suggested by Airola *et al.* [1] with a complete protein structure having both its catalytic and NTD domains. If that is the case, GW4869 may indeed block the salt bridge formation between Asp430 and Lys435 by forming interactions with Asp430.

Taken together, these results suggest that GW4869 can bind to DK switch region by forming favorable interactions with the DK switch residues (Tyr423-Lys435) as proposed by Airola *et al.* [1], most notably through hydrogen bonding with Asn425 and Asp430 residues. The possible binding mode of GW4869 at DK switch region is given in Figure 4.48. The binding free energies and the conformational analysis showed that these binding mode was preserved throughout the simulations.

4.5.5. Comparative Conformational Analysis of Apo, SM-, GW- and GW/SM-Bound Human nSMase2

GW4869 mainly interacted with Ser137-Arg140, Cys397-Asn404 and Leu462-Gln475 regions in addition to DK switch Tyr423-Lys435. Hence a comparative analysis for the MD simulations of apo, SM-bound, GW-bound and GW/SM-bound structures were carried out with a special focus on these regions. GW-bound 5UVG MBW and GW/SM-bound 5UVG WW5M were selected for the analysis of the effect of GW4869 on 5UVG since GW4869 bound to them with better binding free energies. When they were compared with each other, the conformations of the GW-bound 5UVG MBW and GW/SM-bound 5UVG WW5M were similar throughout the simulation except for Leu462-Gln475, Asp553-Thr564 and Phe584-Arg604. The difference in the confor-

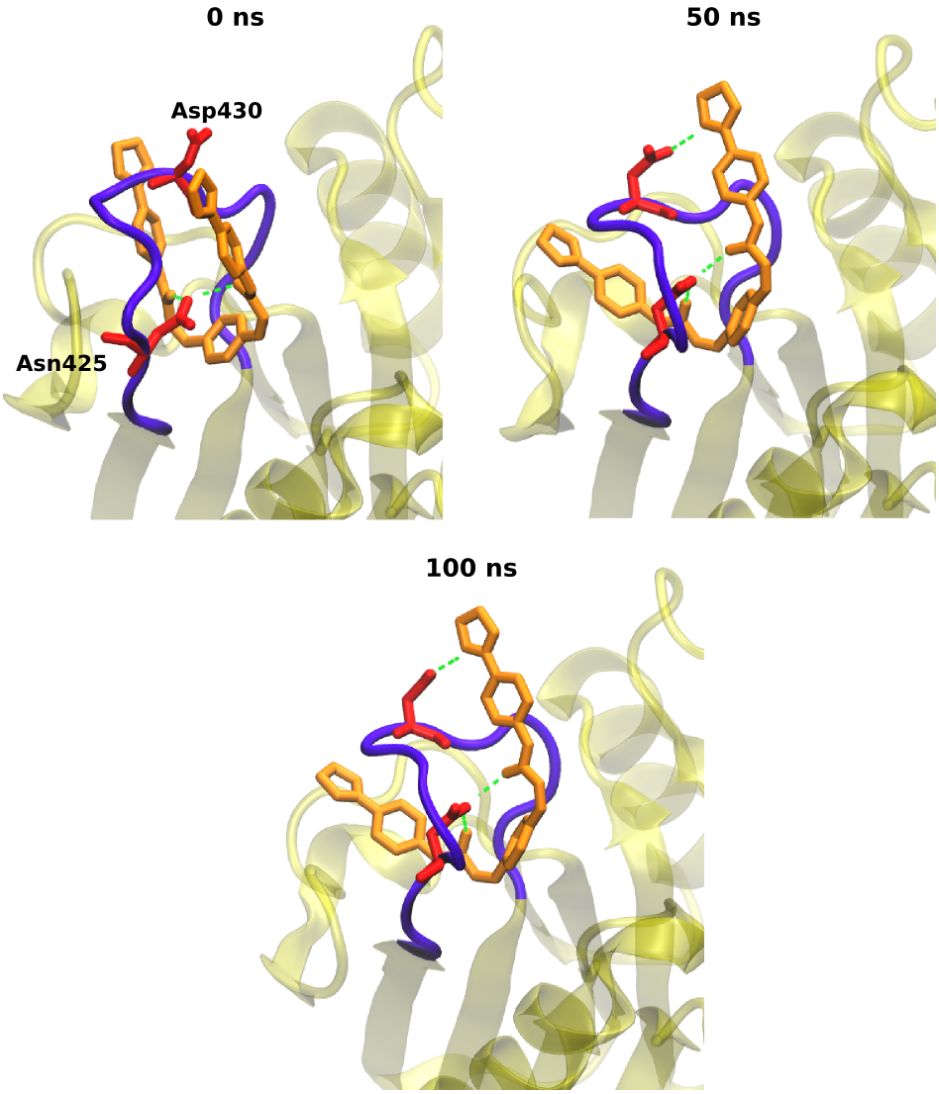

Figure 4.57. Important interactions between GW4869 and GW/SM-bound 5UVG WW5M. GW4869 and the residues; Asn425 and Asp430 are shown in orange and red licorice forms. DK switch loop is colored in violet.

mations of Leu462-Gln475 and Asp553-Thr564 might stem from Ala464 and Tyr558 interacting with SM in GW/SM-bound 5UVG. Cys397-Asn404 and Tyr423-Lys435 are highly similar to each other. However, the missing residues in Cys397-Asn404 and Asp553-Thr564 loop regions were filled by the software. Since the conformations of the loops that are interacting with GW4869 have similar conformations and the differences in their conformations came from the SM bound in the active site of GW/SM-bound 5UVG, only GW/SM-bound 5UVG WW5M were utilized when comparing GW-bound structures with apo and SM-bound structures.

Ser137-Arg140, Cys397-Asn404, Tyr423-Lys435 and Leu462-Gln475 loop regions are conserved according to Airola *et al.* [1]. The comparative analysis of the MD simulation results showed that Gly393-Gly406, Leu462-Gln475, Tyr423-Lys435, Asp553-Thr564 and Phe584-Arg604 regions displayed the largest conformational differences between apo, SM-bound and GW/SM-bound structures. It is important to state that even though conformational differences are seen in these regions (see Figure 4.58), these differences do not seem to explain the catalytic mechanism of human nSMase2 especially the differences in Phe584-Arg604.

Gly393-Gly406 and Tyr423-Lys435 seem to be stabilized with GW4869 binding. They remained less mobile with GW4869 binding. However, Cys394-Lys401 were actually missing in the crystal structure that were filled by the software.

Leu462-Gln475 is an interesting region. It possibly corresponds to Leu152-Gln171 in *Bc*-SMase indicating that it might be coordinated by the metal ion. This region was closer to the active site in apo and GW/SM-bound 5UVG simulations, while it moved away from the active site in SM-bound 5UVG simulations as seen in *Bc*-SMases. Ala464 seems to be important for the movement of this loop. It interacted with SM in GW/SM-bound 5UVG case. However, unlike in *Bc*-SMase case, this region did not seem to be coordinated by the metal ion since it was not close to the calcium ion. The metal coordination might have been seen if there was magnesium ion instead of calcium ion at the active site. This region might be important for the catalytic activity.

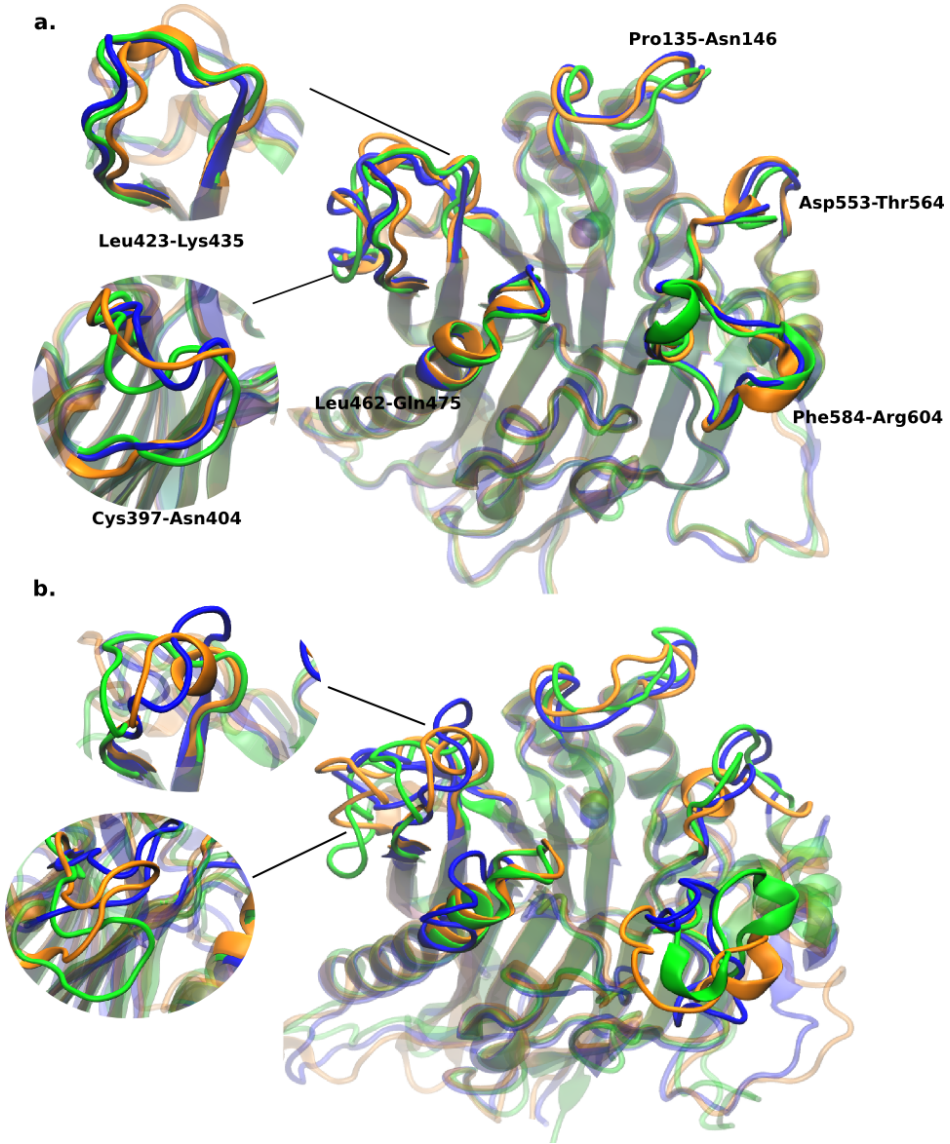

Figure 4.58. Comparative conformational analysis of the apo, SM-bound and GW/SM-bound 5UVG. First frames (a) and last frames (b) of apo (orange), SM-bound (cyan) and GW/SM-bound (green) 5UVG.

Asp553-Thr564 region are similar in conformations for SM- and GW/SM-bound structures. Apo structure attained a helical conformation towards the end of the simulation. This region contained some missing residues/atoms (Gly556-Asp561) which were filled by the software. Hence the helical conformation seen can be misleading. Tyr558 seems to be interacting with the amino group of SM, hence it might be an important residue. However, according to Airola *et al.* [1], this residue is not conserved universally.

Phe584-Arg604 regions of the structures are very different from each other. This region did not seem to take part in the catalytic activity, and according to the sequence alignment conducted by Airola *et al.* this region was not homologous to any part of *Bc*-SMases. Trp232 and Phe244 were very important for the binding of the amino group of *Bc*-SMases hence it was expected to see some aromatic residues taking part in the binding of SM in human nSMase2. Tyr558 seems to be taking part in the binding of SM. The aromatic residues around the amino group of SM were sought besides Tyr558. Phe584 seemed to be promising at first. However, in all simulations, it was directed away from the active site indicating that it might not be important for the catalytic activity.

Taken together, MD simulations conducted on human nSMase2 showed the importance of the missing NTD for the stability of the protein. SM also did not bind to human nSMase2 like in the cases of *Bc*-SMases possibly due to the calcium ion at the active site, missing residues close to the active site and missing NTD. If there was magnesium ion instead of calcium ion, better ligand binding affinity might have been seen for SM. However, even with calcium ion, SM did not diffuse away from the protein, and Glu364 and Asp638 in addition to calcium ion played an important role in the binding of SM.

5. CONCLUSIONS AND RECOMMENDATIONS

5.1. Conclusions

Sphingolipids, most notably ceramide, are membrane lipid molecules that take part in the regulation of diverse cellular signaling pathways involved in inflammation, cell apoptosis and proliferation [4–6, 9, 10]. A major way to generate stress-induced ceramide in the cell is through the hydrolysis of sphingomyelin present in the PM which is catalyzed by nSMase2 at neutral pH. Due to its possible role in exosome secretion, nSMase2 has been implicated in the pathogenesis of Alzheimer's disease and hence, suggested as a therapeutic target for this disease [1, 4].

Several experimental studies are being conducted on mammalian nSMase2 because of its potential as a therapeutic agent and key role in sphingolipid metabolism. However, its complicated structure (having two different domains; catalytic and membrane) and lack of its crystal structure made it difficult to investigate the catalytic mechanism of this protein both computationally and experimentally. The recent discovery of the crystal structure of the catalytic domain of human nSMase2 (PDB ID: 5UVG [1]) facilitated the computational analysis of this enzyme.

The aim of this study was to shed light on the catalytic mechanism of nSMase2 by comparatively investigating and analyzing the simulations performed on apo and SM-bound *Bc*-SMases and human nSMase2 and GW4869-bound human nSMase2, and propose a potential binding site for the experimentally determined nSMase2 inhibitor, GW4869. For this purpose, an integrated computational approach was utilized; molecular docking and MD simulations were performed.

MD simulations performed on the apo and SM-bound structures demonstrated the importance of the membrane domain of human nSMase2 for the stability of this enzyme. Almost in all simulations of SM-bound structures, Glu53 and Mg^{2+}/Co^{2+}

in *Bc*-SMases and Glu364 and Ca^{2+} in human nSMase2 interaction were seen which demonstrated the importance of these residues and ions in SM binding. While SM bound tightly to *Bc*-SMases and human nSMase2 during molecular docking, the comparative analysis of apo and SM-bound simulations showed that the binding of SM stabilized the bacterial SMases while it made human nSMase2 more mobile and caused structural distortions in some regions of the protein. This destabilization is possibly due to the absence of the membrane domain region in the crystal structure of human nSMase2 which contains the palmitoylation and calcineurin sites.

The possible binding site of GW4869 suggested by Airola *et al.* [1] was tested through SiteMap, molecular docking and MD simulations, and a possible binding site and binding mode for GW4869 on the DK Switch region of nSMase2 were identified. Additional MD simulations on GW4869-bound and GW4869/SM-bound human nSMase2 showed that GW4869 bound to DK switch region in the proposed binding mode. Asn425 and Asp430 interactions were observed to play an important role in the binding of GW4869 to the DK switch region of 5UVG.

5.2. Recommendations

MD simulations on human nSMase2 can be conducted by replacing the active site metal ion with magnesium ion. NSMase2 has been suggested to conduct its catalytic activity through magnesium-dependent manner. However, during the crystallization process of human nSMase2, an exogenous calcium ion was bound to human nSMase2 instead of magnesium [1]. Hence magnesium-bound human nSMase2 can be built and further analyzed with MD simulations to have a better understanding of the conformational dynamics of the protein.

Further MD simulations can be performed on the mutant forms of *Bc*-SMases and human nSMase2. The mutations, that were experimentally analyzed such as D430A and K435A in human nSMase2 [1], can be used as the reference when generating the starting structure of the mutant forms of human nSMase2 and *Bc*-SMases *in silico*.

These MD simulations conducted on the mutant form can provide further information on the catalytic mechanism of nSMase2.

MD simulations might be extended to 1 μs to investigate the equilibrium dynamics of nSMase2 better since longer simulations on apo and bound forms of a protein can provide more details, hence improved understanding about the conformational dynamics of the protein.

Different force fields (e.g. CHARMM27) and seed numbers can be investigated when carrying out MD simulations to find the parameters that most successfully capture the conformational dynamics of nSMase2. There are several studies which performed MD simulations on a protein with different force fields and/or other parameters (e.g. [74]). However, to find the most suitable parameters, more experimental data regarding to the catalytic activity of nSMase2 is required as a reference. Experimental data is needed to verify the conformational dynamics observed in MD simulations. Hence the computational results presented in this study should also be further verified by carrying out experiments. Mutagenesis analysis on human nSMase2 can unveil the catalytic mechanism of nSMase2.

Pharmacophore modeling approaches such as structure-based screening can be performed on human nSMase2 to find the molecules that can possibly be used as an inhibitor or chaperone for this enzyme. The identified pharmacological molecules might be used against nSMase2-related diseases such as Alzheimer's disease.

REFERENCES

1. Airola, M. V., P. Shanbhogue, A. A. Shamseddine *et al.*, "Structure of human nSMase2 reveals an interdomain allosteric activation mechanism for ceramide generation", *Proceedings of the National Academy of Sciences*, Vol. 114, No. 28, pp. 5549–5558, 2017.

2. Ago, H., M. Oda, M. Takahashi *et al.*, "Structural basis of the sphingomyelin phosphodiesterase activity in neutral sphingomyelinase from Bacillus cereus", *Journal of Biological Chemistry*, Vol. 281, No. 23, pp. 16157–16167, 2006.

3. Clarke, C. J., C. F. Snook, M. Tani *et al.*, "The extended family of neutral sphingomyelinases", *Biochemistry*, Vol. 45, No. 38, pp. 11247–11256, 2006.

4. Airola, M. V. and Y. A. Hannun, "Sphingolipid metabolism and neutral sphingomyelinases", *Handbook of experimental pharmacology*, No. 215, pp. 57–76, 2013.

5. Milhas, D., C. J. Clarke and Y. A. Hannun, "Sphingomyelin metabolism at the plasma membrane: Implications for bioactive sphingolipids", *FEBS Letters*, Vol. 584, No. 9, pp. 1887–1894, 2010.

6. Obama, T., Y. Kan, H. Ikezawa *et al.*, "Glu-53 of Bacillus cereus sphingomyelinase acts as an indispensable ligand of Mg2+ essential for catalytic activity", *Journal of Biochemistry*, Vol. 133, No. 3, pp. 279–286, 2003.

7. Shamseddine, A. A., M. V. Airola and Y. A. Hannun, "Roles and regulation of neutral sphingomyelinase-2 in cellular and pathological processes", *Advances in Biological Regulation*, Vol. 57, pp. 24–41, 2015.

8. Goñi, F. M. and A. Alonso, "Sphingomyelinases: enzymology and membrane activity", *FEBS Letters*, Vol. 531, No. 1, pp. 38–46, 2002.

9. Pralhada Rao, R., N. Vaidyanathan, M. Rengasamy *et al.*, "Sphingolipid metabolic pathway: an overview of major roles played in human diseases", *Journal of Lipids*, Vol. 2013, p. 178910, 2013.

10. Tirodkar, T. S. and C. Voelkel-Johnson, "Sphingolipids in apoptosis", *Experimental Oncology*, Vol. 34, No. 3, pp. 231–242, 2012.

11. Assi, E., D. Cazzato, C. De Palma *et al.*, "Sphingolipids and brain resident macrophages in neuroinflammation: An emerging aspect of nervous system pathology", *Clinical and Developmental Immunology*, Vol. 2013, pp. 1–8, 2013.

12. Oda, M., M. Takahashi, T. Matsuno *et al.*, "Hemolysis induced by Bacillus cereus sphingomyelinase", *Biochimica et Biophysica Acta (BBA) - Biomembranes*, Vol. 1798, No. 6, pp. 1073–1080, 2010.

13. Wu, B. X., C. J. Clarke and Y. A. Hannun, "Mammalian neutral sphingomyelinases: Regulation and roles in cell signaling responses", *NeuroMolecular Medicine*, Vol. 12, No. 4, pp. 320–330, 2010.

14. Tani, M. and Y. A. Hannun, "Analysis of membrane topology of neutral sphingomyelinase 2", *FEBS letters*, Vol. 581, No. 7, pp. 1323–1328, 2007.

15. Canals, D., D. M. Perry, R. W. Jenkins *et al.*, "Drug targeting of sphingolipid metabolism: Sphingomyelinases and ceramidases", *British Journal of Pharmacology*, Vol. 163, No. 4, pp. 694–712, 2011.

16. Medzhitov, R., "Inflammation 2010: New adventures of an old flame", Vol. 140, No. 6, pp. 771–776, 2010.

17. Dobierzewska, A., N. V. Giltiay, S. Sabapathi *et al.*, "Protein phosphatase 2A and neutral sphingomyelinase 2 regulate IRAK-1 protein ubiquitination and degradation in response to interleukin-1β", *The Journal of Biological Chemistry*, Vol. 286, No. 37, pp. 32064–32073, 2011.

18. Gottipati, S., N. L. Rao and W. P. Fung-Leung, "IRAK1: A critical signaling mediator of innate immunity", *Cellular Signalling*, Vol. 20, No. 2, pp. 269–276, 2008.

19. Rutkute, K., A. A. Karakashian, N. V. Giltiay *et al.*, "Aging in rat causes hepatic hyperresposiveness to interleukin-1β which is mediated by neutral sphingomyelinase-2", *Hepatology*, Vol. 46, No. 4, pp. 1166–1176, 2007.

20. Rutkute, K., R. H. Asmis and M. N. Nikolova-Karakashian, "Regulation of neutral sphingomyelinase-2 by GSH: A new insight to the role of oxidative stress in aging-associated inflammation", *Journal of Lipid Research*, Vol. 48, No. 11, pp. 2443–2452, 2007.

21. Clarke, C. J., T. G. Truong and Y. A. Hannun, "Role for neutral sphingomyelinase-2 in tumor necrosis factor α-stimulated expression of vascular cell adhesion molecule-1 (VCAM) and intercellular adhesion molecule-1 (ICAM) in lung epithelial cells: p38 MAPK is an upstream regulator of nSMase2", *Journal of Biological Chemistry*, Vol. 282, No. 2, pp. 1384–1396, 2007.

22. Dinkins, M. B., S. Dasgupta, G. Wang *et al.*, "Exosome reduction in vivo is associated with lower amyloid plaque load in the 5XFAD mouse model of Alzheimer's disease", *Neurobiology of Aging*, Vol. 35, No. 8, pp. 1792–1800, 2014.

23. Obama, T., S. Fujii, H. Ikezawa *et al.*, "His151 and His296 are the acid-base catalytic residues of Bacillus cereus sphingomyelinase in sphingomyelin hydrolysis", *Biological & Pharmaceutical Bulletin*, Vol. 26, No. 7, pp. 920–926, 2003.

24. Berman, H. M., J. Westbrook, Z. Feng *et al.*, "The Protein Data Bank", *Nucleic Acids Research*, Vol. 28, No. 1, pp. 235–242, 2000.

25. Filosto, S., W. Fry, A. A. Knowlton *et al.*, "Neutral sphingomyelinase 2 (nSMase2) is a phosphoprotein regulated by calcineurin (PP2B)", *Journal of Biological Chemistry*, Vol. 285, No. 14, pp. 10213–10222, 2010.

26. The UniProt Consortium, "UniProt: The universal protein knowledgebase", *Nucleic Acids Research*, Vol. 45, No. D1, pp. D158–D169, 2017.

27. UniProt, *Q9NY59 (NSMA2_HUMAN)*, `http://www.uniprot.org/uniprot/Q9NY59`, accessed at March 2018.

28. Aicart-Ramos, C., R. A. Valero and I. Rodriguez-Crespo, "Protein palmitoylation and subcellular trafficking", *Biochimica et Biophysica Acta (BBA) - Biomembranes*, Vol. 1808, No. 12, pp. 2981–2994, 2011.

29. Altschul, S. F., W. Gish, W. Miller *et al.*, "Basic local alignment search tool", *Journal of Molecular Biology*, Vol. 215, No. 3, pp. 403–410, 1990.

30. Sergelius, C., S. Niinivehmas, T. Maula *et al.*, "Structure–activity relationship of sphingomyelin analogs with sphingomyelinase from Bacillus cereus", *Biochimica et Biophysica Acta (BBA) - Biomembranes*, Vol. 1818, No. 3, pp. 474–480, 2012.

31. Gorelik, A., K. Illes, L. X. Heinz *et al.*, "Crystal structure of mammalian acid sphingomyelinase", *Nature Communications*, Vol. 7, p. 12196, 2016.

32. Slotte, J. P. and B. Ramstedt, "The functional role of sphingomyelin in cell membranes", *European Journal of Lipid Science and Technology*, Vol. 109, No. 10, pp. 977–981, 2007.

33. Zhou, Y. F., M. C. Metcalf, S. C. Garman *et al.*, "Human acid sphingomyelinase structures provide insight to molecular basis of Niemann–Pick disease", *Nature Communications*, Vol. 7, p. 13082, 2016.

34. Barenholz, Y. and T. E. Thompson, "Sphingomyelin: Biophysical aspects", *Chemistry and Physics of Lipids*, Vol. 102, No. 1, pp. 29–34, 1999.

35. Piotto, S., L. Sessa, P. Iannelli *et al.*, "Computational study on human sphingomyelin synthase 1 (hSMS1)", *Biochimica et Biophysica Acta (BBA) - Biomembranes*, Vol. 1859, No. 9, Part B, pp. 1517–1525, 2017.

36. Piotto, S., L. Sessa and S. Concilio, "The Role of Sphingomyelin in the Regulation of Membrane Physical State", A. Catala (Editor), *Sphingolipids: Biology, Synthesis and Functions*, chap. The Role of Sphingomyelin in the Regulation of Membrane Physical State, Nova Publishers, 2015.

37. Maestro, version 10.4, Schrödinger, LLC, New York, NY, 2015.

38. Madhavi Sastry, G., M. Adzhigirey, T. Day *et al.*, "Protein and ligand preparation: Parameters, protocols, and influence on virtual screening enrichments", *Journal of Computer-Aided Molecular Design*, Vol. 27, No. 3, pp. 221–234, 2013.

39. Protein Preparation Wizard; Epik version 2.4, Schrödinger, LLC, New York, NY, 2015; Impact version 5.9, Schrödinger, LLC, New York, NY, 2015; Prime version 3.2, Schrödinger, LLC, New York, NY, 2015.

40. Olsson, M. H. M., C. R. Søndergaard, M. Rostkowski *et al.*, "PROPKA3: Consistent treatment of internal and surface residues in empirical pKa predictions", *Journal of Chemical Theory and Computation*, Vol. 7, No. 2, pp. 525–537, 2011.

41. LigPrep, version 3.6, Schrödinger, LLC, New York, NY, 2015.

42. SiteMap, version 3.7, Schrödinger, LLC, New York, NY, 2015.

43. Halgren, T. A., "Identifying and characterizing binding sites and assessing druggability", *Journal of Chemical Information and Modeling*, Vol. 49, No. 2, pp. 377–389, 2009.

44. Halgren, T., "New method for fast and accurate binding-site identification and analysis", *Chemical Biology & Drug Design*, Vol. 69, No. 2, pp. 146–148, 2007.

45. Schrödinger Suite 2015-4 Induced Fit Docking protocol 2015-4, Glide version 6.4, Prime version 3.7, Schrödinger, LLC, New York, NY, 2015.

46. Farid, R., T. Day, R. A. Friesner *et al.*, "New insights about HERG blockade obtained from protein modeling, potential energy mapping, and docking studies", *Bioorganic and Medicinal Chemistry*, Vol. 14, No. 9, pp. 3160–3173, 2006.

47. Sherman, W., T. Day, M. P. Jacobson *et al.*, "Novel procedure for modeling ligand/receptor induced fit effects", *Journal of Medicinal Chemistry*, Vol. 49, No. 2, pp. 534–553, 2006.

48. Sherman, W., H. S. Beard and R. Farid, "Use of an induced fit receptor structure in virtual screening", *Chemical Biology and Drug Design*, Vol. 67, No. 1, pp. 83–84, 2006.

49. Desmond Molecular Dynamics System, version 4.5, D. E. Shaw Research, New York, NY, 2016. Maestro-Desmond Interoperability Tools, version 4.5, Schrödinger, New York, NY, 2016.

50. Bowers, K. J., D. E. Chow, H. Xu *et al.*, "Scalable algorithms for molecular dynamics simulations on commodity clusters", *Proceedings of the ACM/IEEE Conference on Supercomputing (SC06)*, p. 43, ACM, Tampa, Florida, 2006.

51. Prime, version 4.2, Schrödinger, LLC, New York, NY, 2015.

52. National Center for Biotechnology Information, *PubChem Compound Database; CID=9939941*, https://pubchem.ncbi.nlm.nih.gov/compound/9939941, accessed at February 2018.

53. National Center for Biotechnology Information, *PubChem Compound Database; CID=16078967*, https://pubchem.ncbi.nlm.nih.gov/compound/16078967, accessed at February 2018.

54. Epik, version 3.4, Schrödinger, LLC, New York, NY, 2015.

55. Shelley, J. C., A. Cholleti, L. L. Frye *et al.*, "Epik: A software program for pKa prediction and protonation state generation for drug-like molecules", *Journal of Computer-Aided Molecular Design*, Vol. 21, No. 12, pp. 681–691, 2007.

56. Greenwood, J. R., D. Calkins, A. P. Sullivan *et al.*, "Towards the comprehensive, rapid, and accurate prediction of the favorable tautomeric states of drug-like molecules in aqueous solution", *Journal of Computer-Aided Molecular Design*, Vol. 24, No. 6, pp. 591–604, 2010.

57. Xu, M. and M. A. Lill, "Induced fit docking, and the use of QM/MM methods in docking", *Drug Discovery Today: Technologies*, Vol. 10, No. 3, pp. e411–e418, 2013.

58. Glide, version 6.9, Schrödinger, LLC, New York, NY, 2015.

59. Friesner, R. A., J. L. Banks, R. B. Murphy *et al.*, "Glide: A new approach for rapid, accurate docking and scoring. 1. Method and assessment of docking accuracy", *Journal of Medicinal Chemistry*, Vol. 47, No. 7, pp. 1739–1749, 2004.

60. Halgren, T. A., R. B. Murphy, R. A. Friesner *et al.*, "Glide: A new approach for rapid, accurate docking and scoring. 2. Enrichment factors in database screening", *Journal of Medicinal Chemistry*, Vol. 47, No. 7, pp. 1750–1759, 2004.

61. Friesner, R. A., R. B. Murphy, M. P. Repasky *et al.*, "Extra precision Glide: Docking and scoring incorporating a model of hydrophobic enclosure for protein−ligand complexes", *Journal of Medicinal Chemistry*, Vol. 49, No. 21, pp. 6177–6196, 2006.

62. Jacobson, M. P., D. L. Pincus, C. S. Rapp *et al.*, "A hierarchical approach to all-atom protein loop prediction", *Proteins: Structure, Function, and Bioinformatics*, Vol. 55, No. 2, pp. 351–367, 2004.

63. Jacobson, M. P., R. A. Friesner, Z. Xiang *et al.*, "On the role of the crystal environment in determining protein side-chain conformations", *Journal of Molecular Biology*, Vol. 320, No. 3, pp. 597–608, 2002.

64. Yang, L. Q., P. Sang, Y. Tao *et al.*, "Protein dynamics and motions in relation to their functions: several case studies and the underlying mechanisms", *Journal of Biomolecular Structure & Dynamics*, Vol. 32, No. 3, pp. 372–393, 2014.

65. Salsbury, F. R., "Molecular dynamics simulations of protein dynamics and their relevance to drug discovery", *Current Opinion in Pharmacology*, Vol. 10, No. 6, pp. 738–744, 2010.

66. Elloumi, M. and A. Y. Zomaya, *Biological Knowledge Discovery Handbook: Preprocessing, Mining and Postprocessing of Biological Data*, Wiley, 2013.

67. Guliaev, A. B., S. Cheng and B. Hang, "Protein dynamics via computational microscope", *World Journal of Methodology*, Vol. 2, No. 6, pp. 42–49, 2012.

68. Anandakrishnan, R., A. Drozdetski, R. C. Walker *et al.*, "Speed of conformational change: Comparing explicit and implicit solvent molecular dynamics simulations", *Biophysical Journal*, Vol. 108, No. 5, pp. 1153–1164, 2015.

69. Reddy, M. R. and M. D. Erion, *Free Energy Calculations in Rational Drug Design*, Springer Science & Business Media, 2001.

70. Humphrey, W., A. Dalke and K. Schulten, "VMD molecular dynamics", *J. Molec. Graphics*, Vol. 14, pp. 33–38, 1996.

71. Frishman, D. and P. Argos, "Knowledge-based protein secondary structure assignment", *Proteins: Structure, Function, and Bioinformatics*, Vol. 23, No. 4, pp. 566–579, 1995.

72. Hou, T., J. Wang, Y. Li *et al.*, "Assessing the performance of the MM/PBSA and MM/GBSA methods. 1. The accuracy of binding free energy calculations based on molecular dynamics simulations", *Journal of Chemical Information and Modeling*, Vol. 51, No. 1, pp. 69–82, 2011.

73. Li, J., R. Abel, K. Zhu *et al.*, "The VSGB 2.0 model: A next generation energy model for high resolution protein structure modeling", *Proteins*, Vol. 79, No. 10, pp. 2794–2812, 2011.

74. Kundu, S., "Effects of different force fields on the structural character of α synuclein β-hairpin peptide (35–56) in aqueous environment", *Journal of Biomolecular Structure and Dynamics*, Vol. 36, No. 2, pp. 302–317, 2018.

APPENDIX A: ANALYSIS OF MOLECULAR DYNAMICS SIMULATIONS

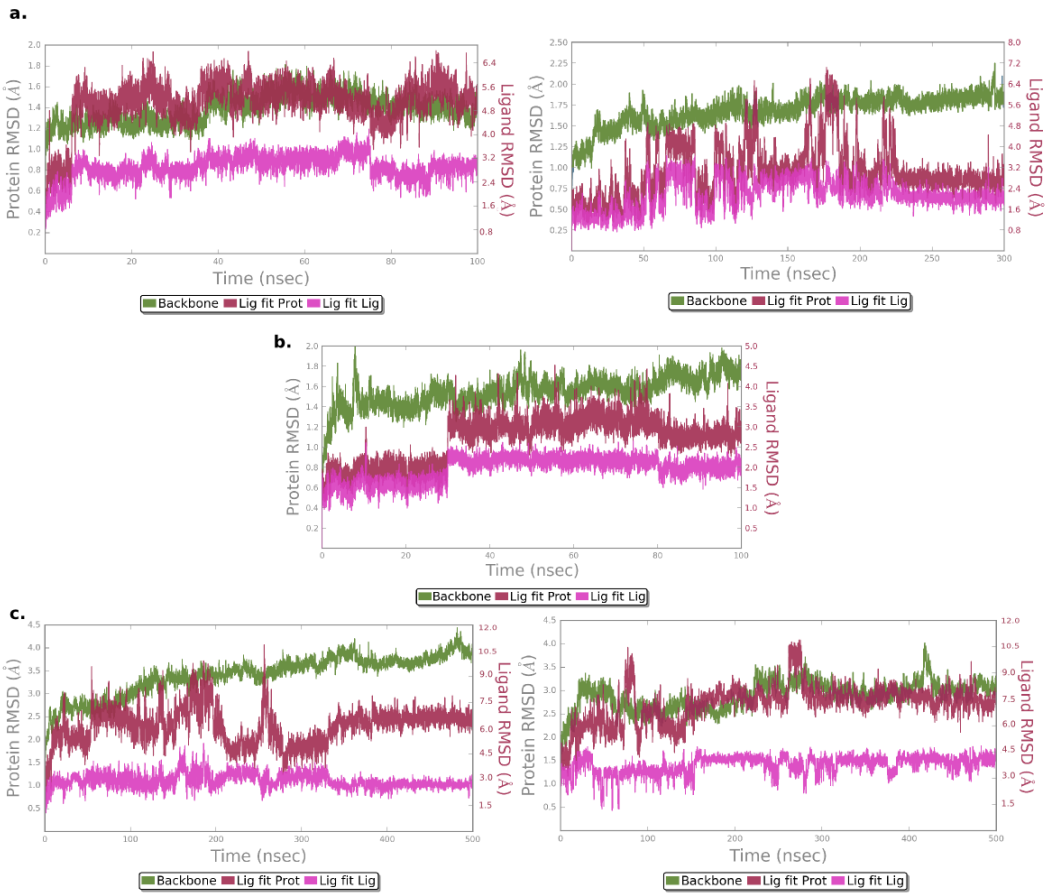

Figure A.1. RMSD profiles of the protein and ligand. (a.) RMSD profiles of 2UYR MBW (left) and 2UYR WW5M (right) and SM, (b.) RMSD profiles of 2DDS MBW and SM, (c.) RMSD profiles of 5UVG MBW (left) and 5UVG WW5M (right) and SM.

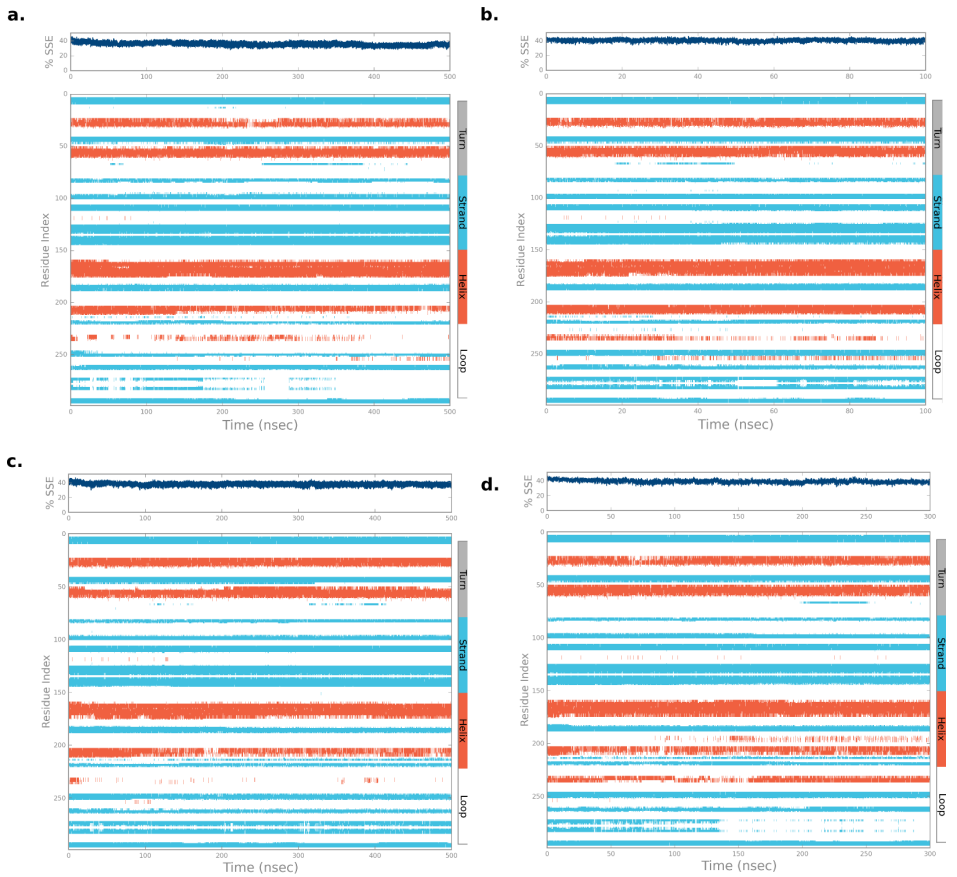

Figure A.2. SSE analysis of 2UYR. (a.) MD simulation of apo 2UYR MBW, (b.) MD simulation of SM-bound 2UYR MBW, (c.) MD simulation of apo 2UYR WW5M, (d.) MD simulation of SM-bound 2UYR WW5M.

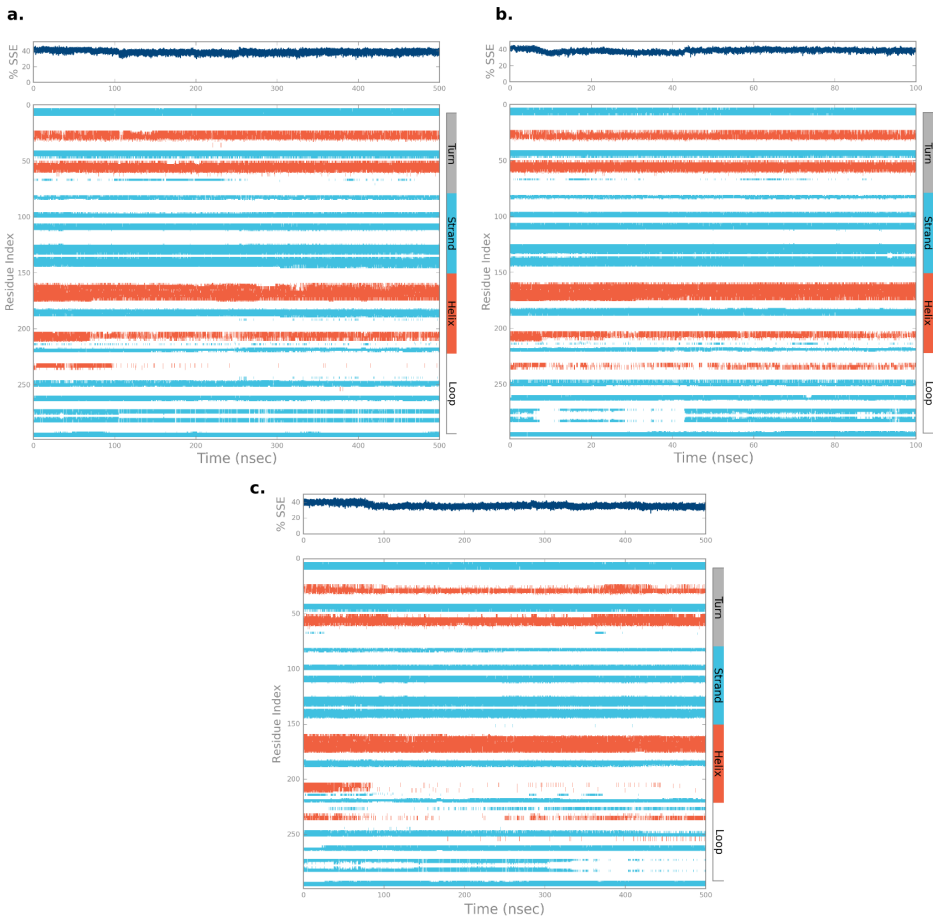

Figure A.3. SSE analysis of 2DDS. (a.) MD simulation of apo 2DDS MBW, (b.) MD simulation of SM-bound 2DDS MBW, (c.) MD simulation of apo 2DDS WW5M.

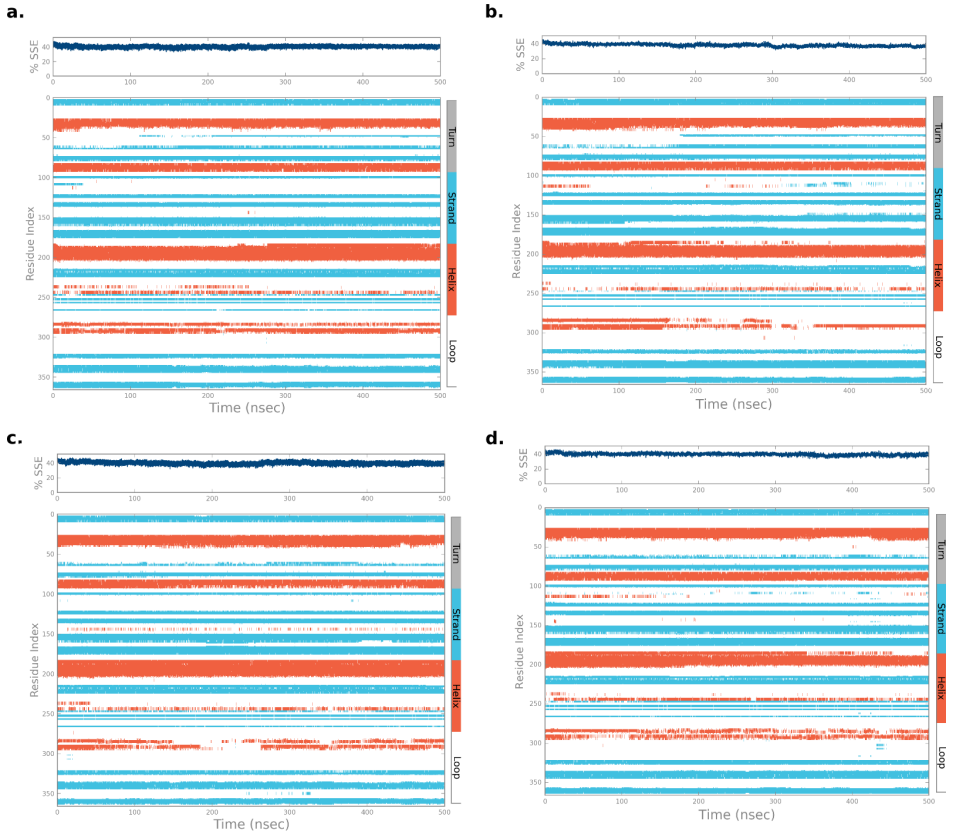

Figure A.4. SSE analysis of 5UVG. (a.) MD simulation of apo 5UVG MBW, (b.) MD simulation of SM-bound 5UVG MBW, (c.) MD simulation of apo 5UVG WW5M, (d.) MD simulation of SM-bound 5UVG WW5M.

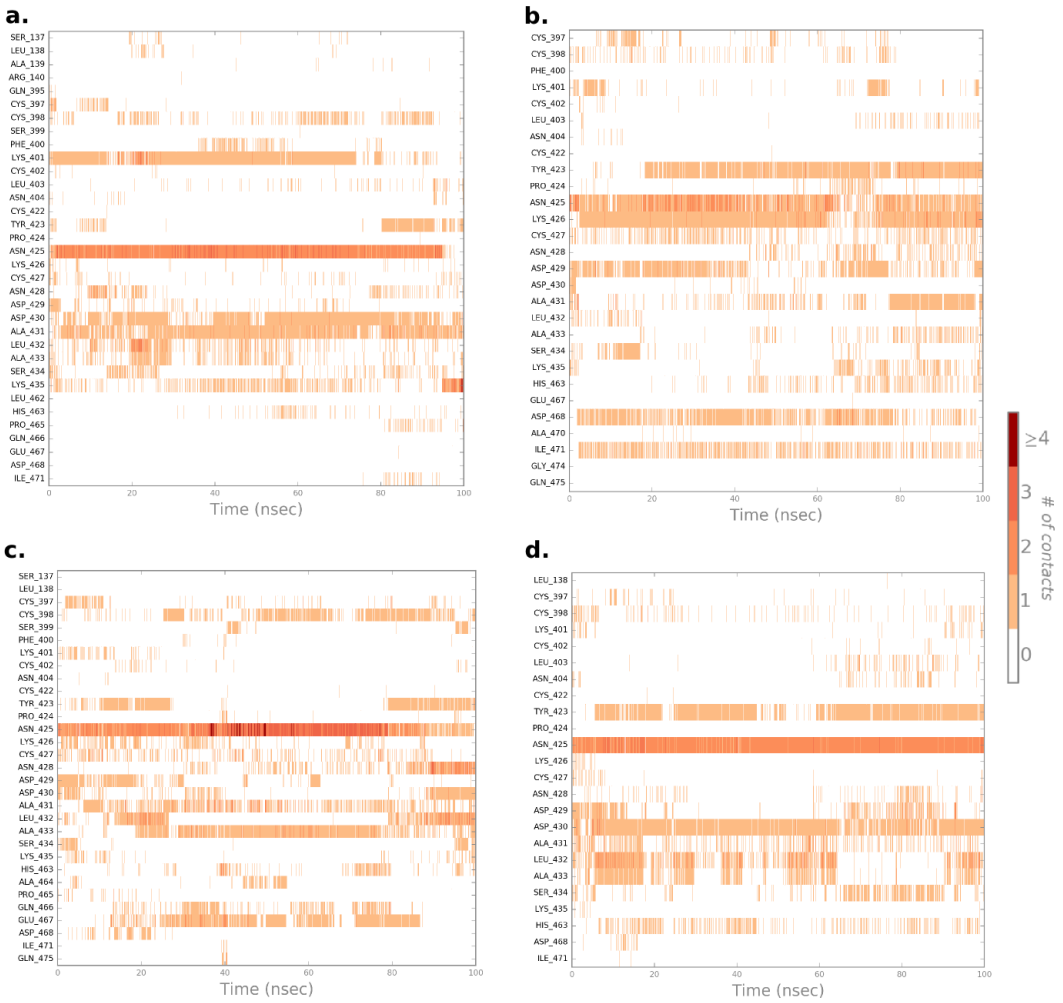

Figure A.5. Protein-ligand interaction timeline of GW-bound 5UVG MBW (a) and WW5M (b), and GW/SM-bound 5UVG MBW (c) and WW5M (d). The number of contacts includes h-bond, hydrophobic, water-bridge and ionic interactions.

Table A.1. Important protein-ligand interactions reported by Schrödinger Suite. Hydrogen bonding, water-bridge and hydrophobic interactions are denoted by H-bond, Wb and Hyd, respectively.

Residues	**2UYR WW5M**	**2UYR MBW**	**2DDS MBW**	**Residues**	**5UVG WW5M**	**5UVG MBW**
Tyr18	H-bond, Wb	Wb	-	-	-	-
Tyr25	Hyd	Hyd	Hyd	-	-	-
Glu53	Wb, Ionic	Wb, Ionic, H-bond	-	**Glu364**	Ionic, Wb, H-bond	Ionic, Wb
Phe55	Hyd	Hyd	Hyd	**Phe366**	-	Hyd
Pro125	Hyd	-	-	-	-	-
Asp126	H-bond, Wb	Ionic, Wb	-	**Asp430**	-	-
Leu128	-	Hyd	-	-	-	-
Lys131	-	H-bond, Wb	H-bond, Wb	**Lys435**	H-bond, Wb	H-bond, Wb
His151	-	Wb, Ionic	Wb	**His461**	-	-
Ala154	Hyd, Wb	-	-	**Ala464**	-	-
Glu155	Wb, Ionic	-	-	-	-	-
Asp156	Wb, H-bond	Wb	-	-	-	-
Asp195	Wb	-	Wb	**Asp510**	-	-
Asn197	Wb, H-bond	-	Wb	**Asn512**	Wb	Wb
Trp232	Hyd	Hyd	-	**Trp546**		
Asn243	-	Wb, H-bond	-	-	-	-
Phe244	Hyd	Hyd	-	-	-	-
Asp295	-	Wb	Wb, Ionic	**Asp638**	Wb, Ionic	Wb, Ionic